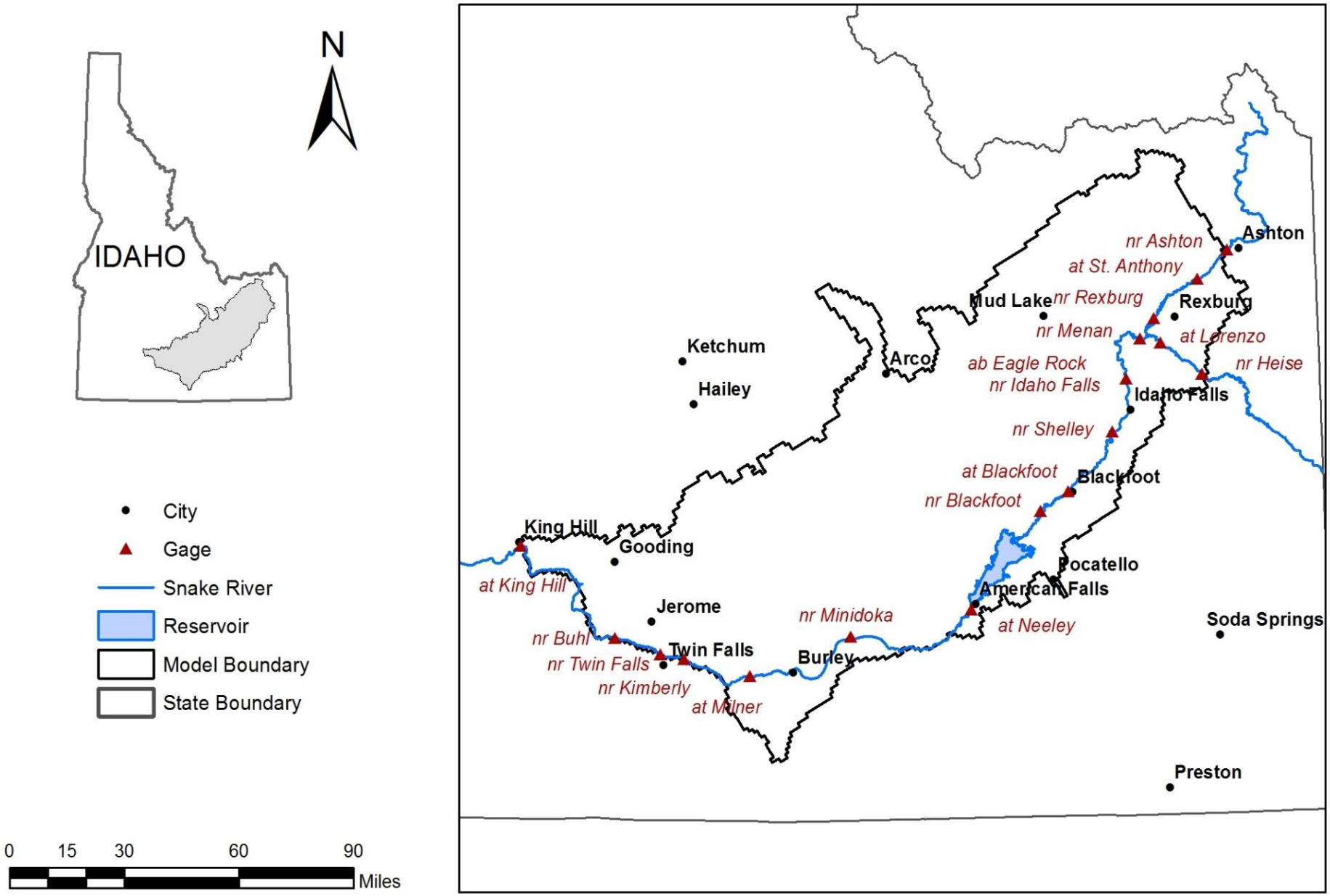

Figure 1. Study area and the Enhanced Snake Plain Aquifer Model version 2.1 (ESPAM2.1) boundary.

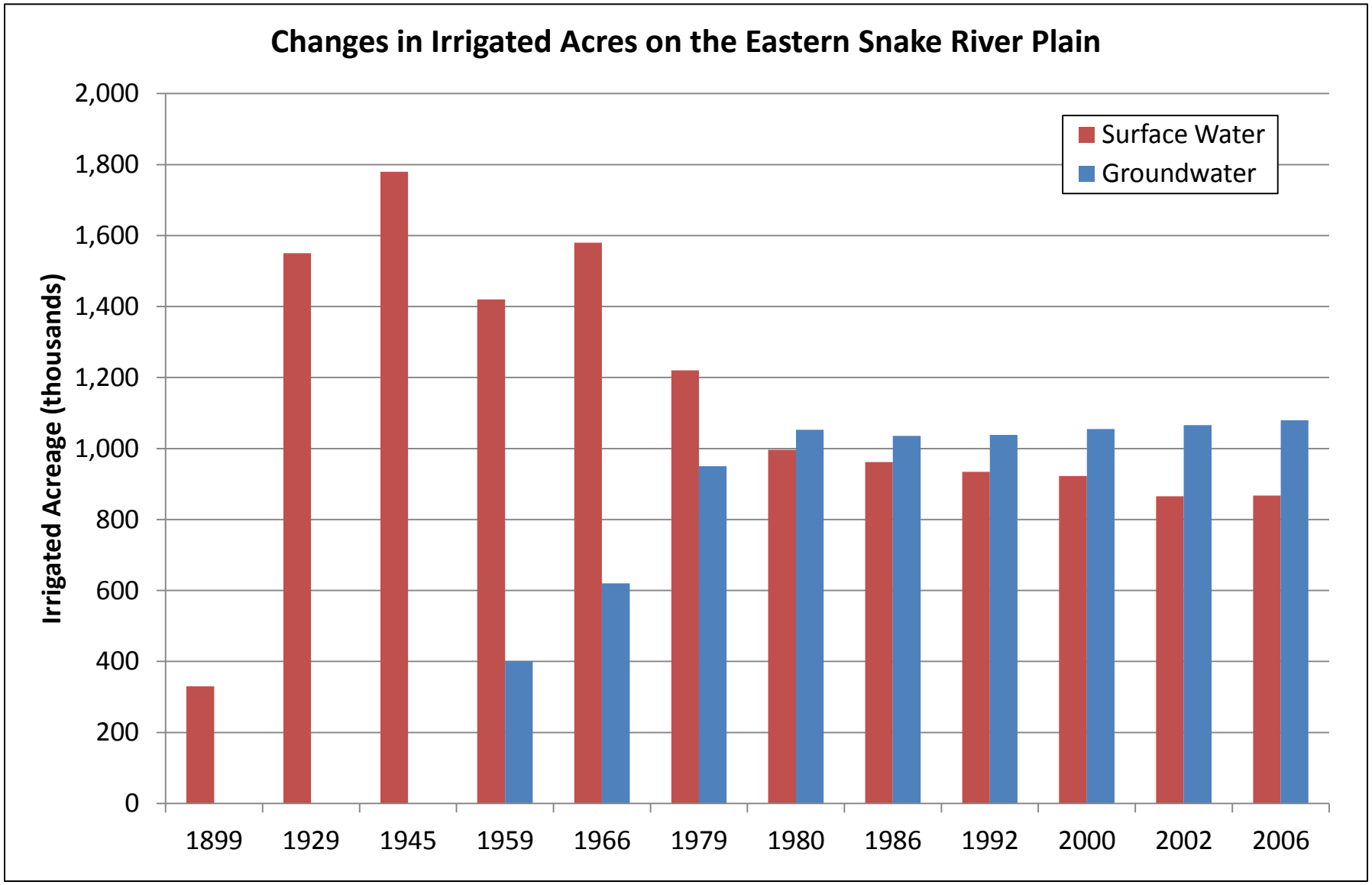

Figure 2. Surface-water and groundwater irrigated acres on the eastern Snake Plain (after Garabedian, 1992 and IDWR GIS shapefiles). The years 1899 through 1979 are represented in Garabedian (1992). The years 1980 – 2006 were acquired from IDWR GIS shapefiles.

Figure 3. Conceptual illustration of variation in average annual flow of the Snake River (after the US Bureau of Reclamation, 1996). Average annual flow values updated using 1980-2008 gage data.

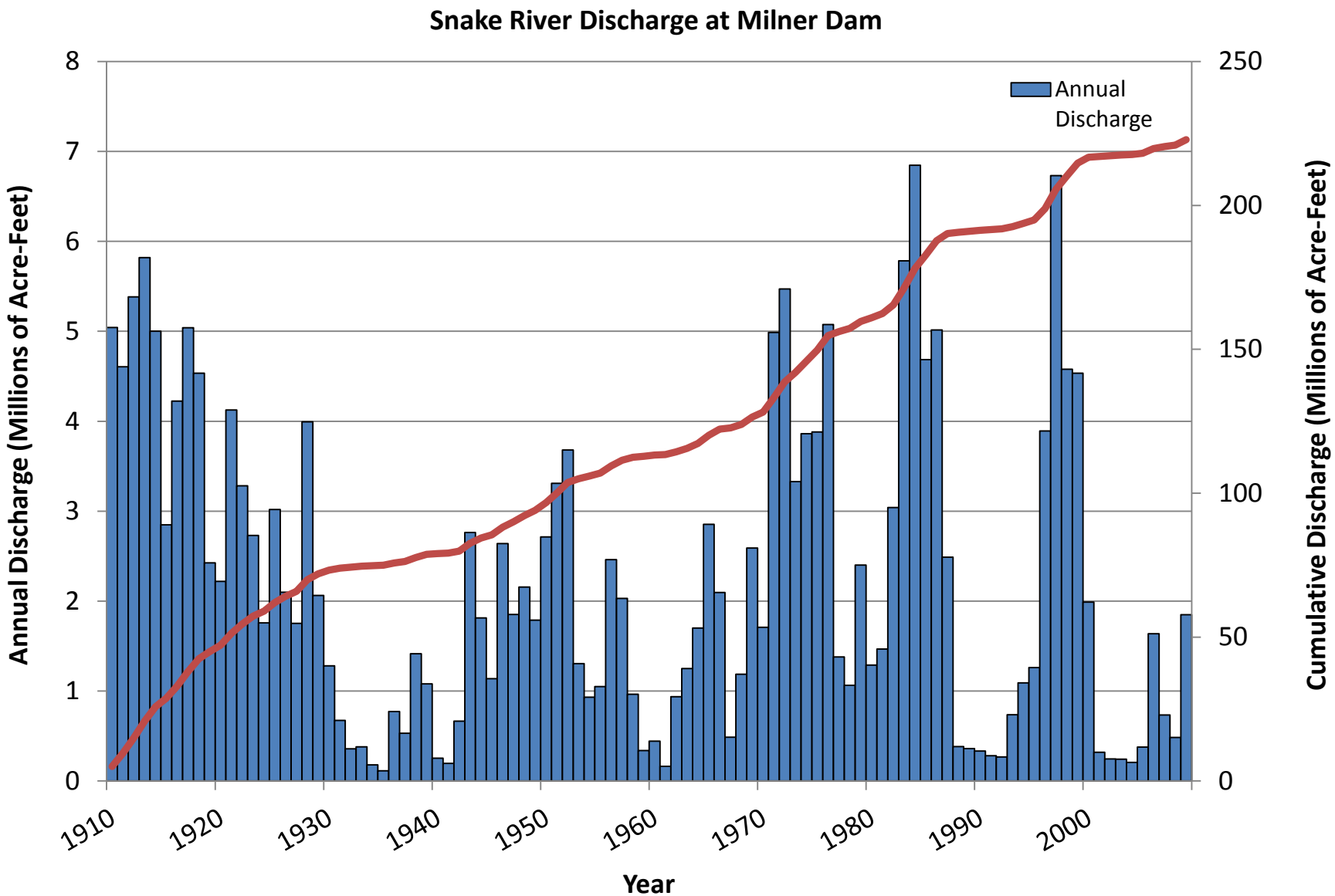

Figure 4. Annual and cumulative discharge of the Snake River at Milner Dam (US Geological Survey data).

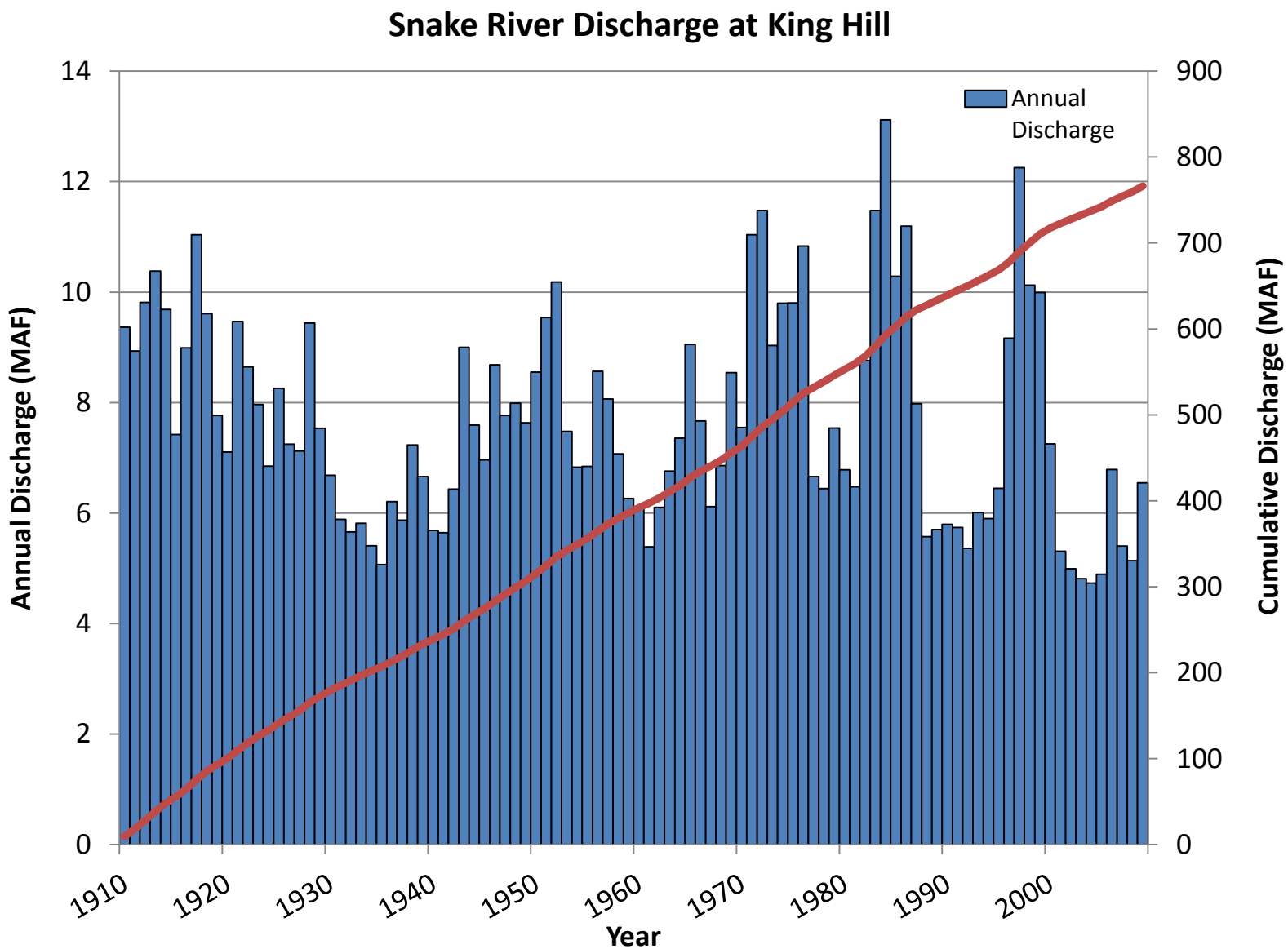

Figure 5. Annual and cumulative discharge of the Snake River at King Hill (US Geological Survey data).

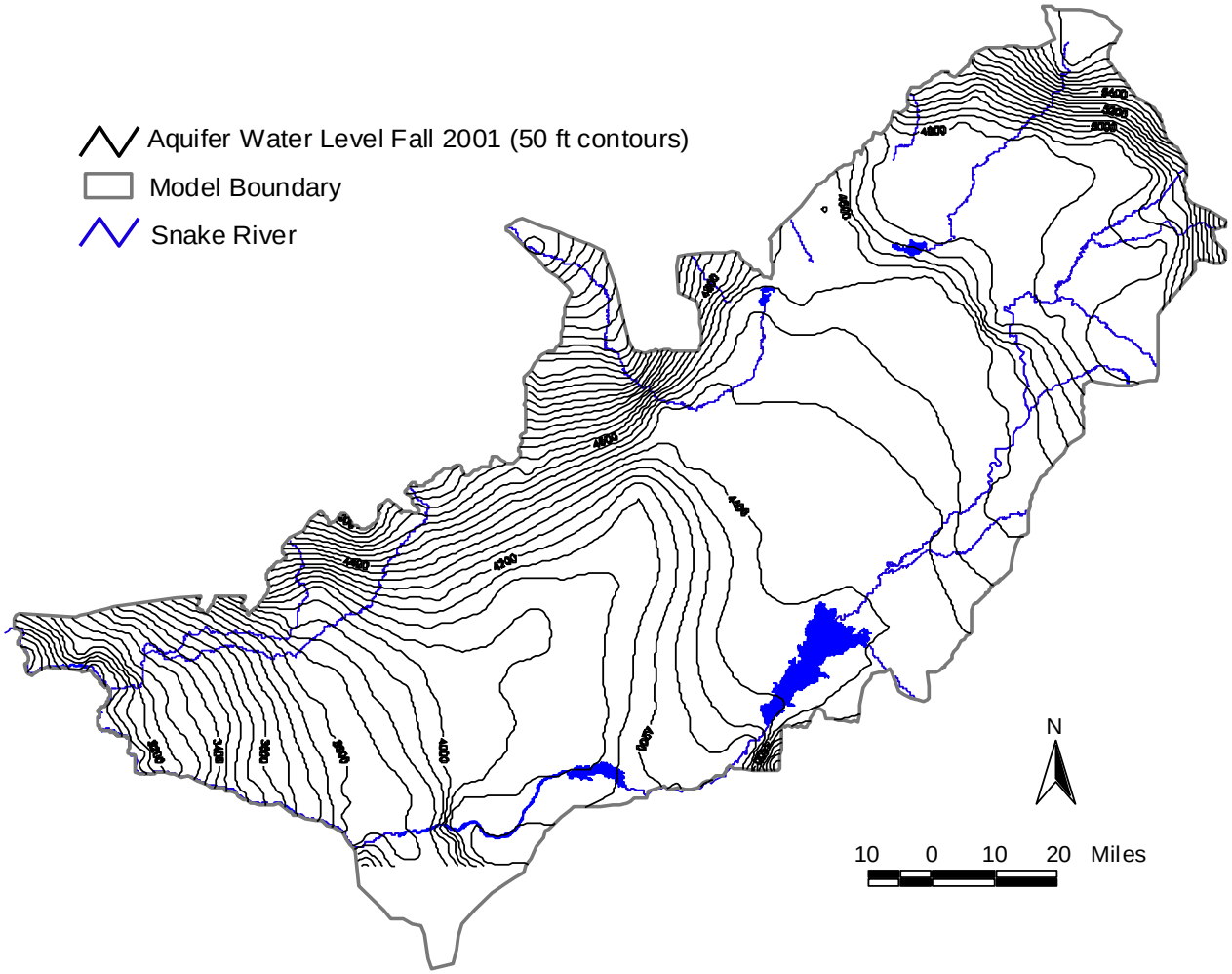

Figure 6. Contours of the Fall 2001 potentiometric surface of the eastern Snake Plain aquifer.

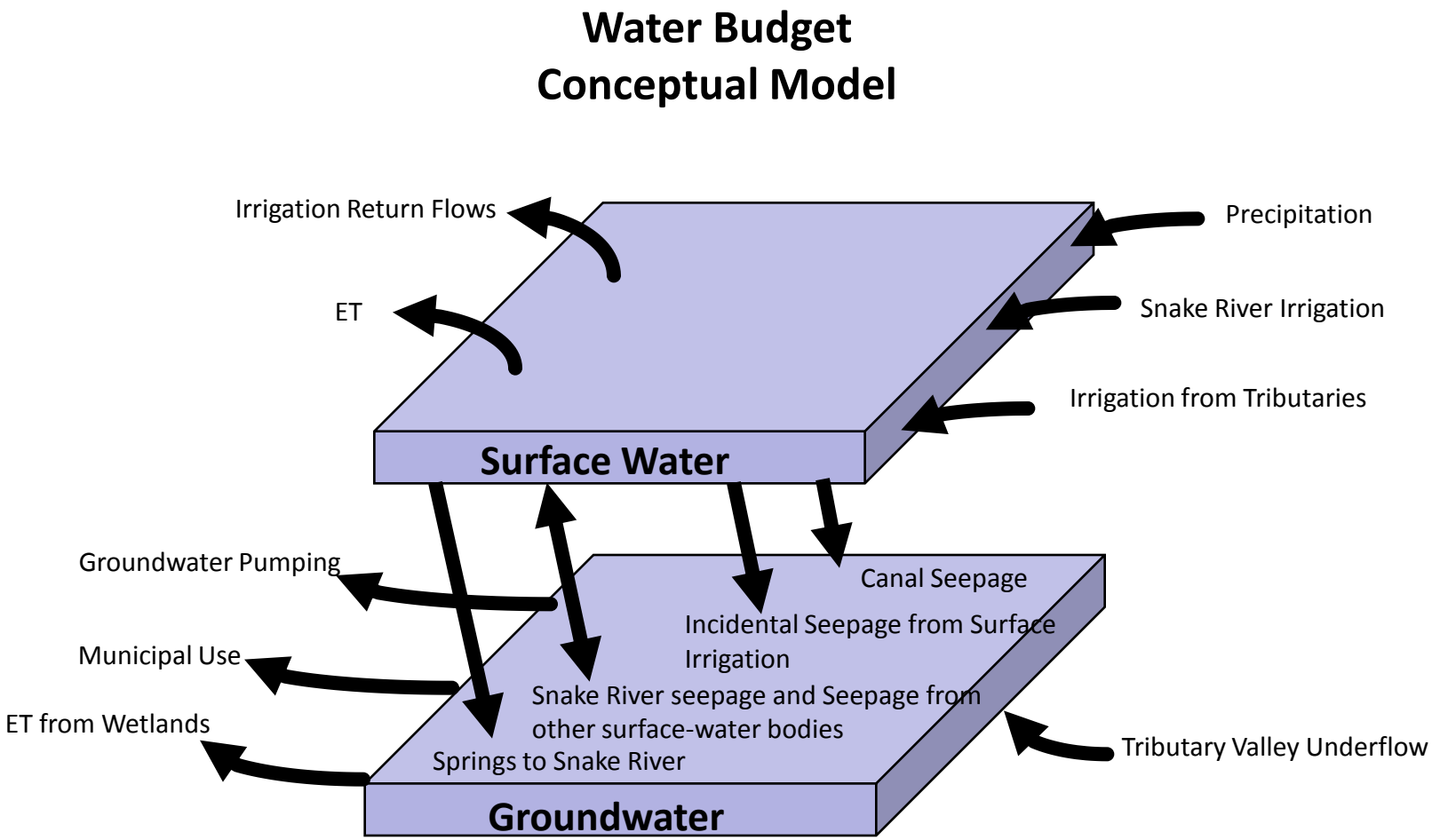

Figure 7. Conceptual water budget for the eastern Snake Plain aquifer. Adapted from ESPAM1.1 report.

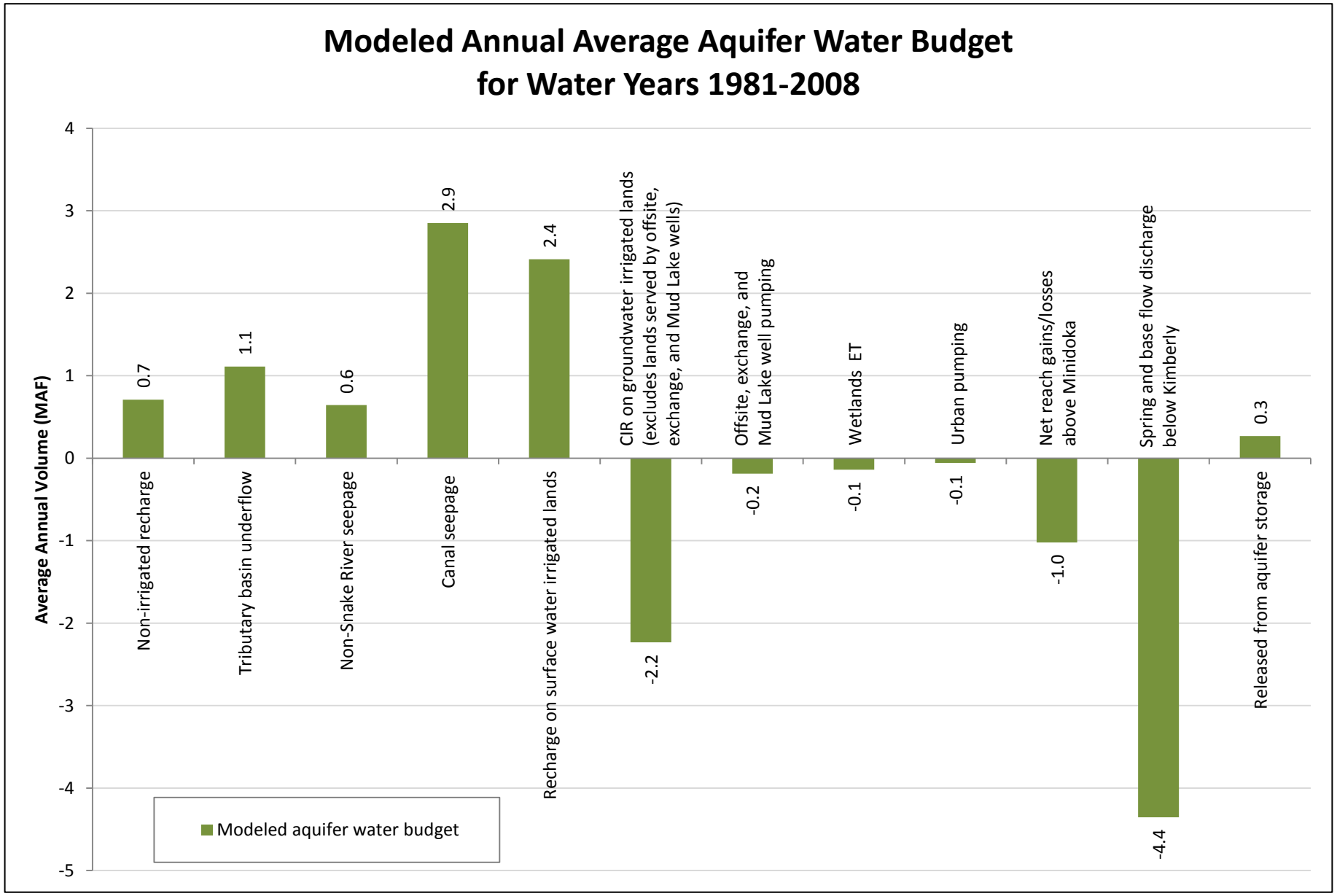

Figure 8. Enhanced Snake Plain Aquifer Model 2.1 average annual aquifer water budget. Positive values of aquifer storage represent water released from storage into the aquifer flow system. Negative values of aquifer storage represent water placed into storage.

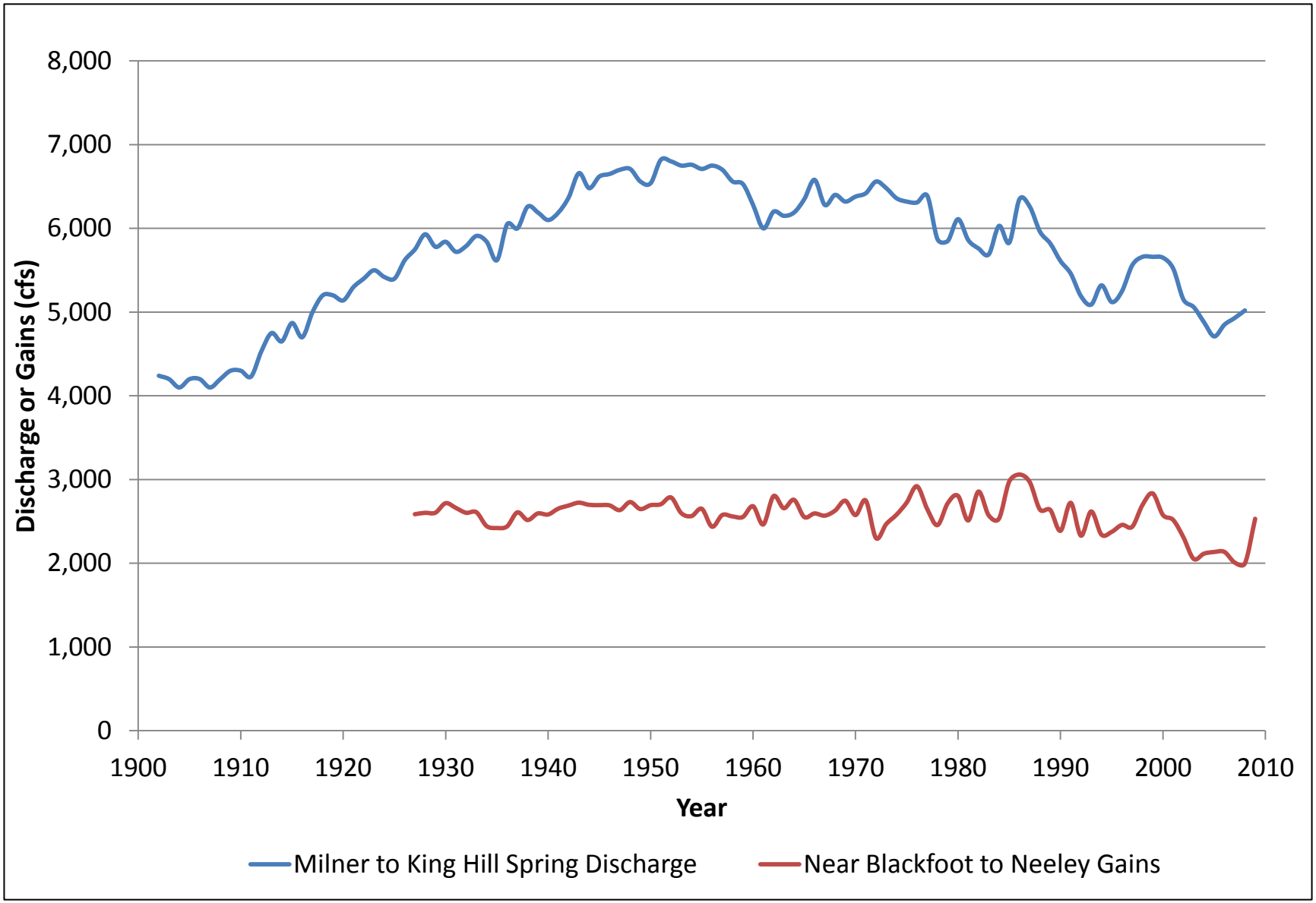

Figure 9. Average annual spring discharge for Milner-to-King Hill and near Blackfoot-to-Neeley river gains (from IDWR data).

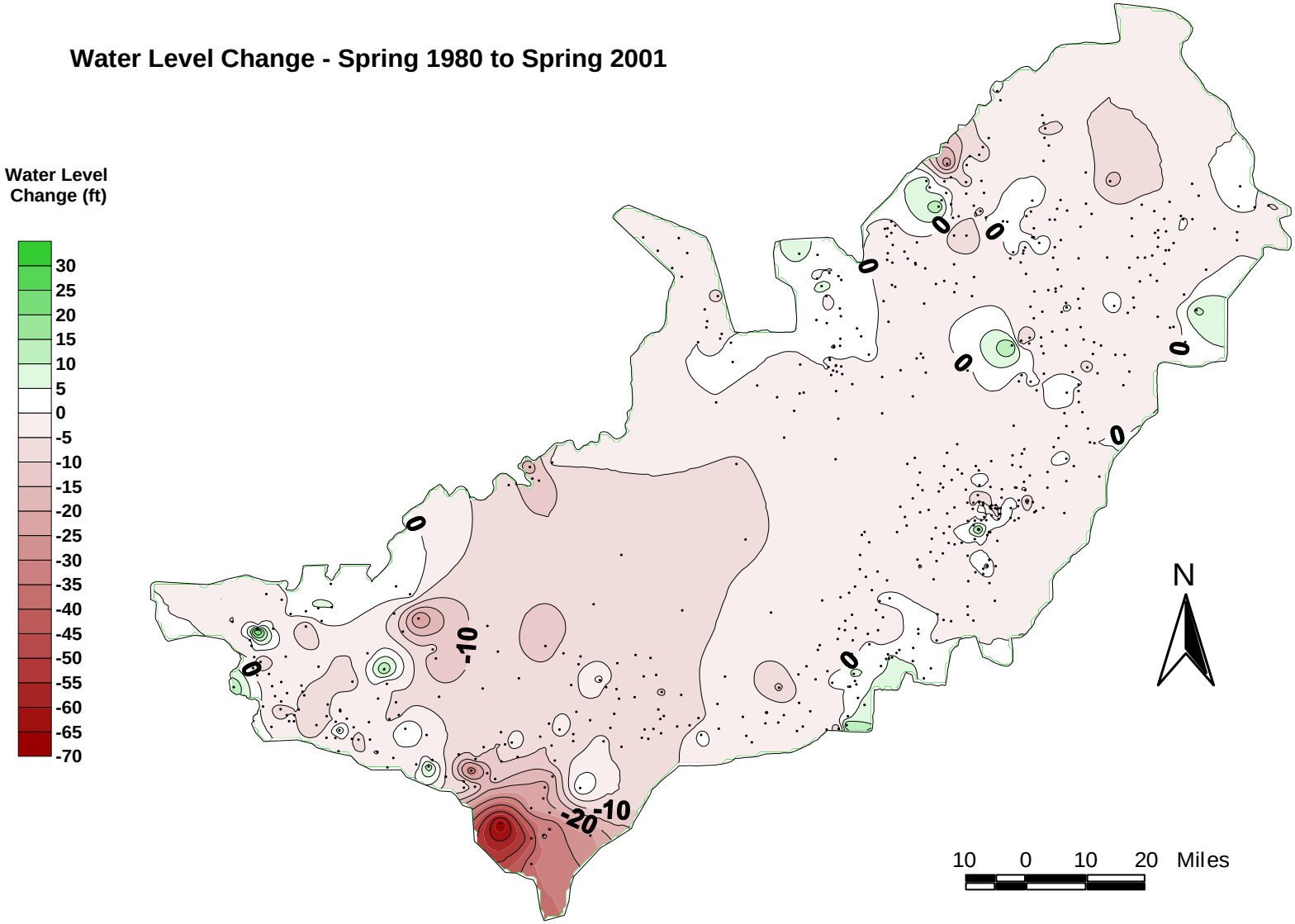

Figure 10. Water level change map, Spring 1980 – Spring 2001.

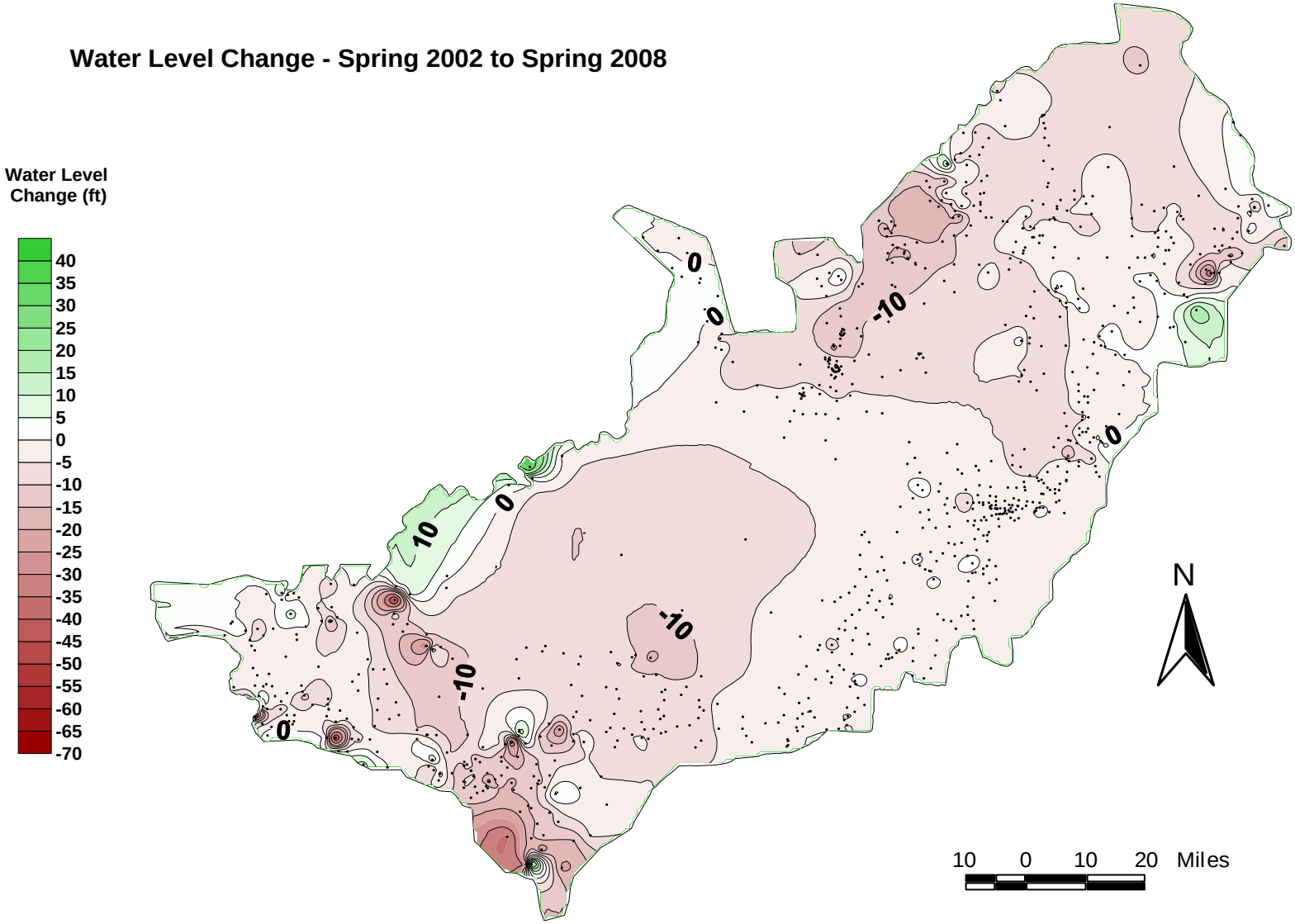

Figure 11. Water level change map, Spring 2002 – Spring 2008.

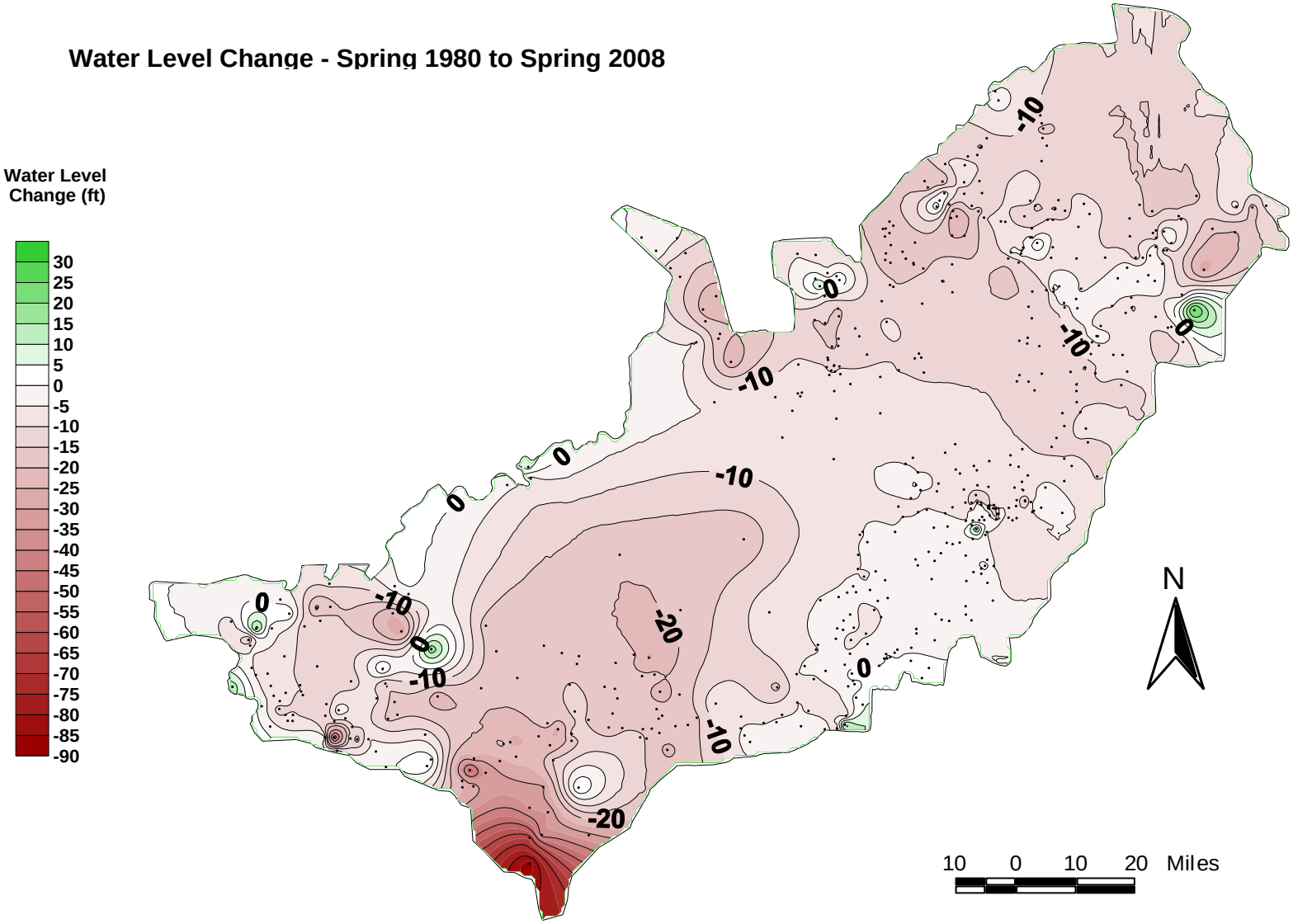

Figure 12. Water level change map, Spring 1980 - Spring 2008.

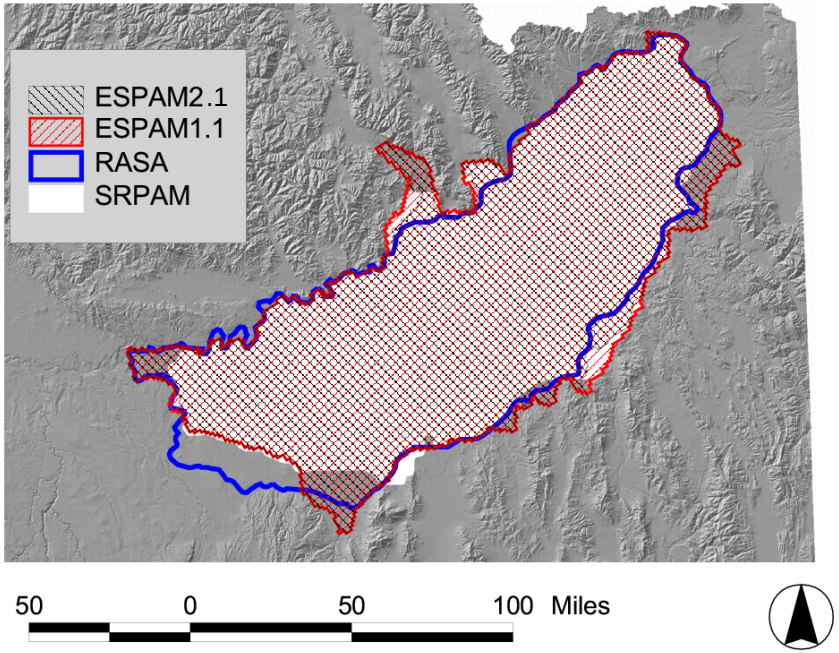

Figure 13a. Comparison of model boundaries.

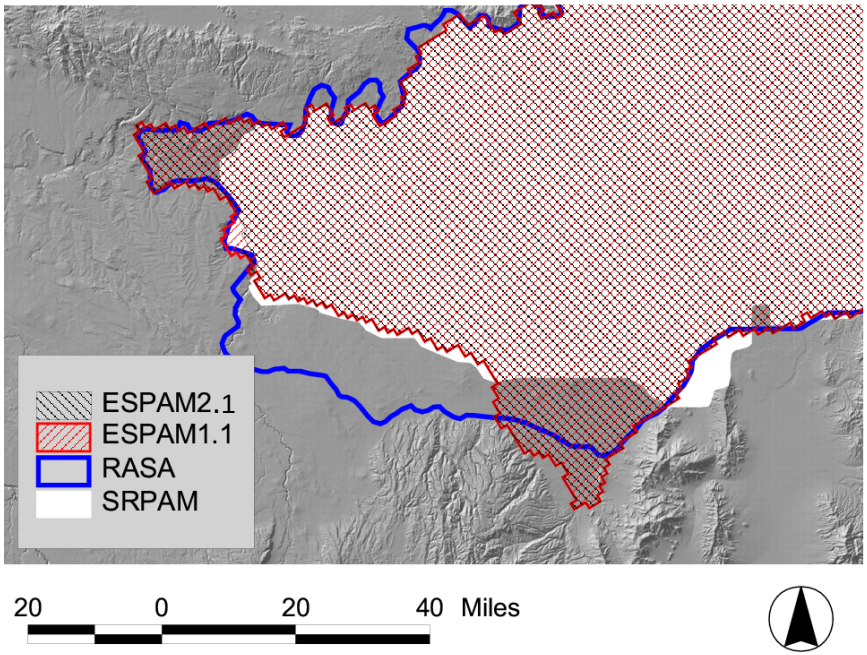

Figure 13b. Close-up of the southwestern area of Figure 15a.

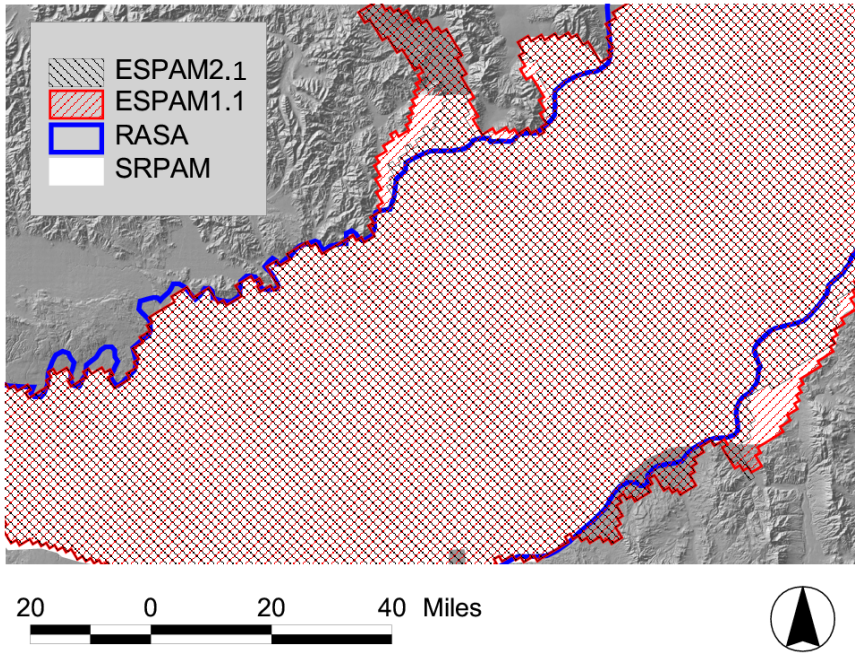

Figure 13c. Close-up of the central area of Figure 15a.

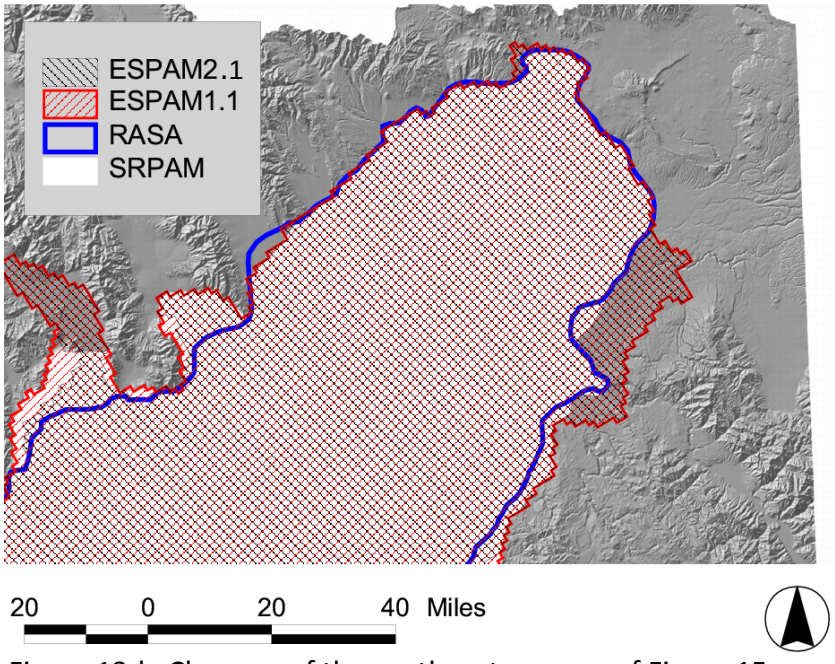

Figure 13d. Close-up of the northeastern area of Figure 15a.

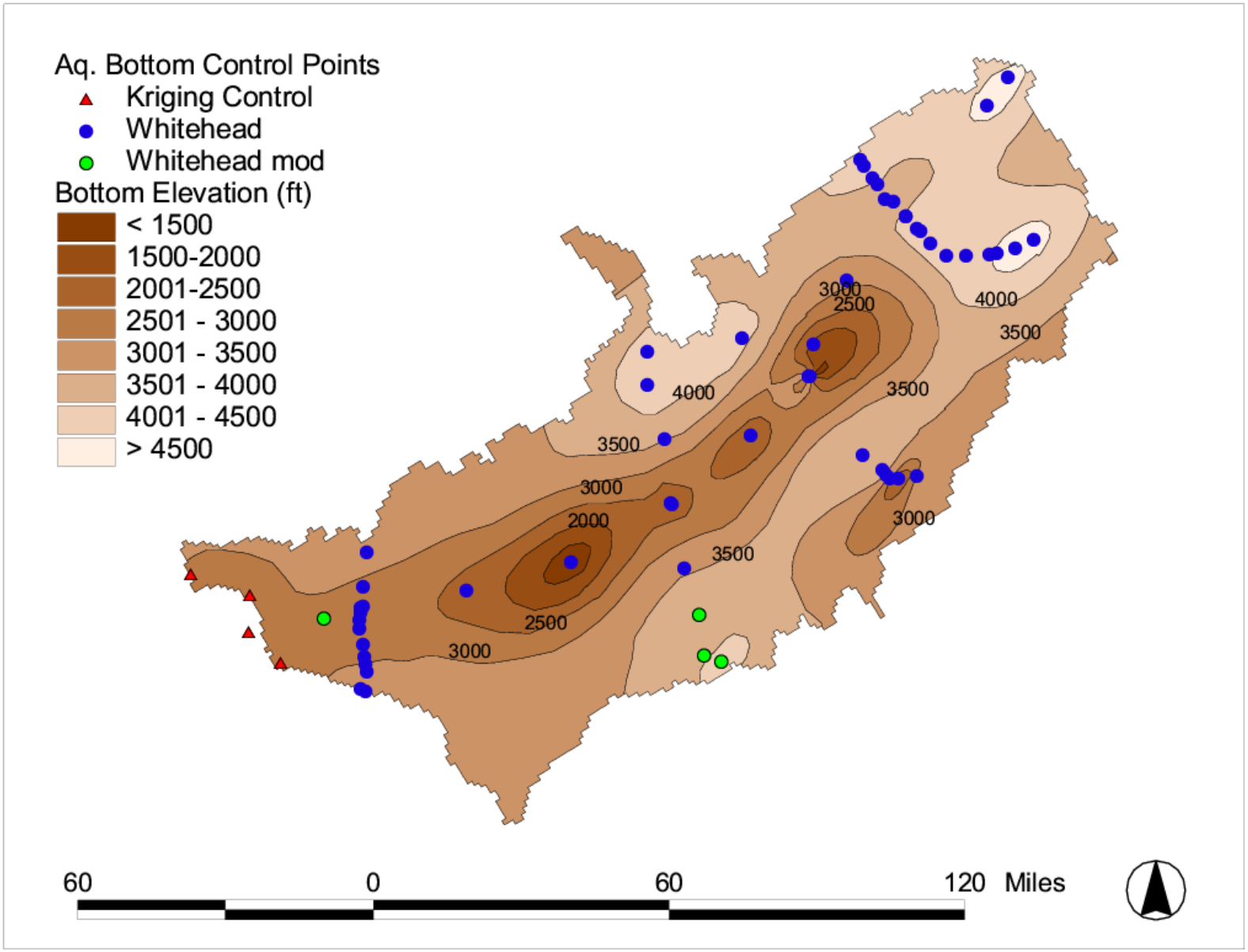

Figure 14. Aquifer bottom elevations with estimated elevation points. Based on modified Whitehead (1986) data. Blue dots represent locations used by Whitehead, green dots represent modified Whitehead data points, and red triangles represent points added to anchor the Kriged surface.

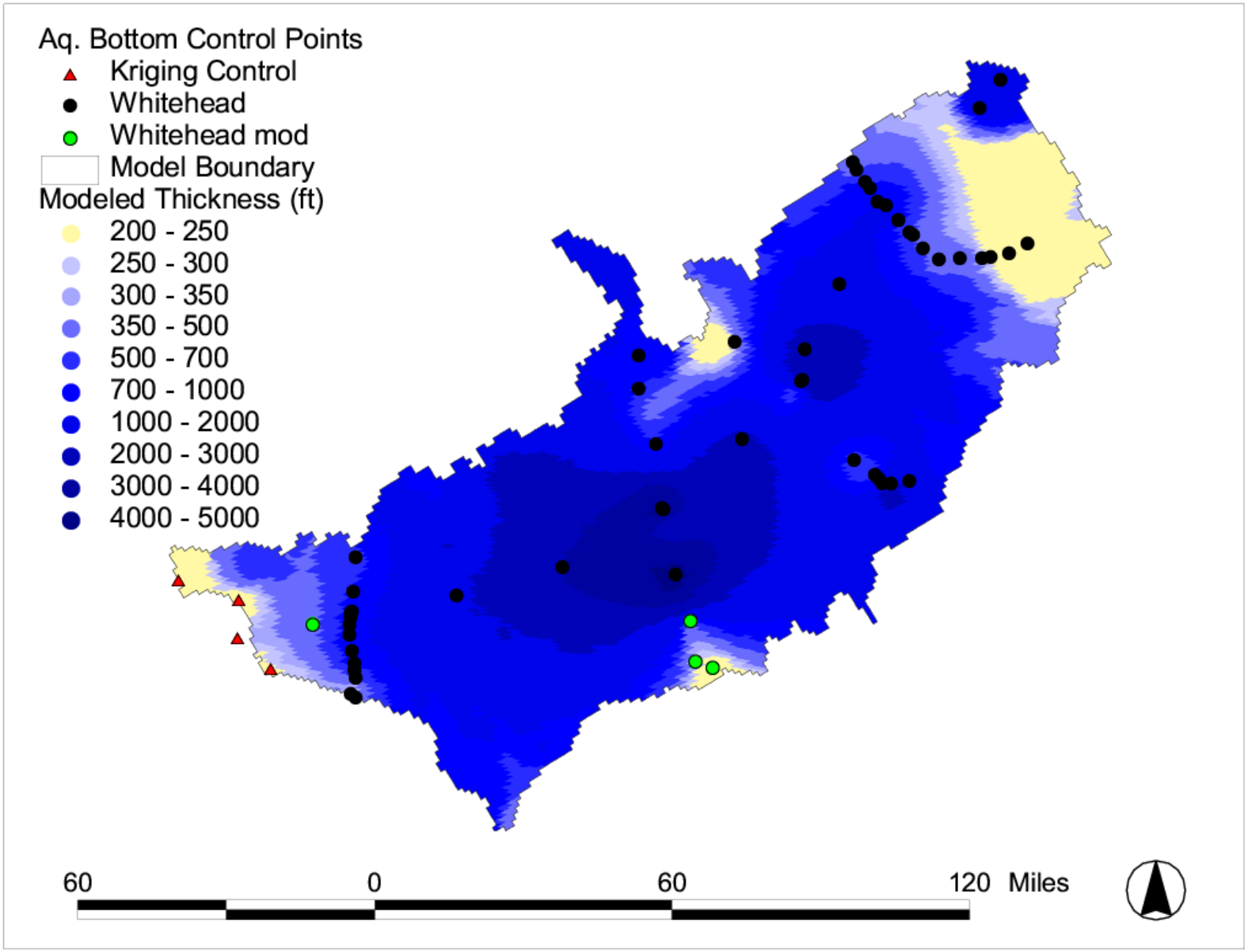

Figure 15. Delineation of aquifer thickness.

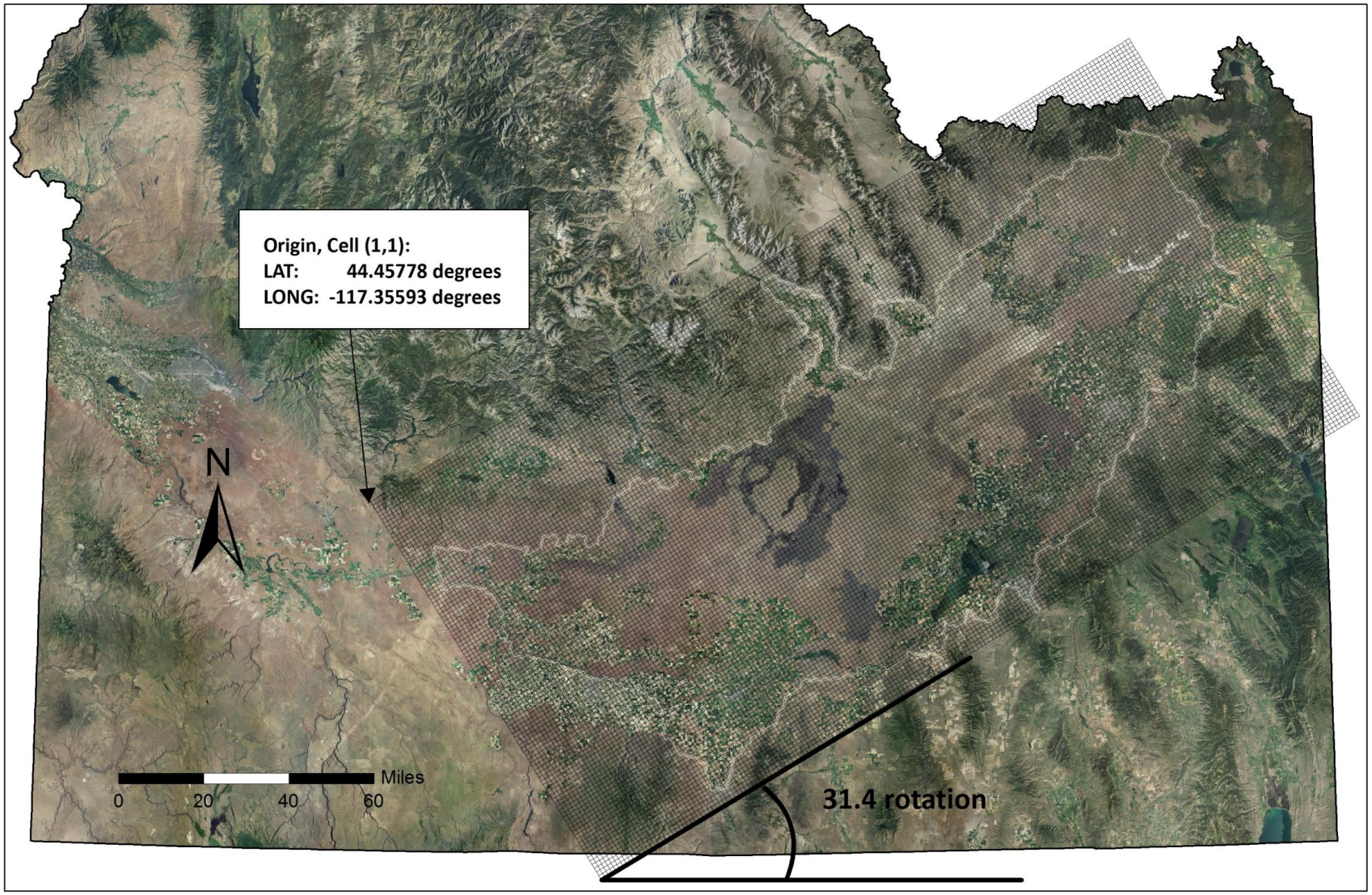

Figure16. Model grid and origin.

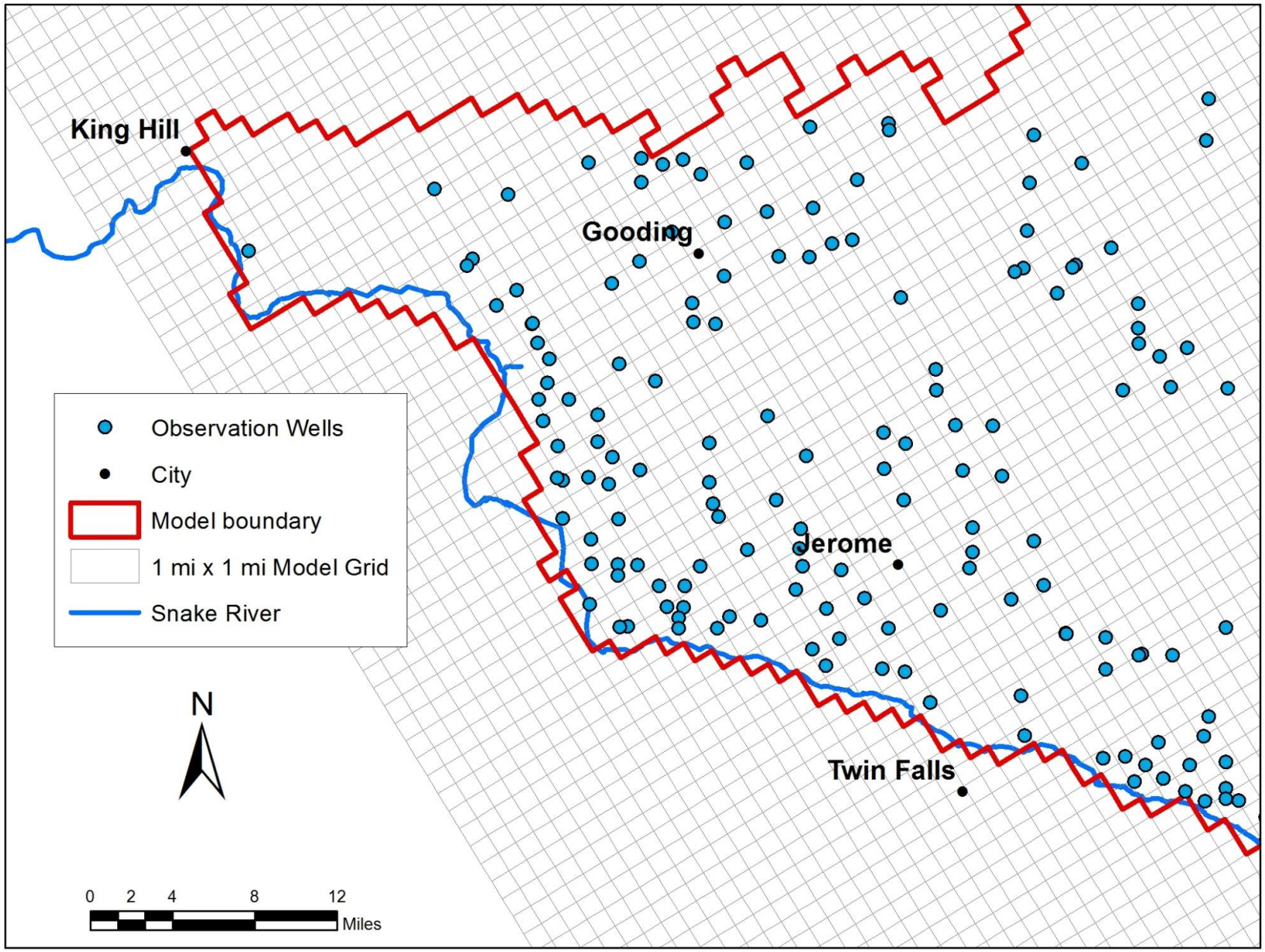

Figure 17. Close-up of model grid in the Thousand Springs area.

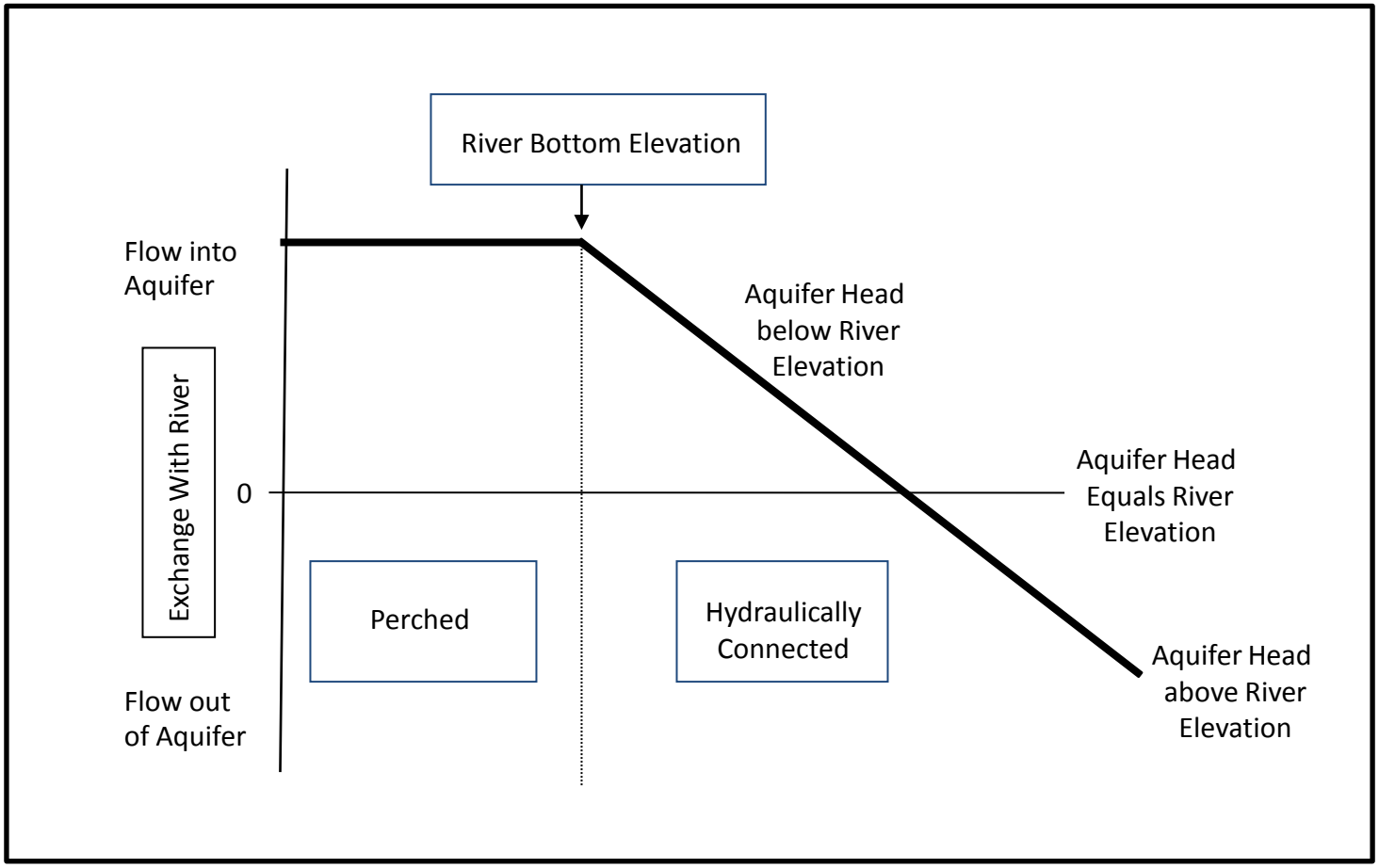

Figure 18. Conceptual illustration of river leakage computation in MODFLOW (after McDonald and Harbaugh, 1988).

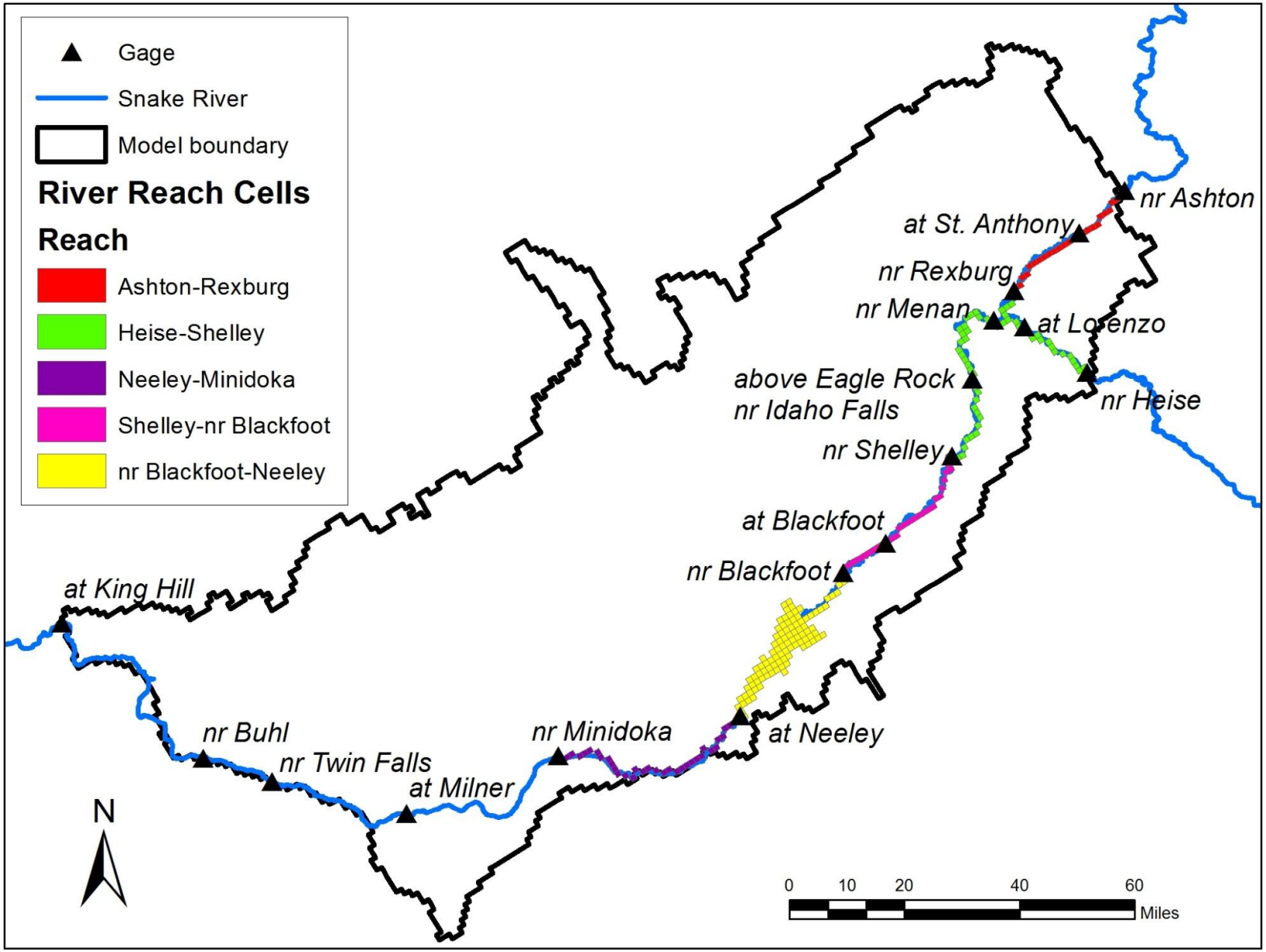

Figure 19. Head-dependent river reaches.

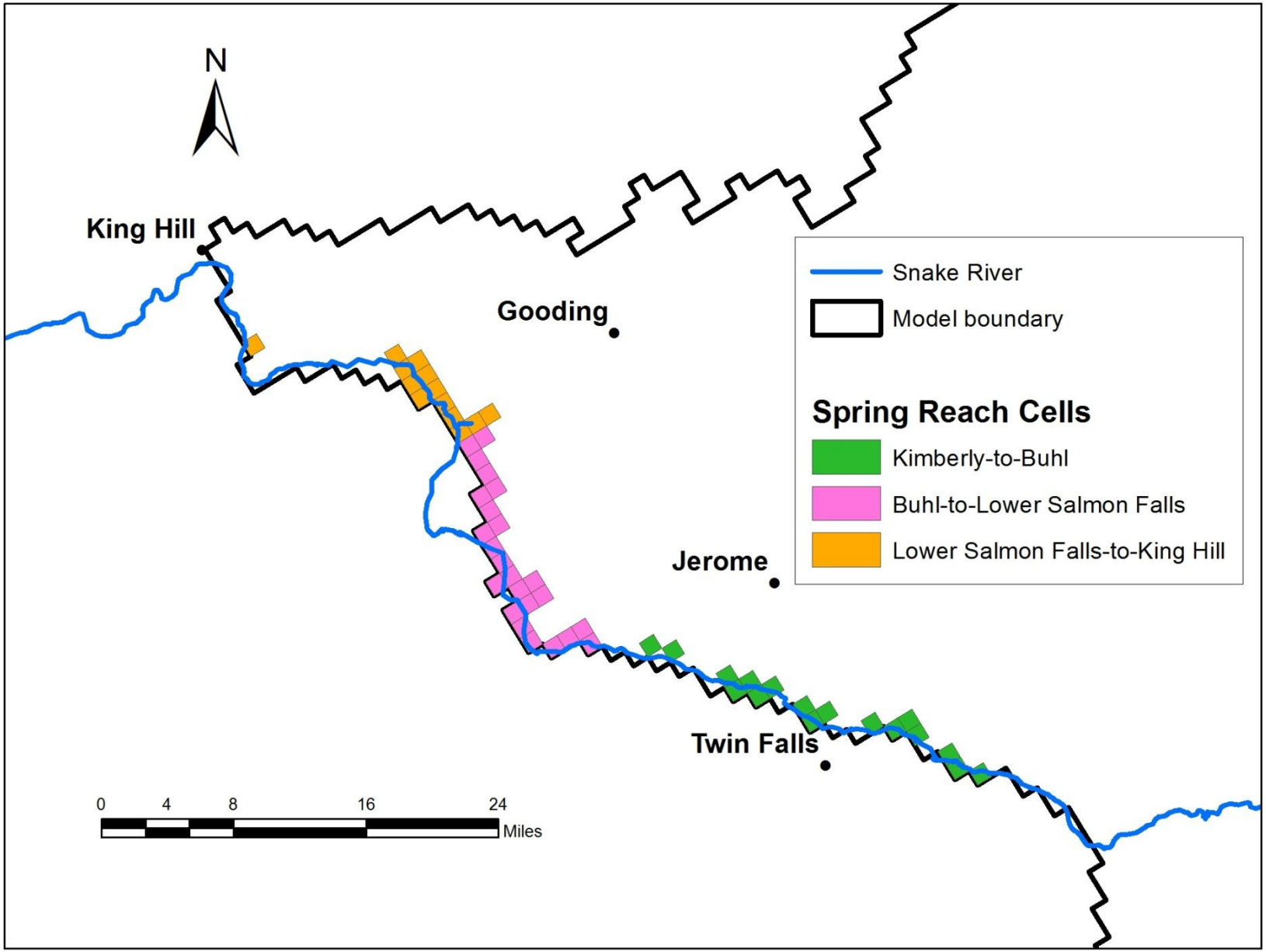

Figure 20. Head-dependent spring reaches.

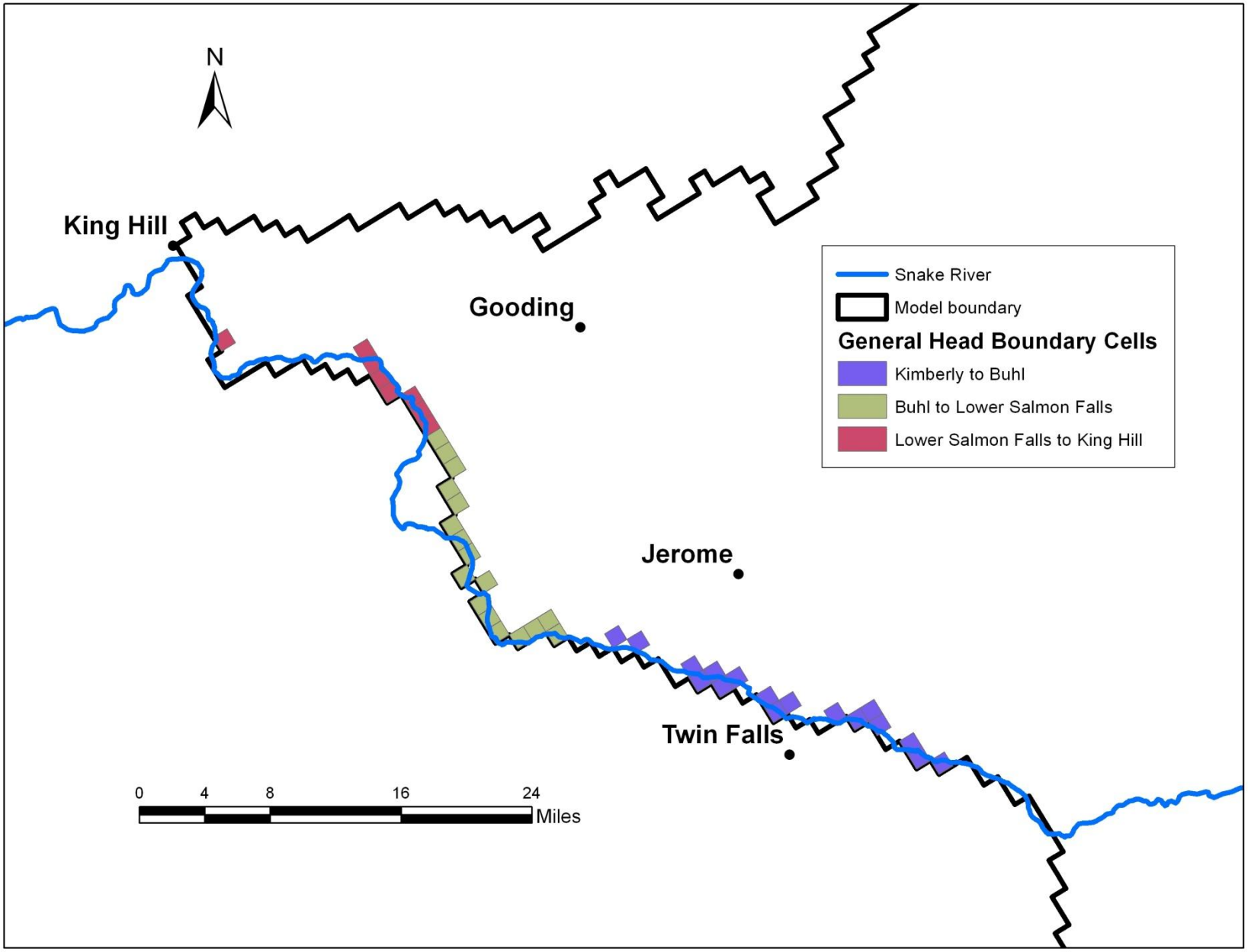

Figure 21. General head boundary cells.

Figure 22a – 22f. Irrigated lands for the years 1980, 1986, 1992, 2000, 2002, and 2006.
See 11x17 Figures.

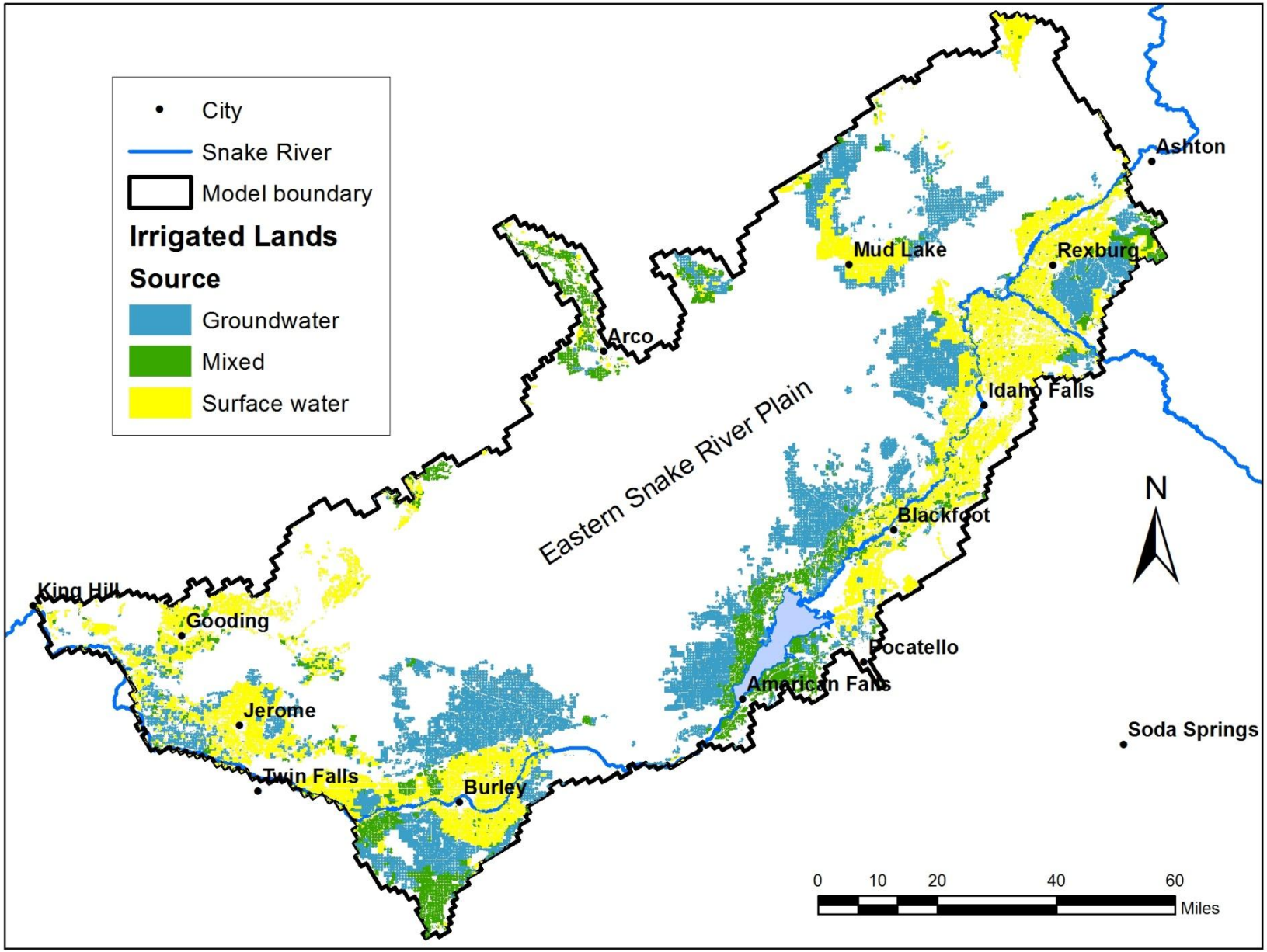

Figure 23. Irrigation water source determined from adjudication data. Water source was adjusted in Mud Lake and Monteview area to account for water delivery from offsite irrigation wells.

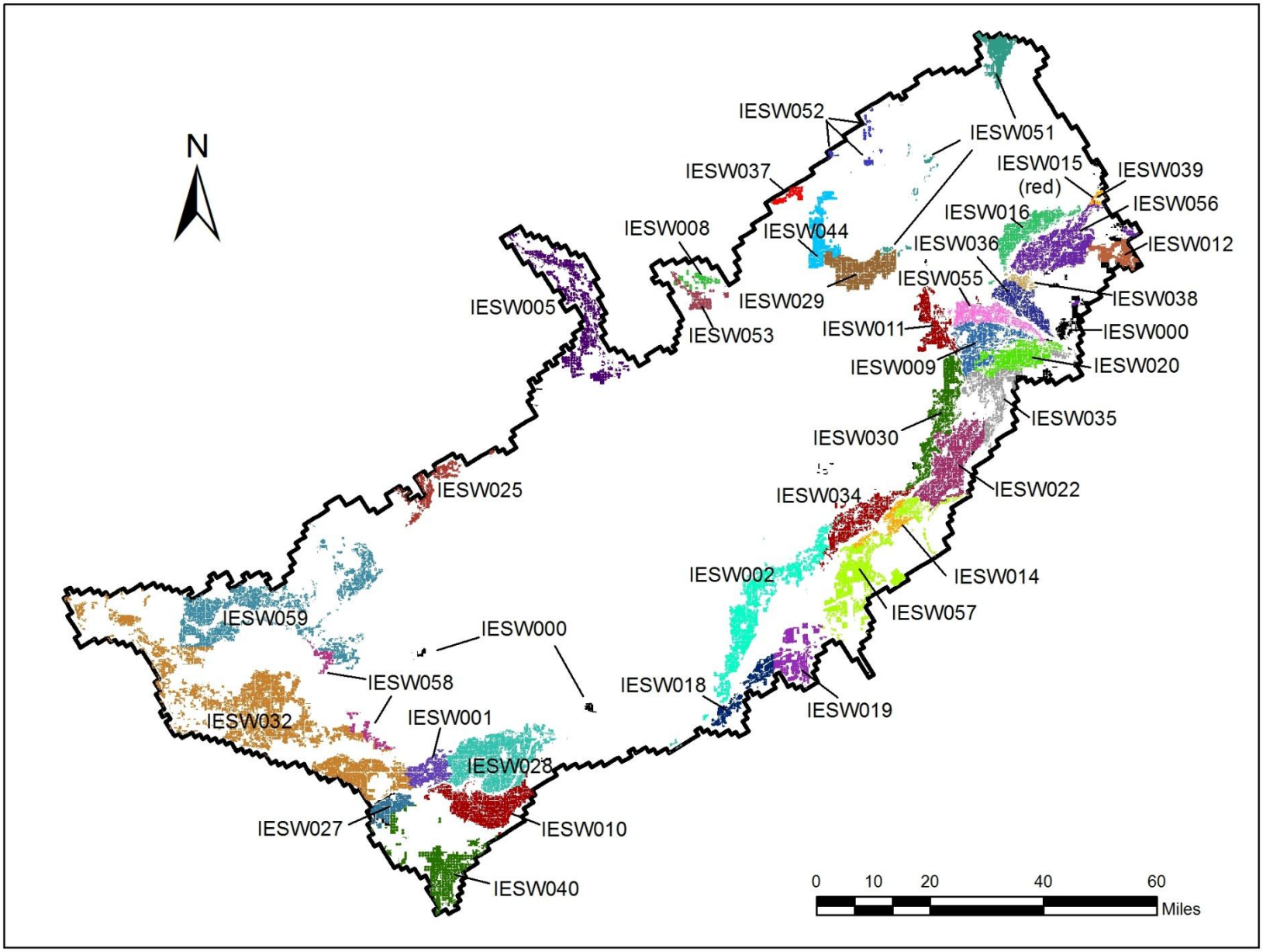

Figure 24. Surface-water irrigation entities.

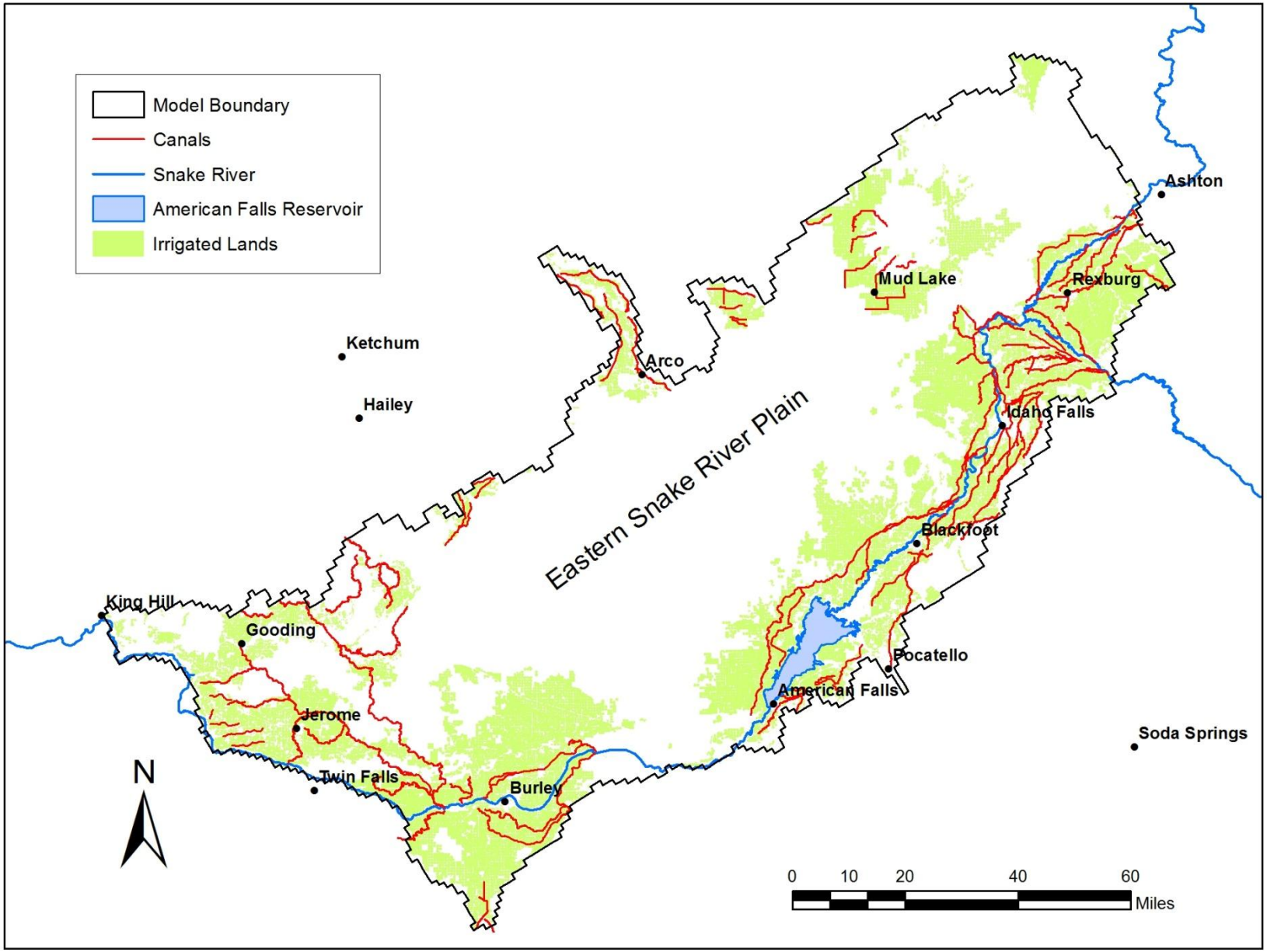

Figure 25. Locations of canals where leakage is simulated in the model.

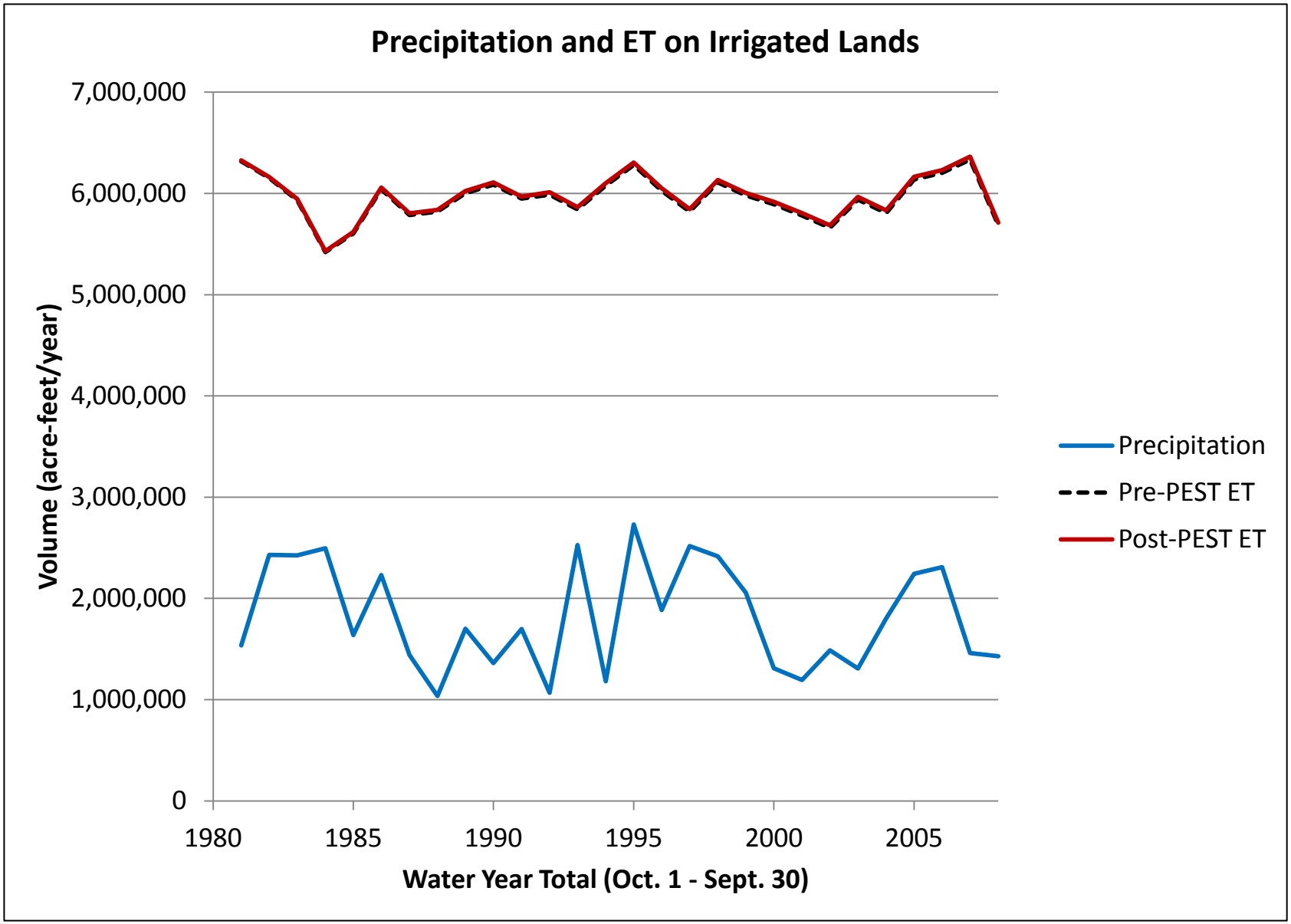

Figure 26. Precipitation and evapotranspiration (ET) for irrigated lands for water years 1981-2008.

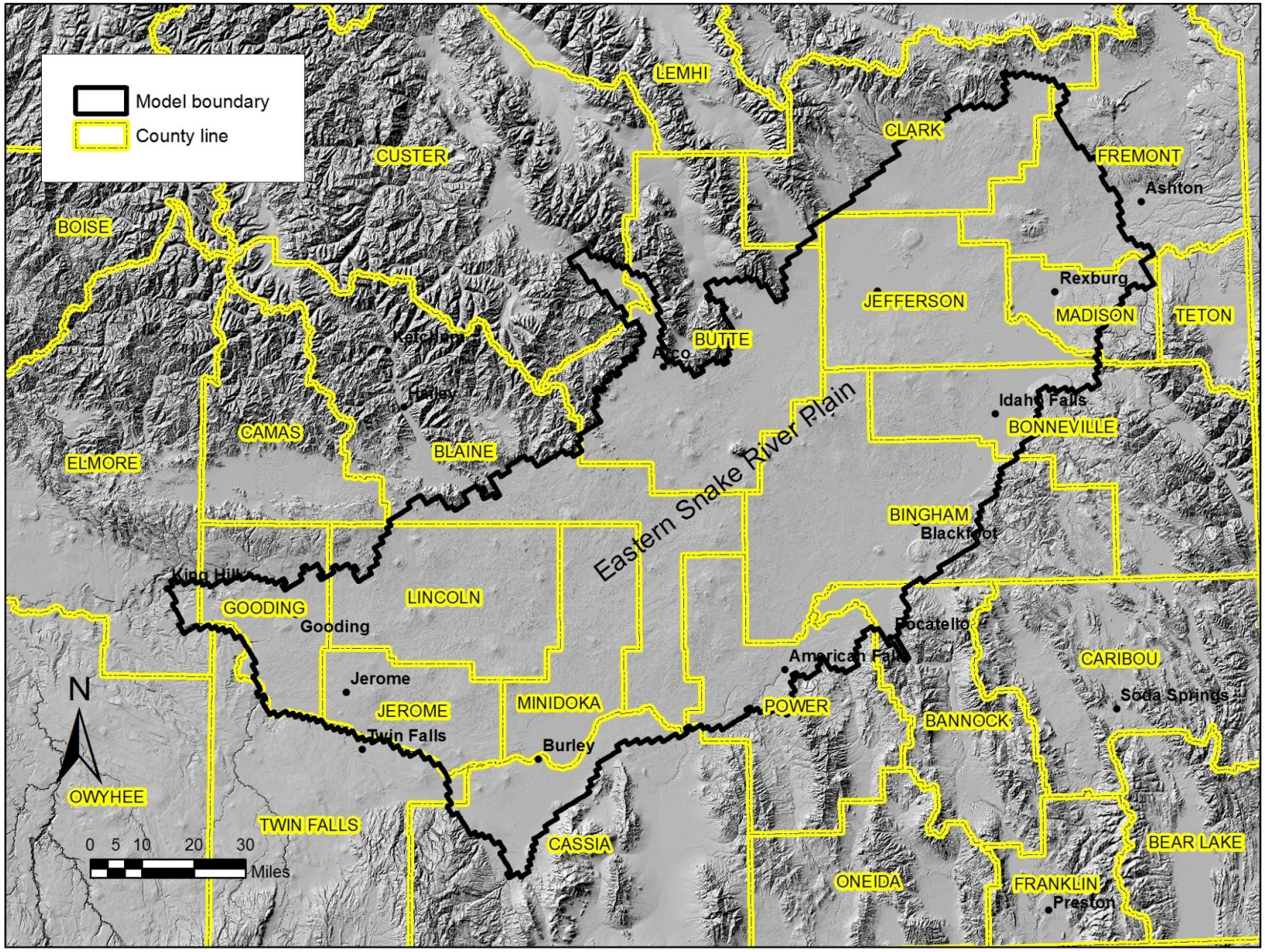

Figure 27. Idaho counties in the study area.

DRAFT

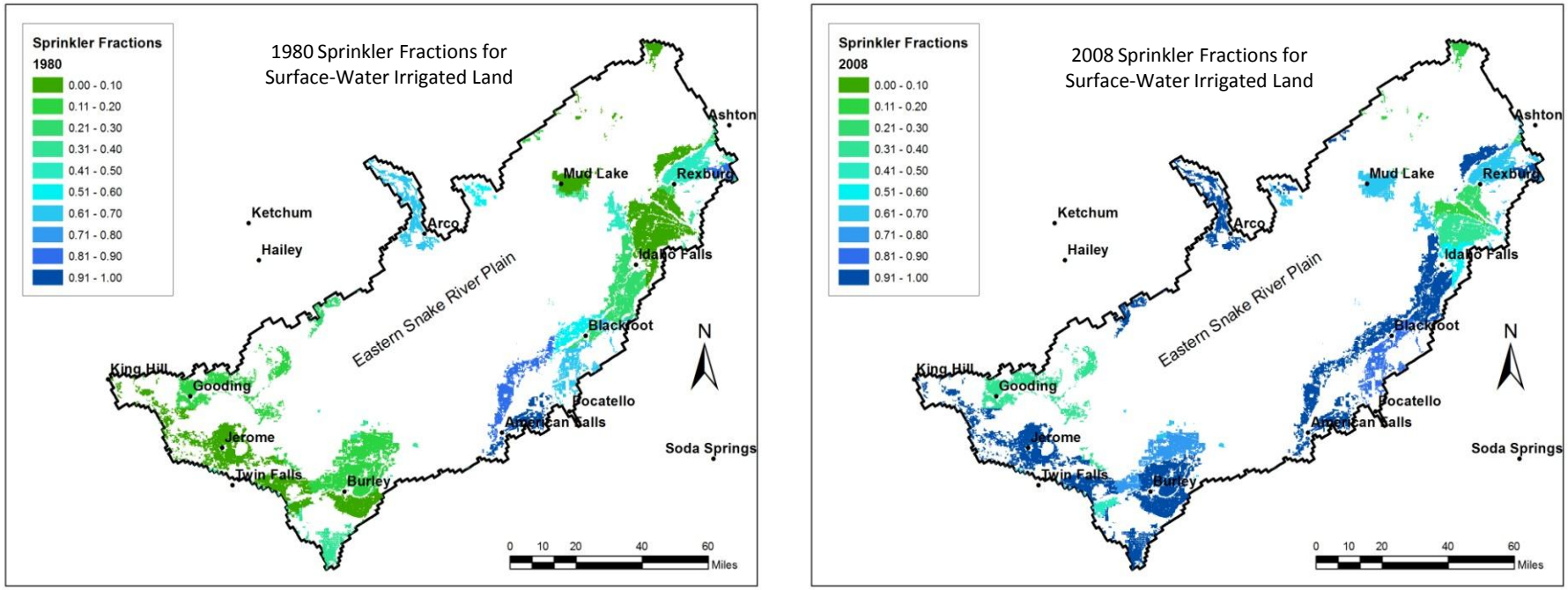

Figure 28. Sprinkler fraction by surface-water entity, 1980 and 2008.

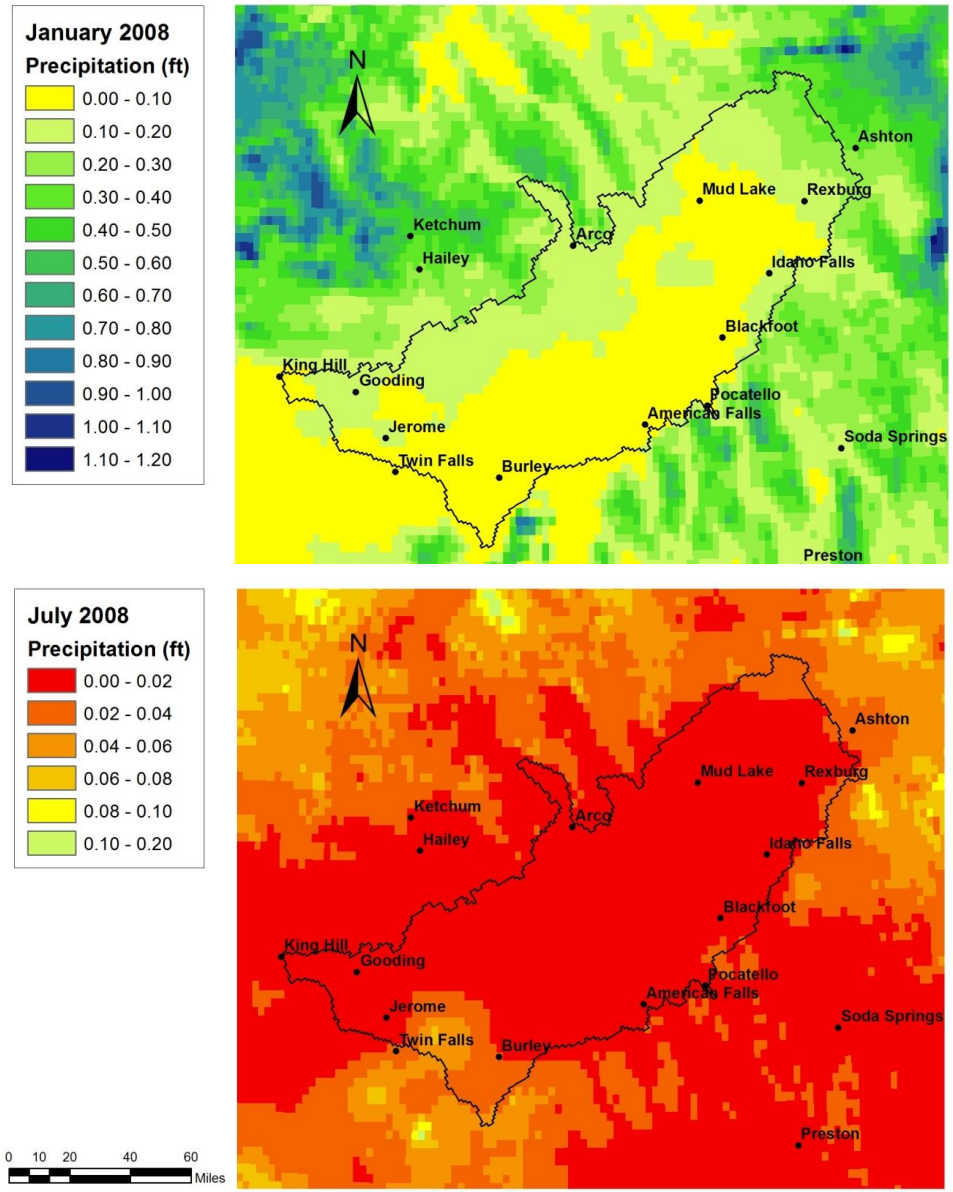

Figure 29. PRISM precipitation maps for one month in the non-irrigation season (January 2008 - top) and the irrigation season (July 2008 - bottom).

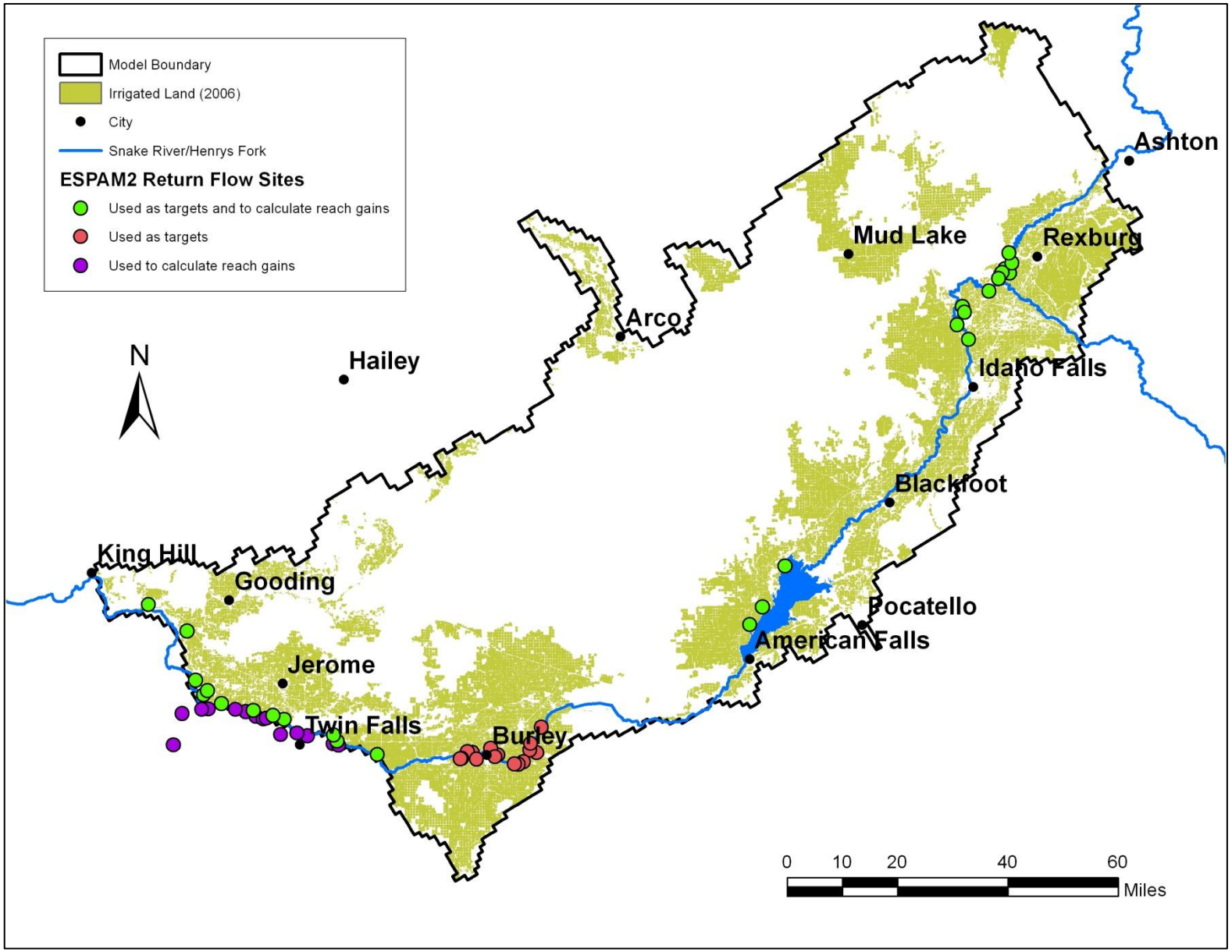

Figure 30. Return-flow measurement locations.

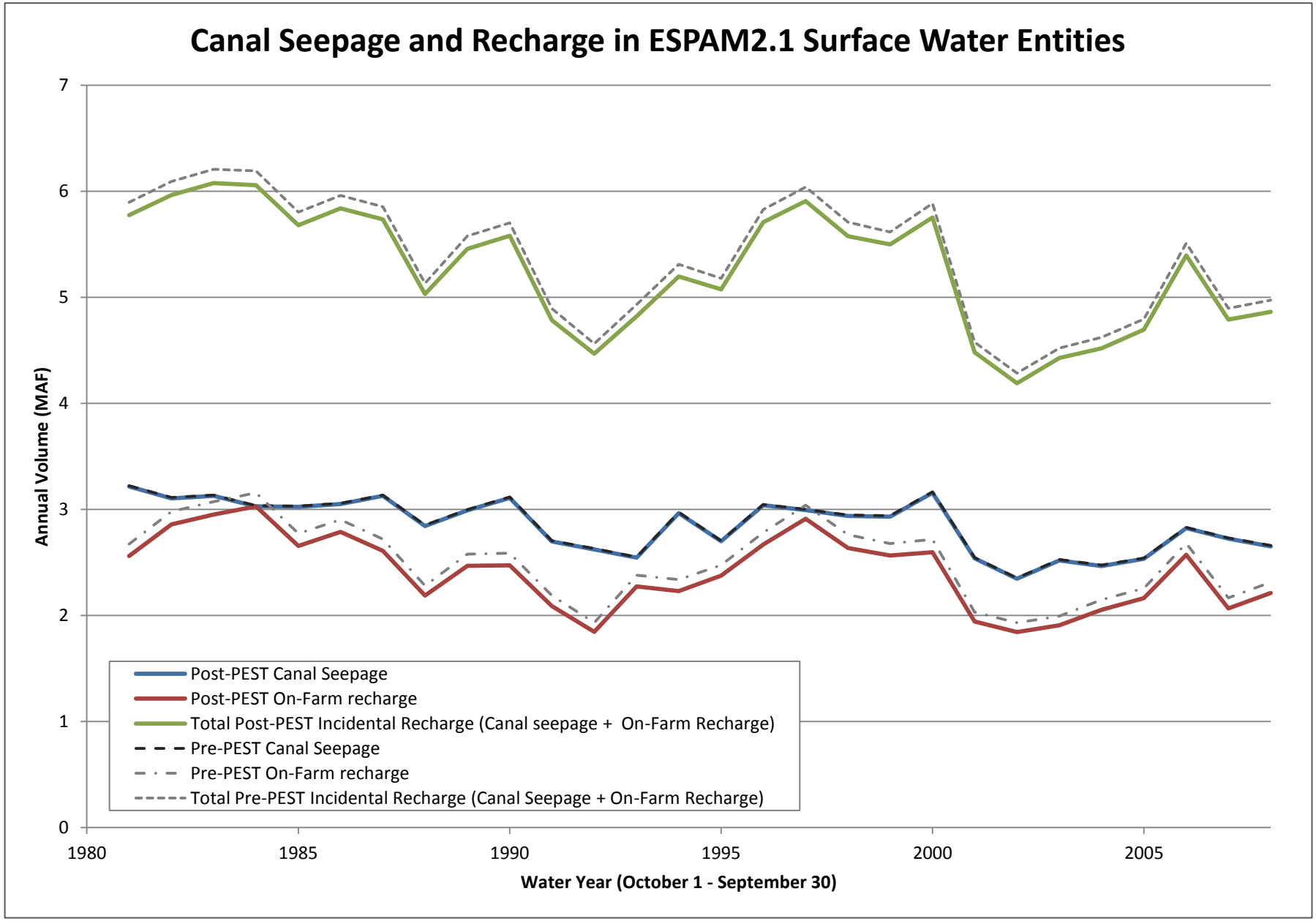

Figure 31. Annual volume of canal seepage and recharge incidental to irrigation in ESPAM2.1 surface water entities.

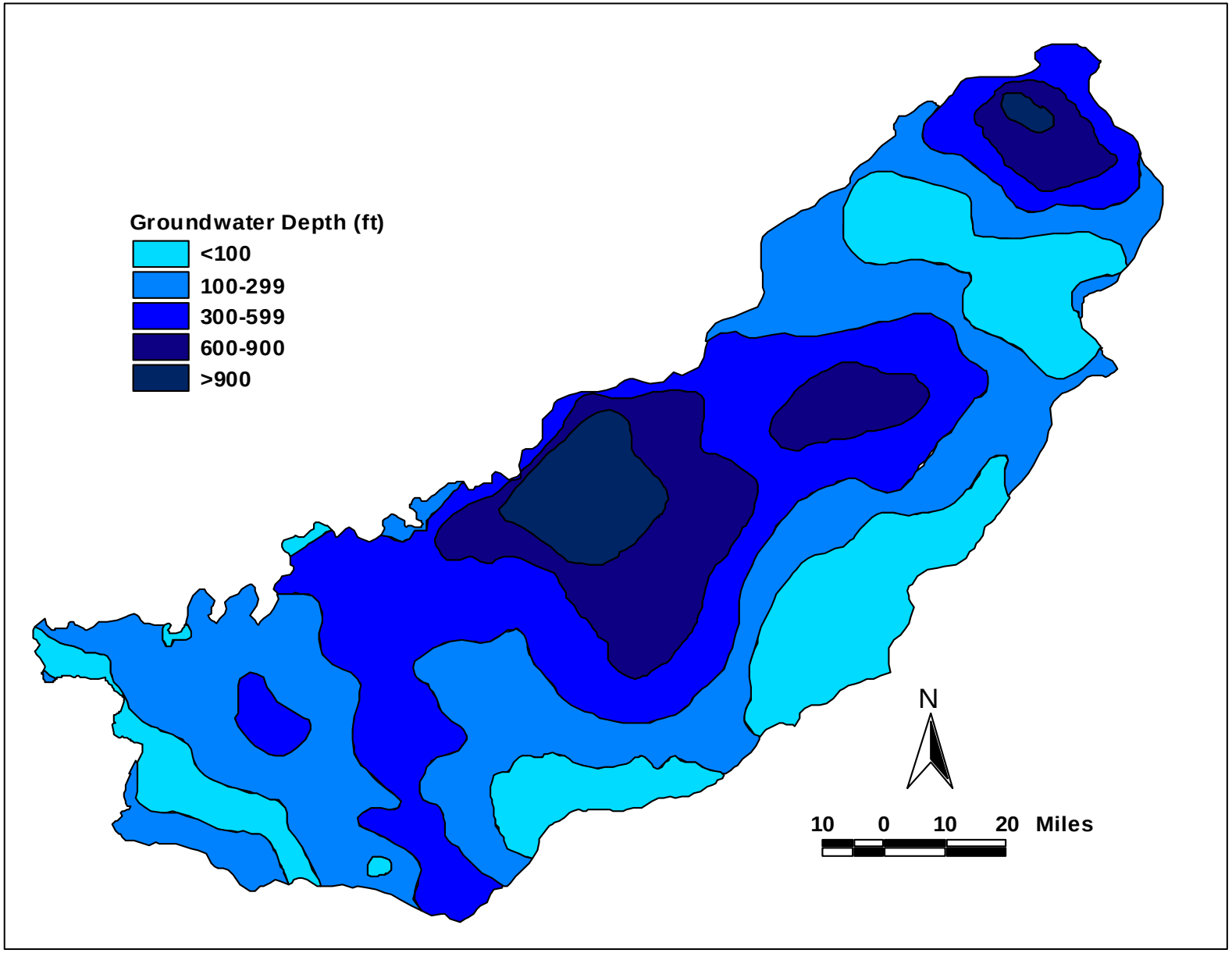

Figure 32. Depth to water in 1980 (digitized from Lindholm and others, 1988).

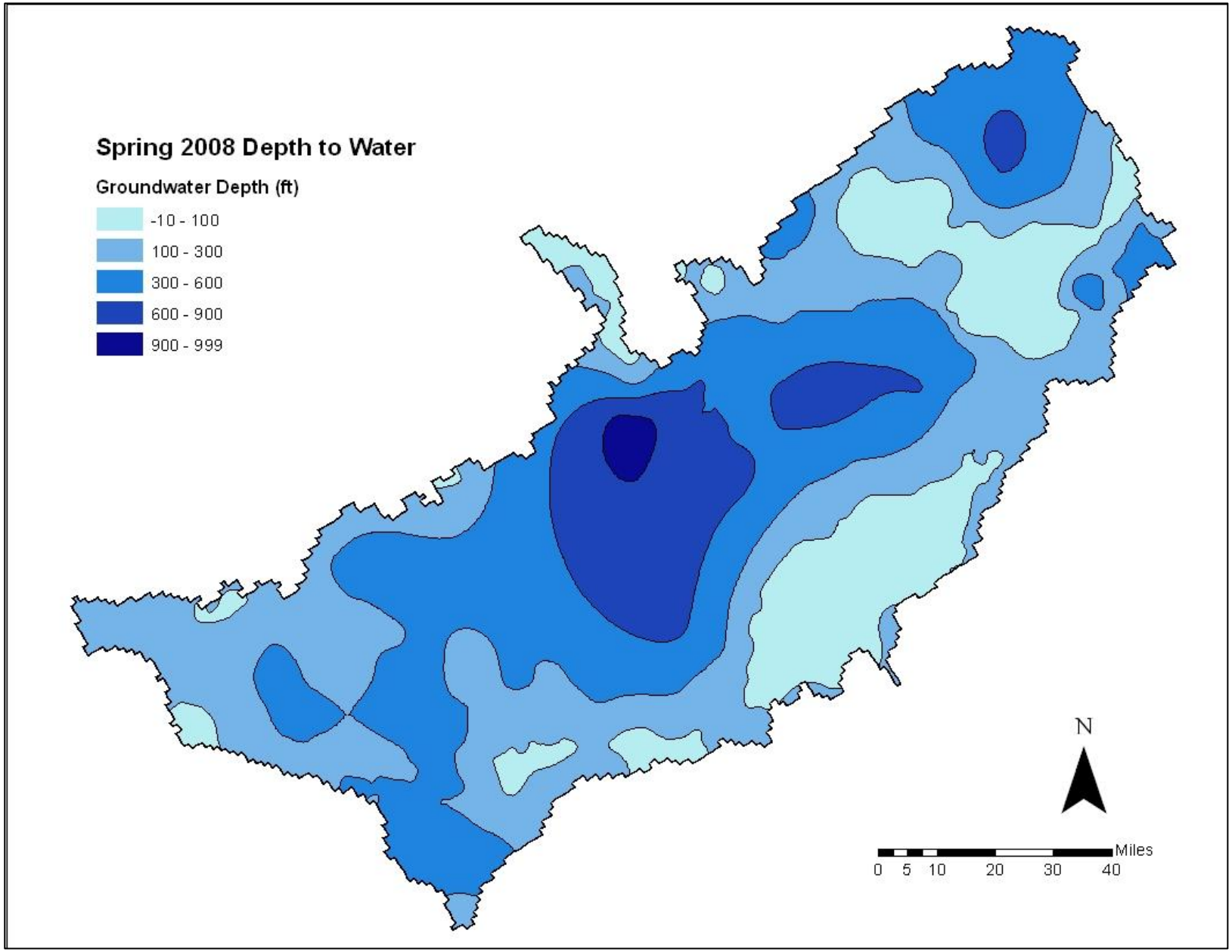

Figure 33. Depth to water based on Spring 2008 synoptic water levels.

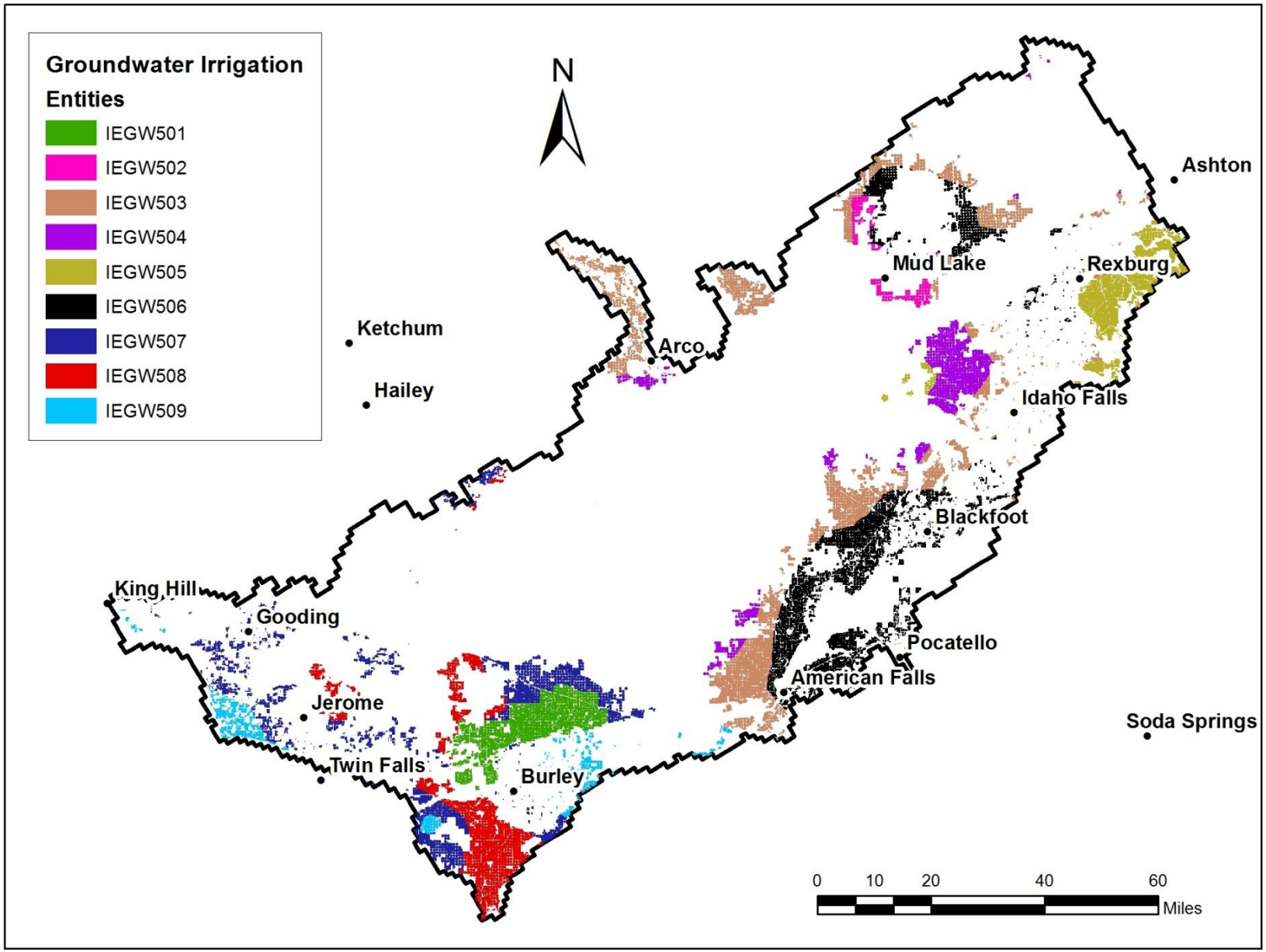

Figure 34. Groundwater irrigation polygons. The central portion of the plain absent of irrigation is represented as IEGW600 (not labeled in the figure).

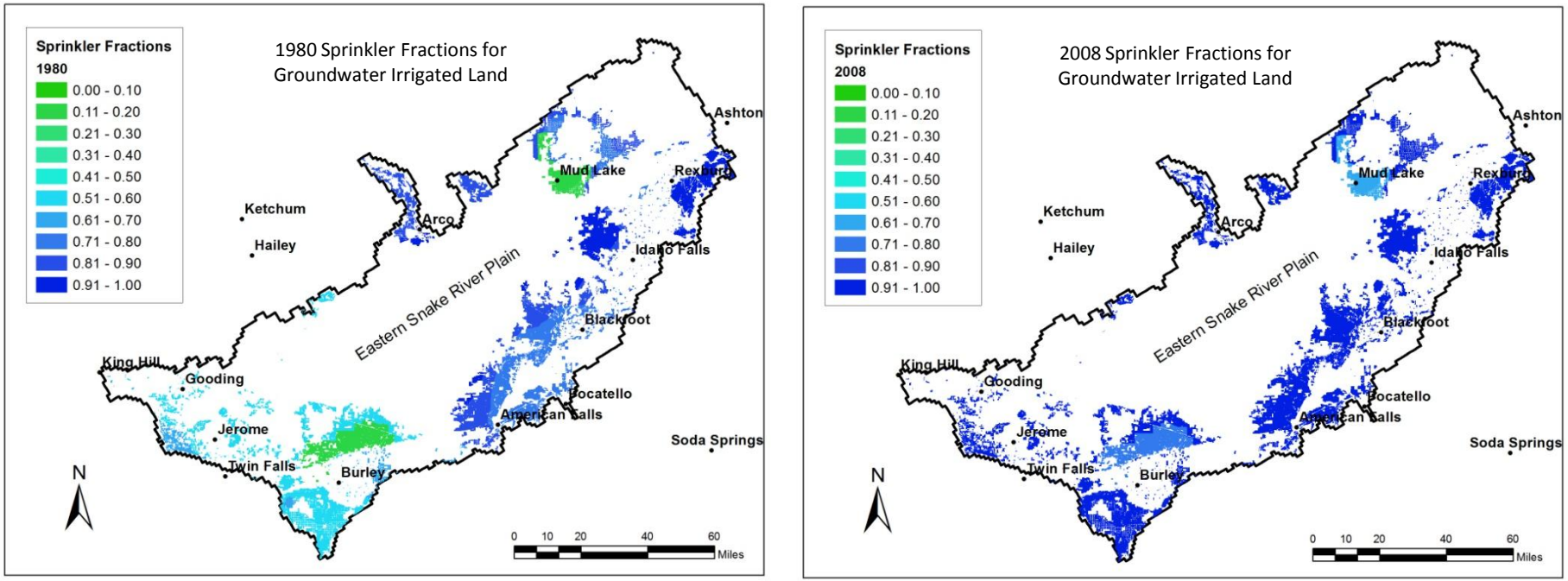

Figure 35. Sprinkler fraction by groundwater polygon, 1980 and 2008.

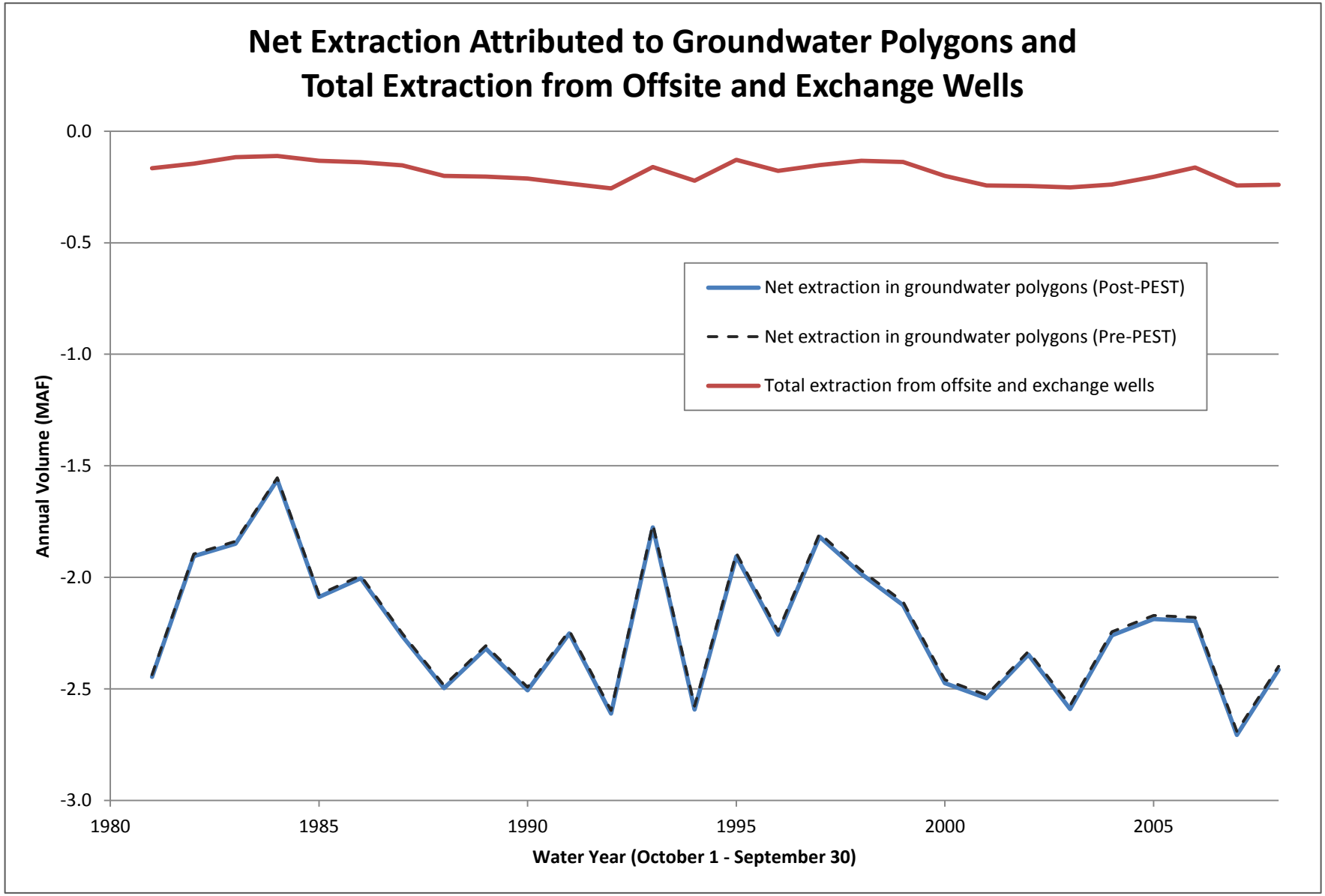

Figure 36. Net extraction in groundwater polygons and total extraction from offsite and exchange wells. Net extraction in groundwater polygons is equivalent to the crop irrigation requirement attributed to groundwater polygons. Total extraction from offsite and exchange wells includes water recharged via canal seepage and On-Farm recharge. Extraction from offsite and exchange wells is not adjusted during model calibration.

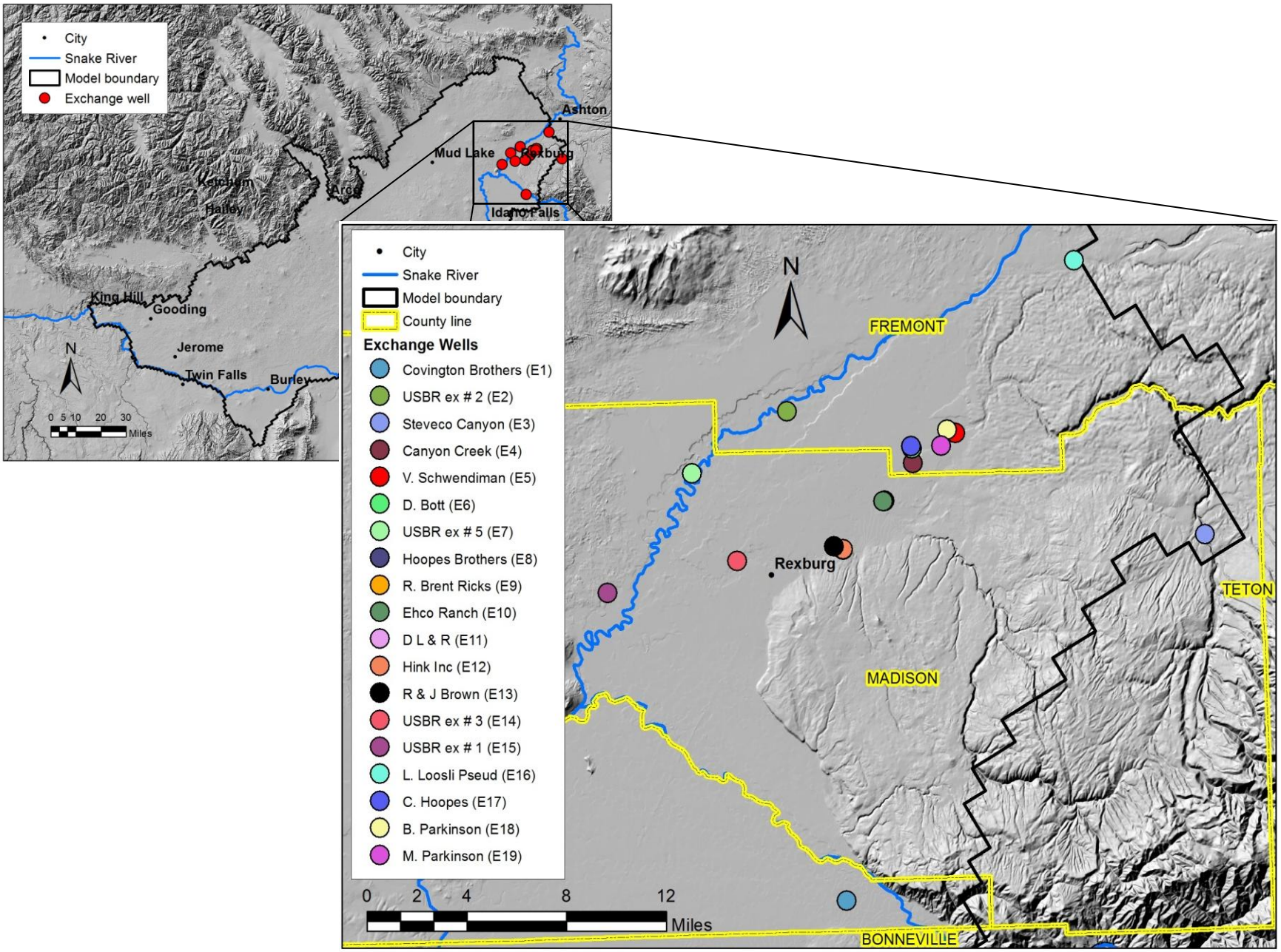

Figure 37. Teton and Snake River exchange wells.

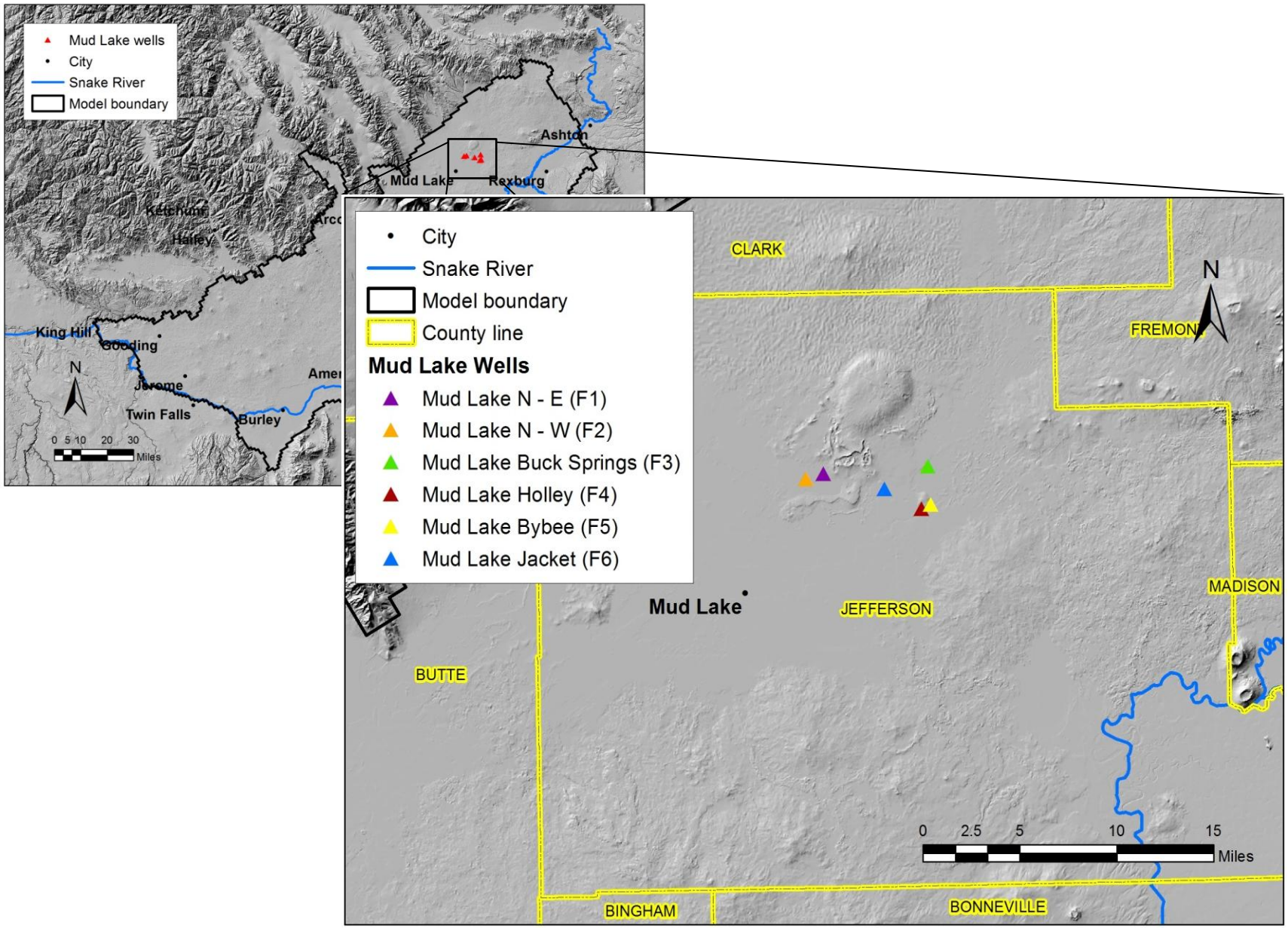

Figure 38. Mud Lake area exchange well groups.

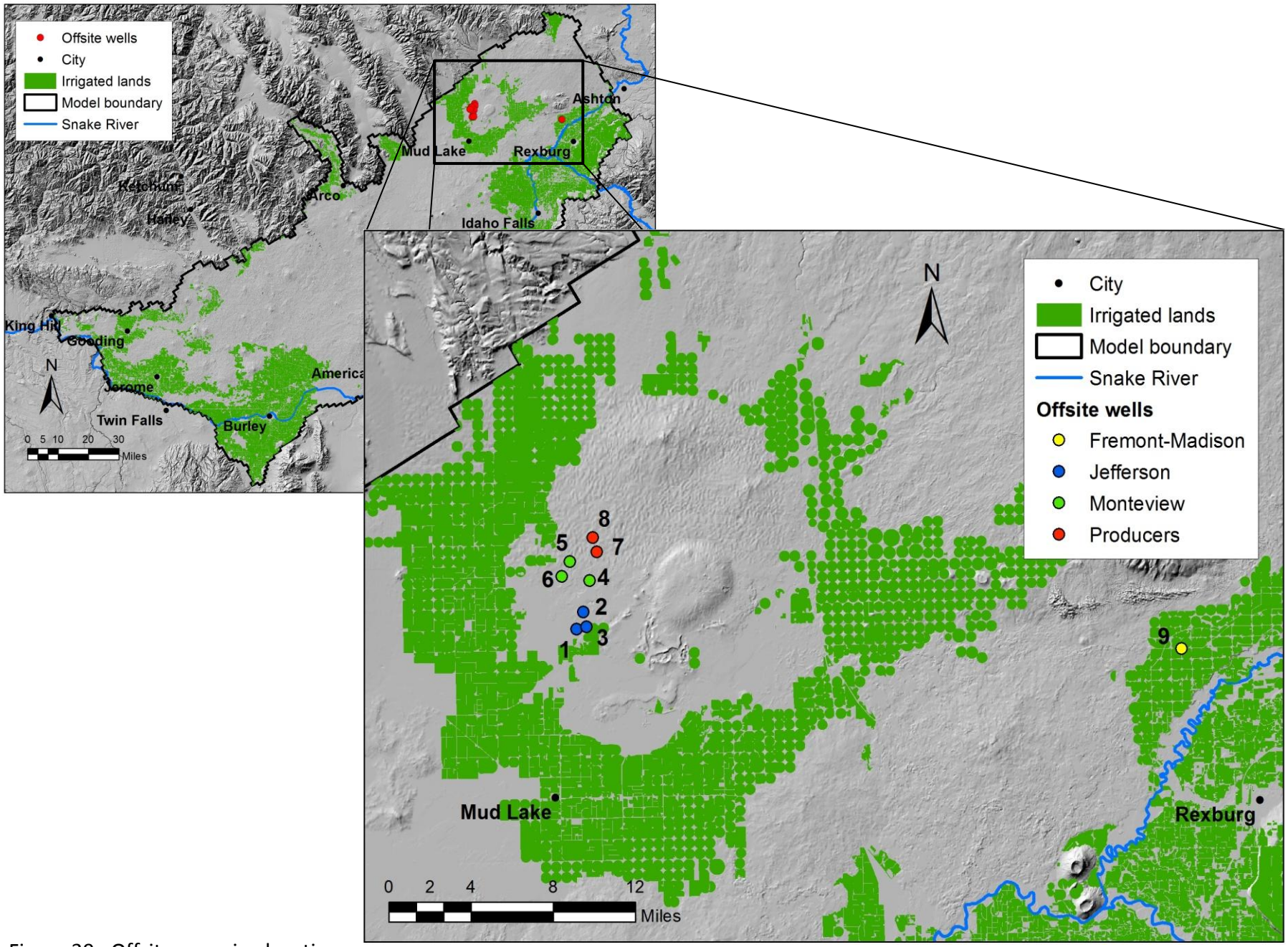

Figure 39. Offsite pumping locations.

Figure 40a – 40d. Time series of fixed point pumping volumes for exchange wells. See 11x17 Figures.

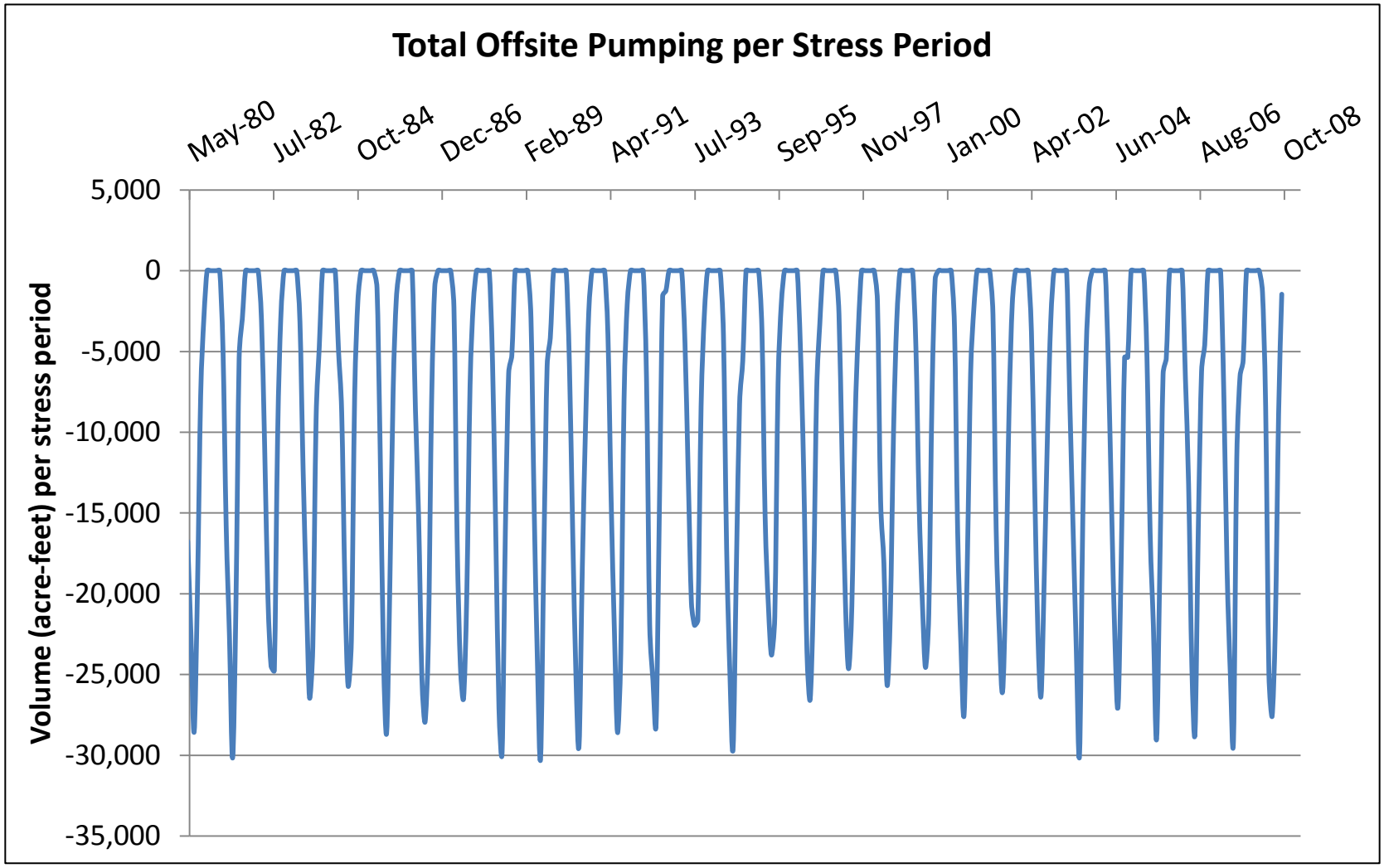

Figure 41. Time series of total offsite pumping in the eastern Snake Plain aquifer.

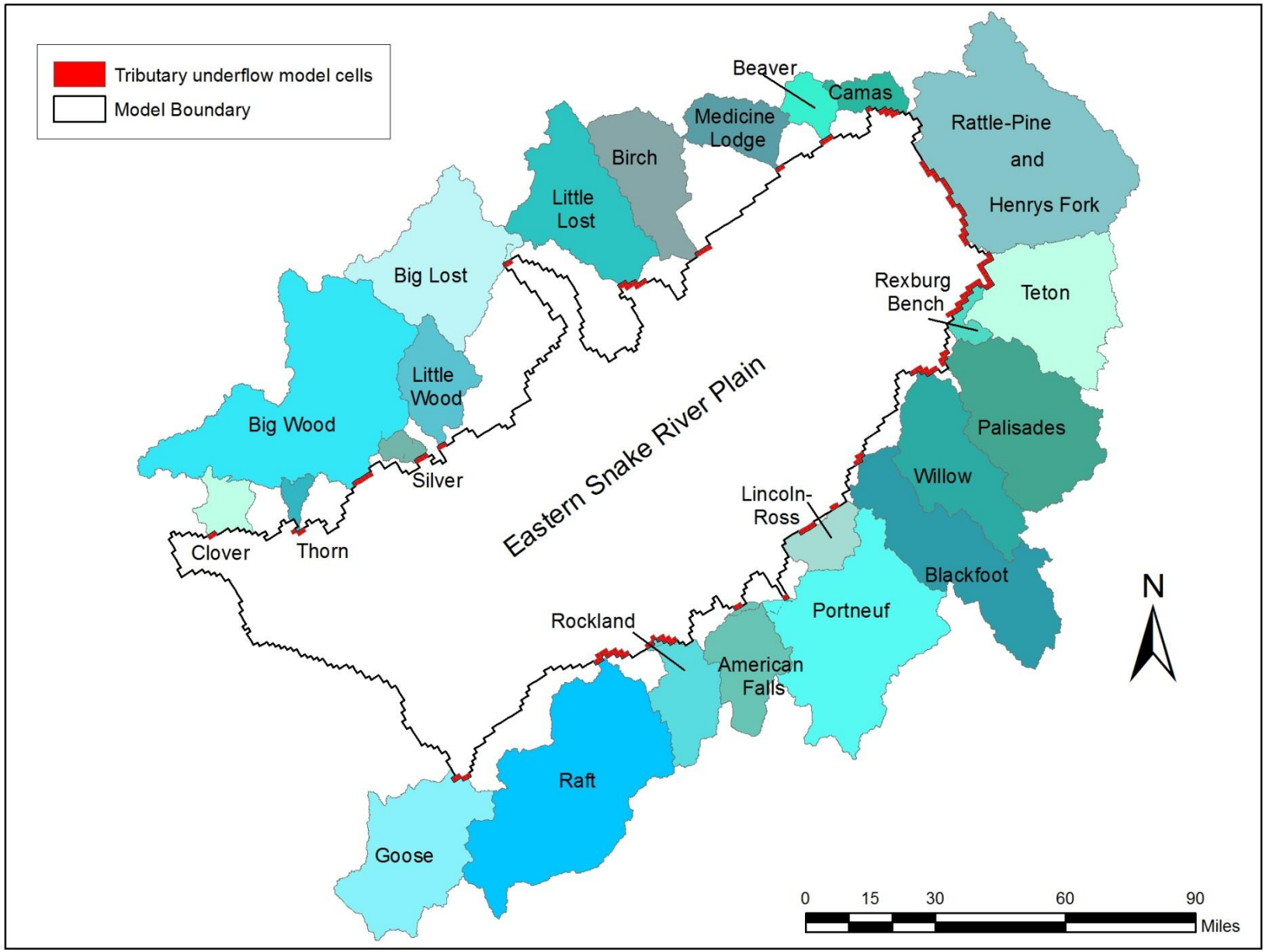

Figure 42. Tributary underflow basins and model cells.

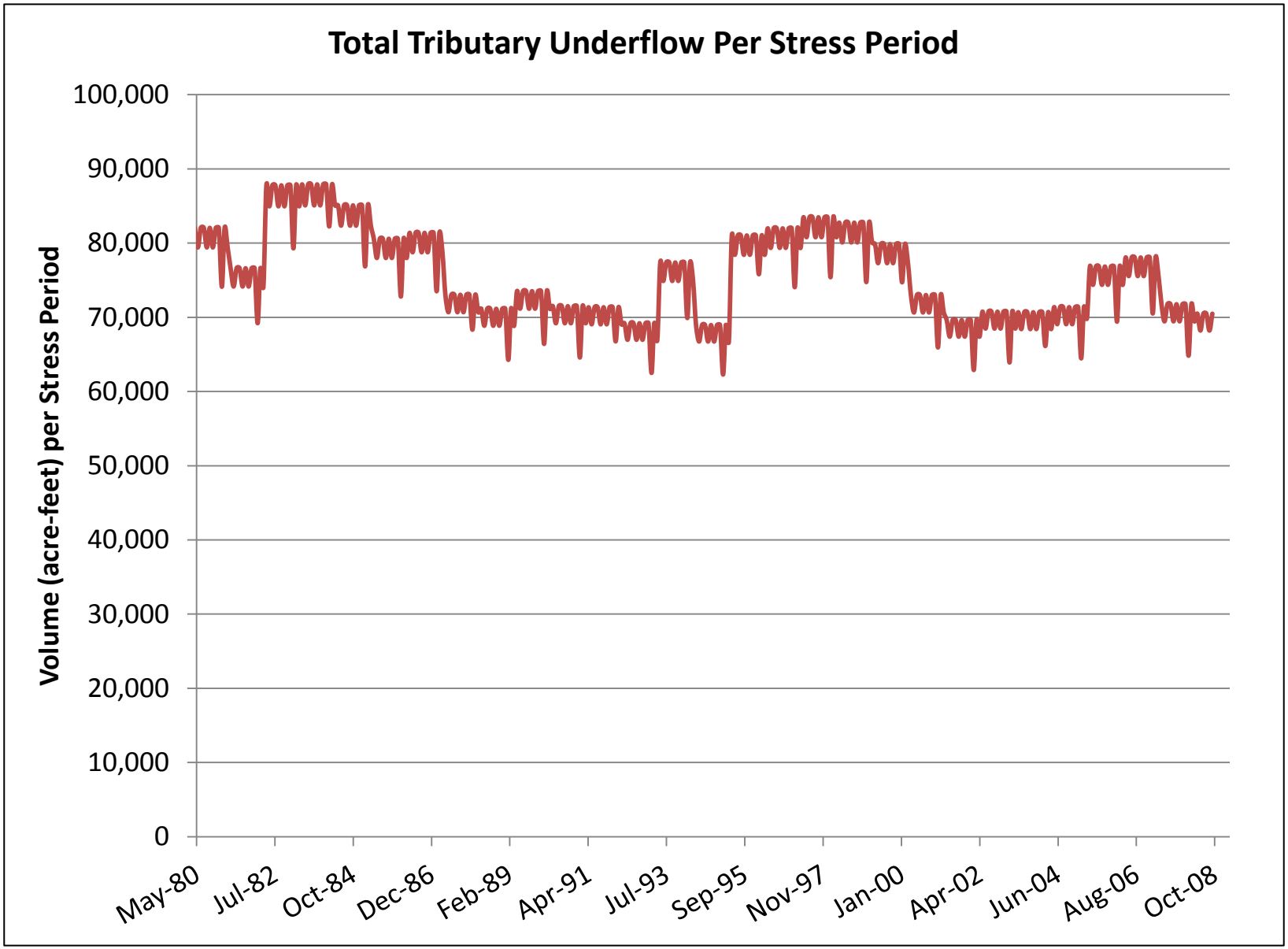

Figure 43. Pre-PEST tributary underflow volume over the calibration period 1980-2008.

Figure 44a – 44f. Pre-PEST tributary underflow in volume (acre-feet) in individual tributary basins.
See 11x17 Figures.

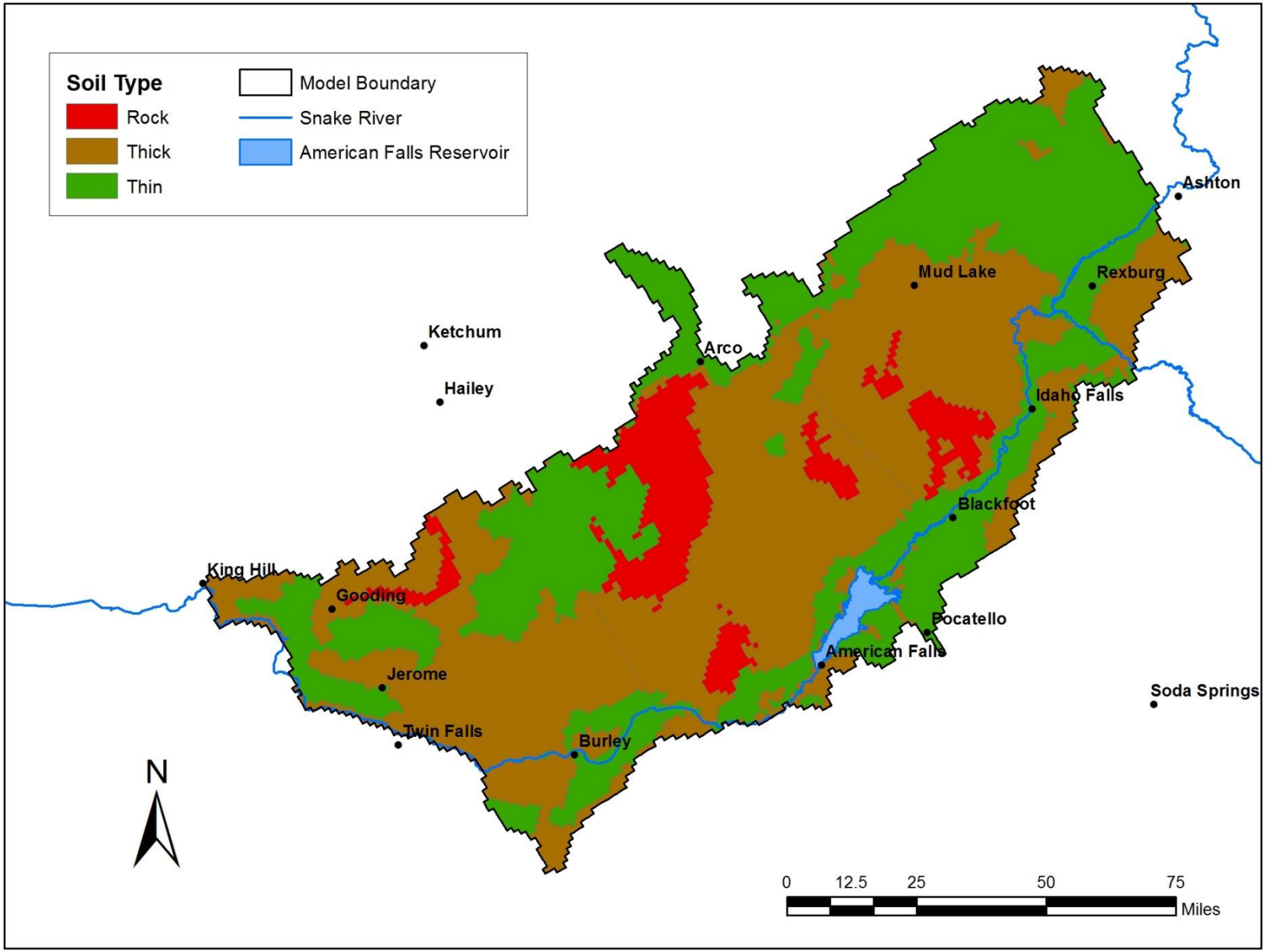

Figure 45. Generalized soil type.

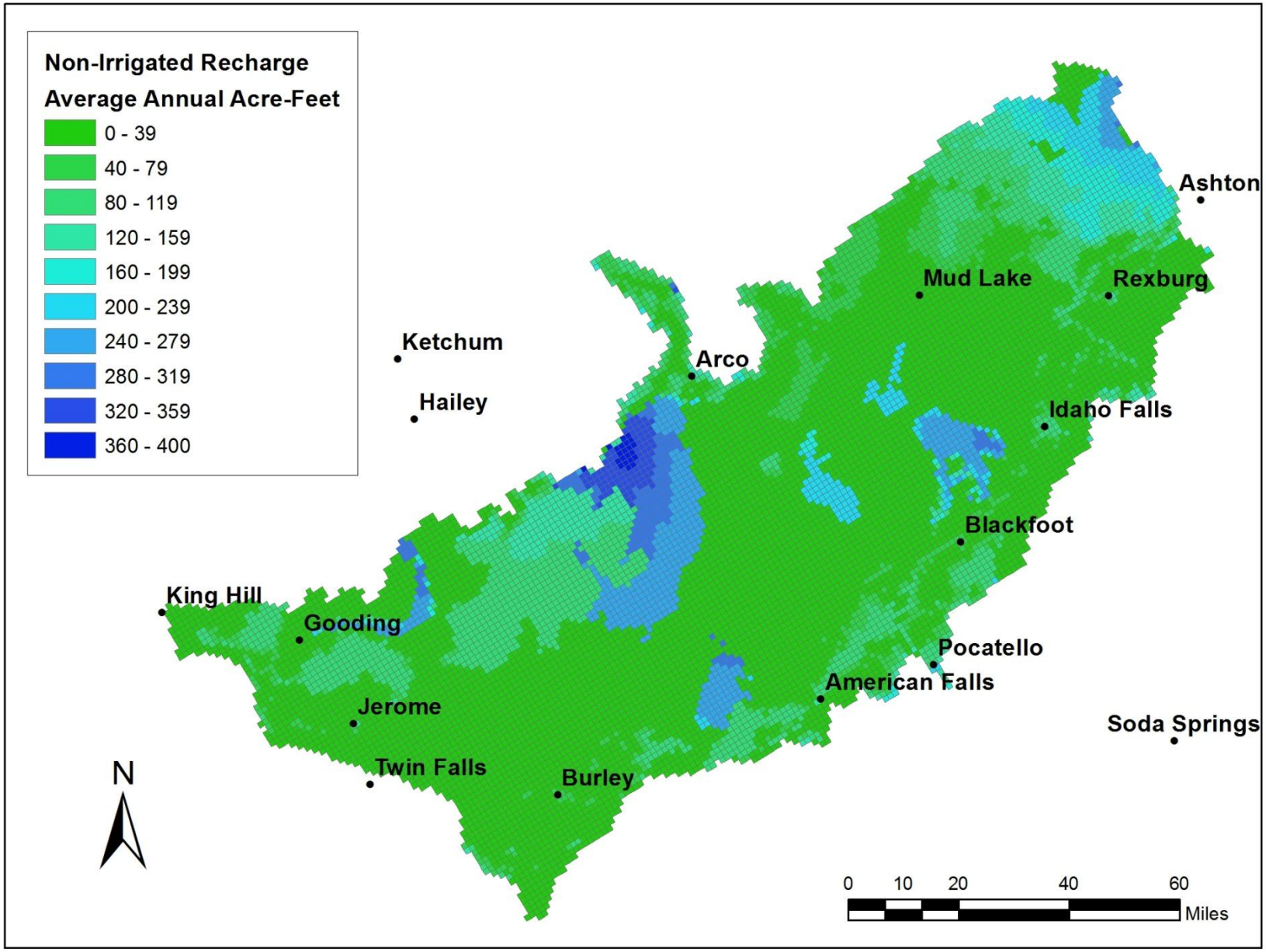

Figure 46. Spatial distribution of pre-PEST non-irrigated recharge averaged for water years 1981-2008.

Figure 47a-47d. Time series of Pre-PEST non-irrigated recharge. See 11x17 figures.

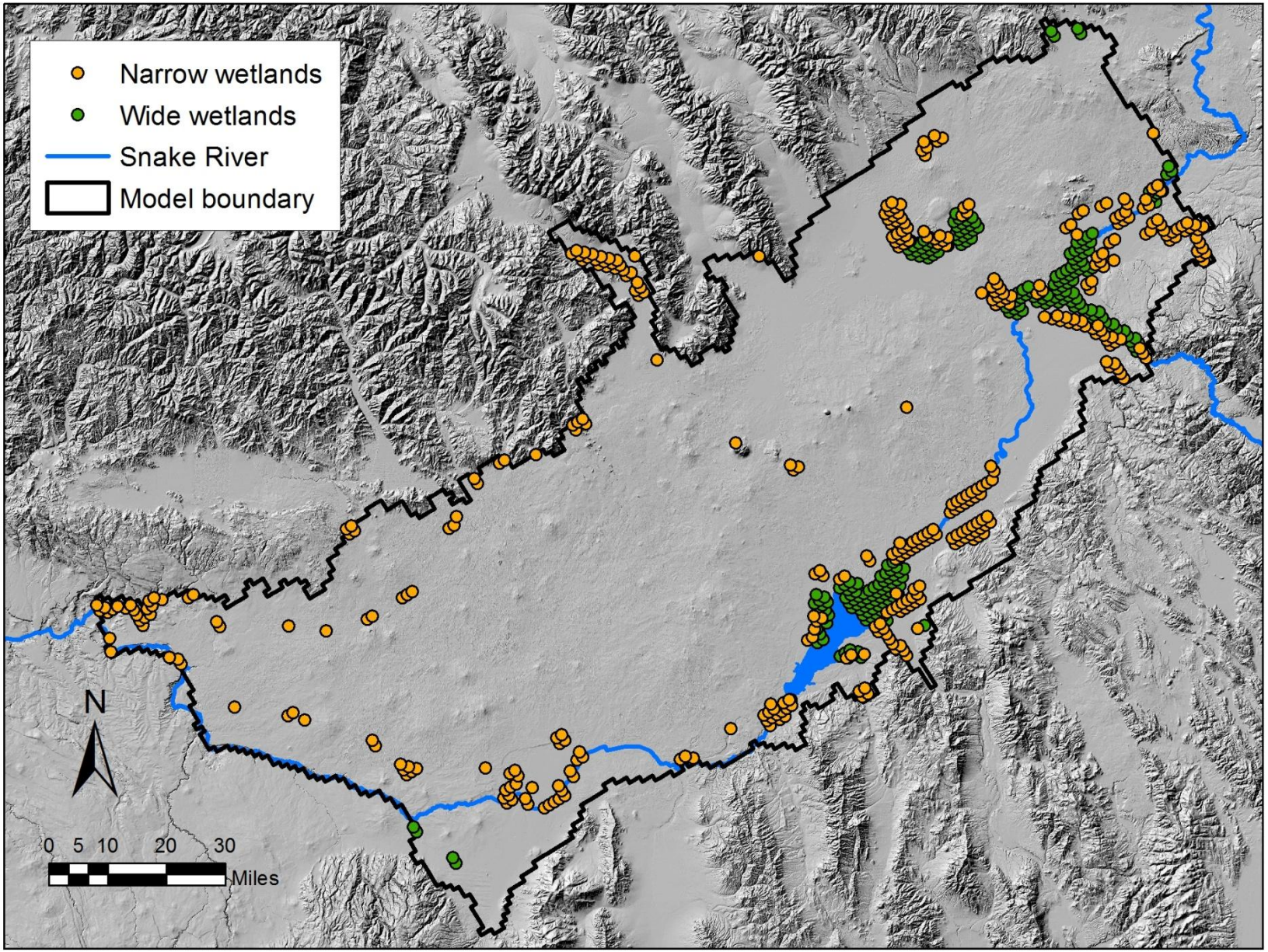

Figure 48. Locations of wetlands represented in the fixed point extraction dataset.

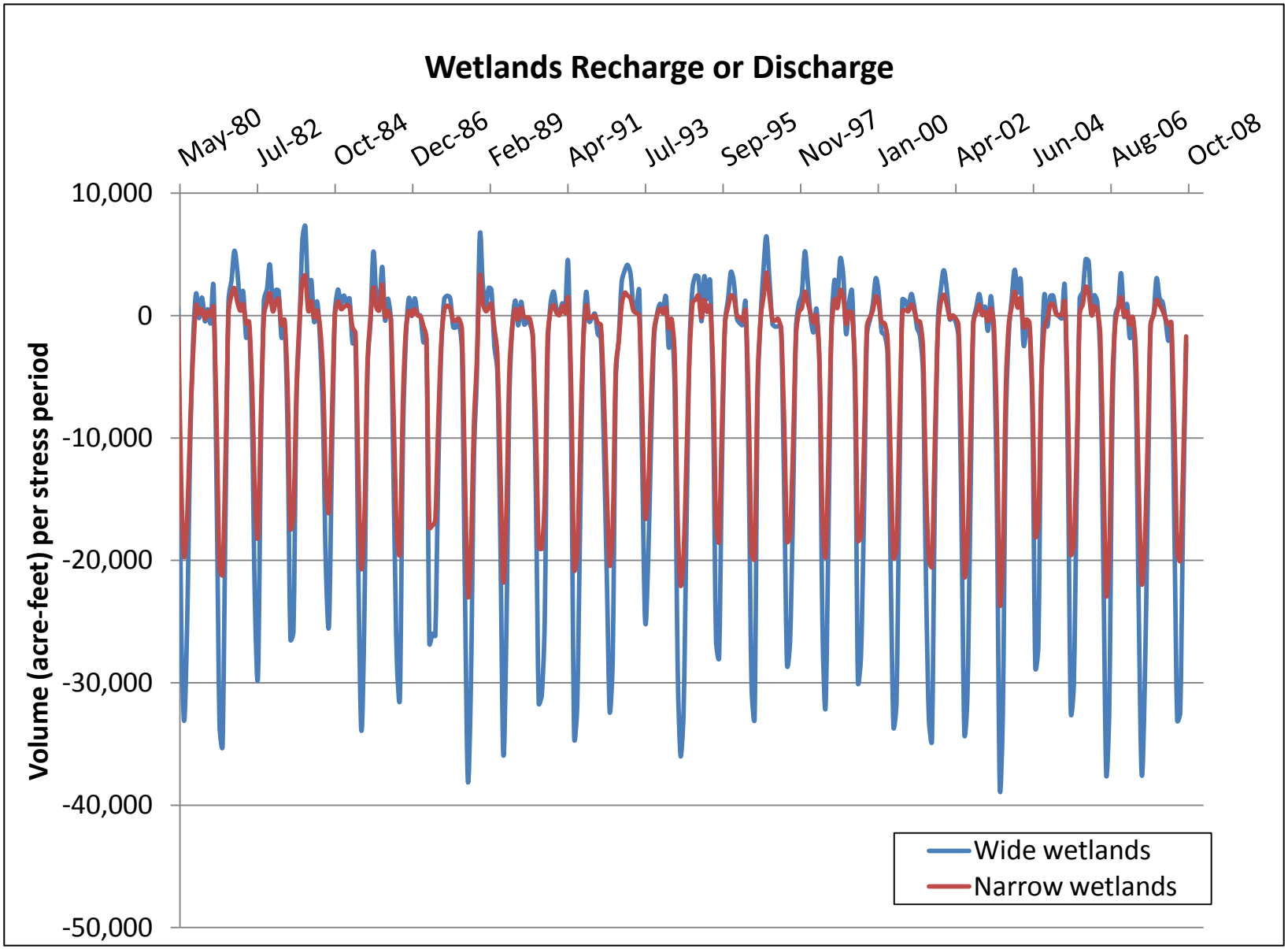

Figure 49. Time series of pre-PEST recharge or discharge from wetlands (wide and narrow). Recharge is indicated by negative values and discharge is indicated by positive values.

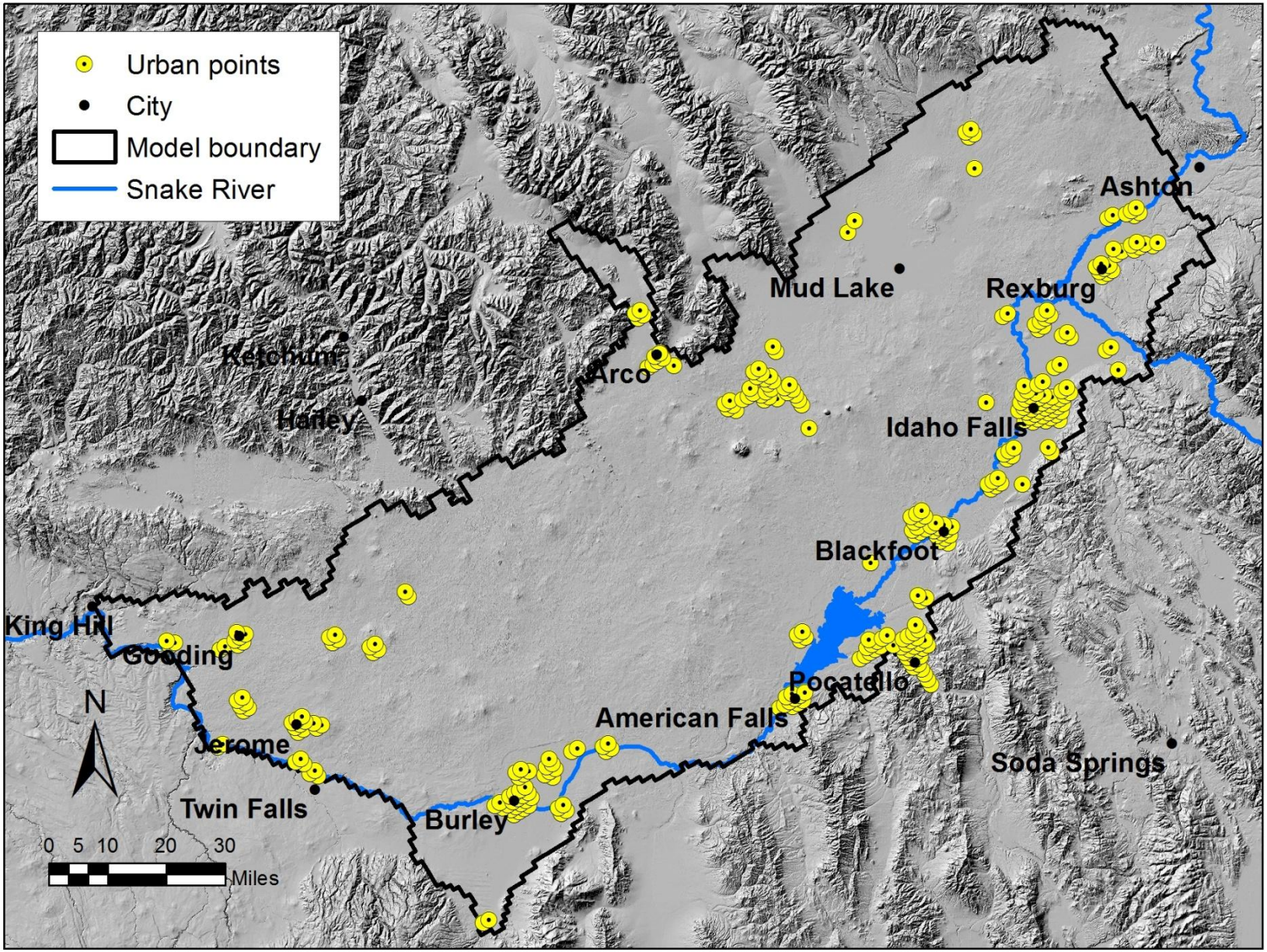

Figure 50. Locations of urban extraction points represented in fixed point extraction dataset.

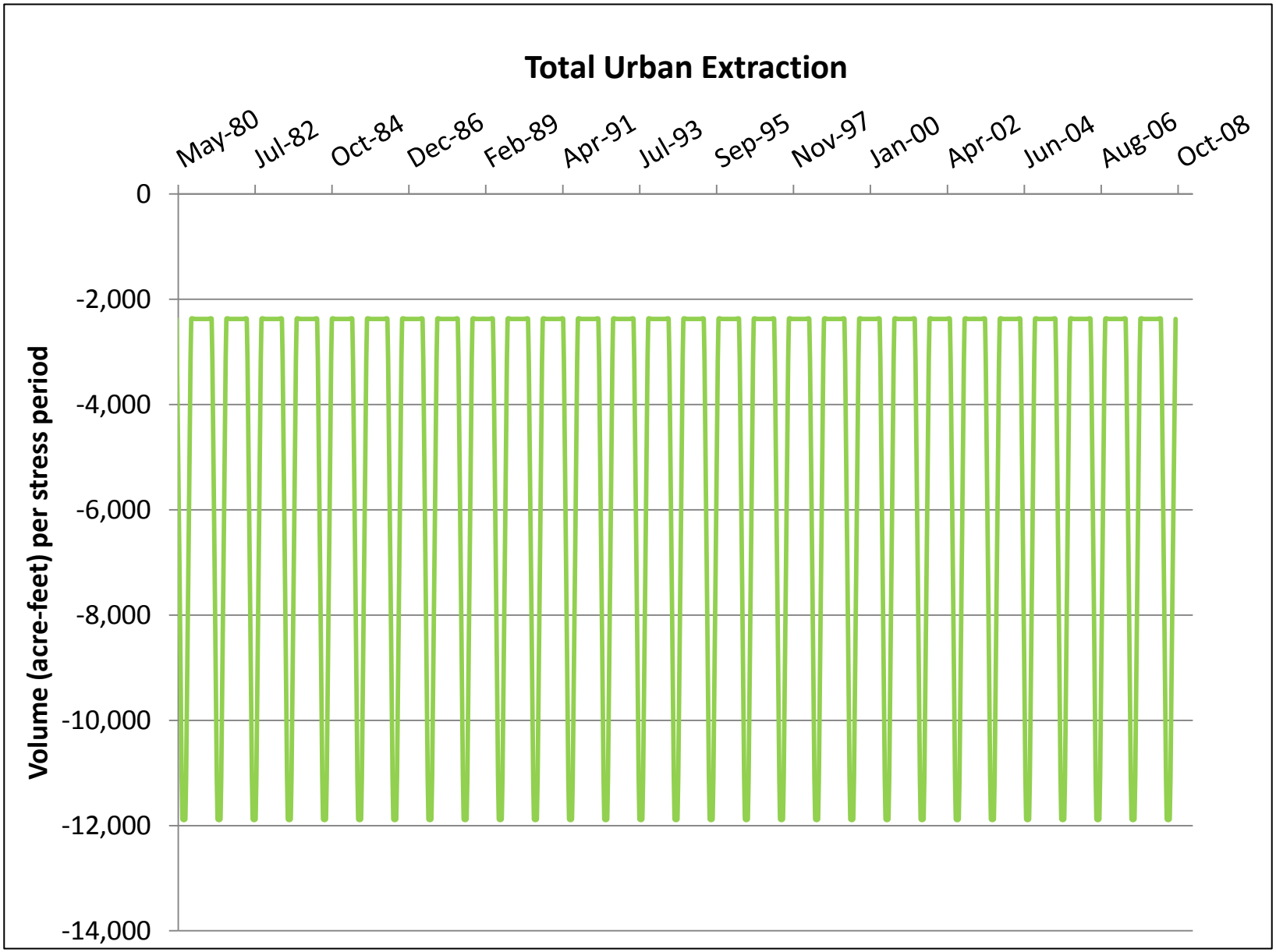

Figure 51. Time series of urban extraction.

Figure 52a – 52c. Non-Snake River sources of surface water seepage. See 11x17 figures.

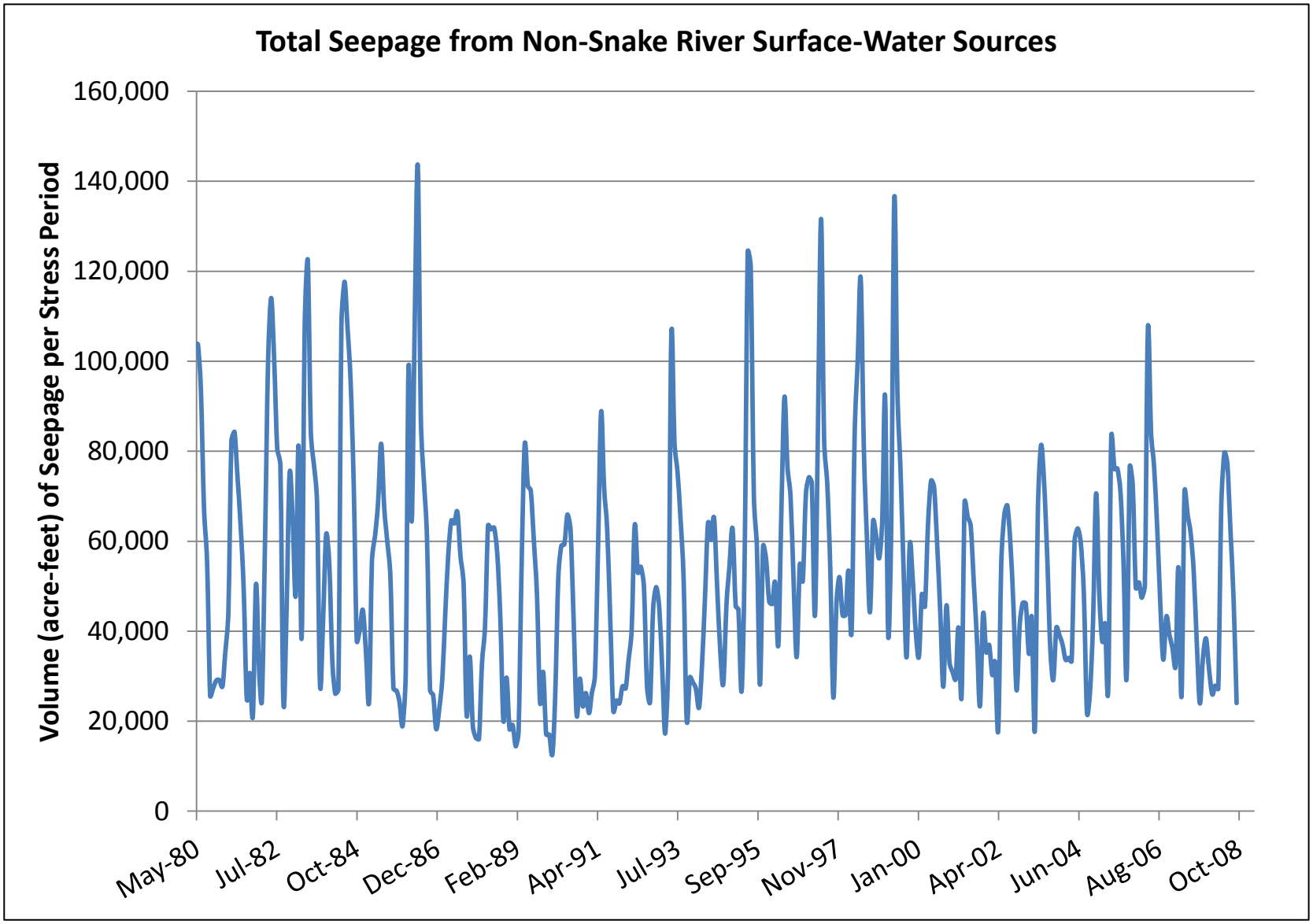

Figure 53. Total volume of seepage from non-Snake River surface-water sources.

Figure 54a – 54d. Pre-PEST volume of seepage per stress period from non-Snake River surface-water sources.
See 11x17 figures.

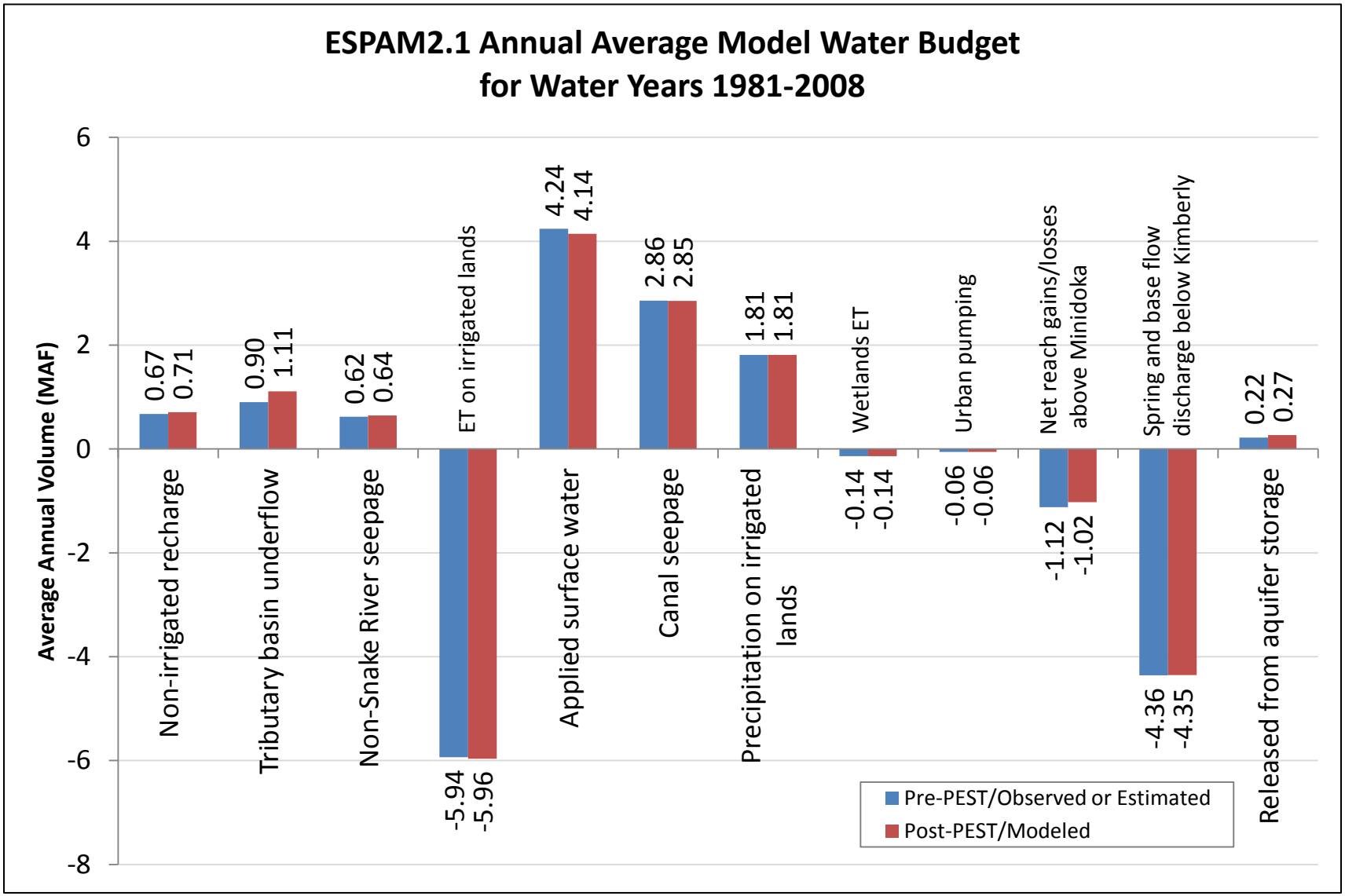

Figure 55. Enhanced Snake Plain Aquifer Model 2.1 average annual model water budget. Positive values of aquifer storage represent water released from storage into the aquifer flow system. Negative values of aquifer storage represent water placed into storage. Applied surface water is defined as (*Agricultural diversions – canal seepage – returns – offsite, exchange, and Mud Lake pumping*). Precipitation on agricultural lands and urban pumping were not adjustable during model calibration.

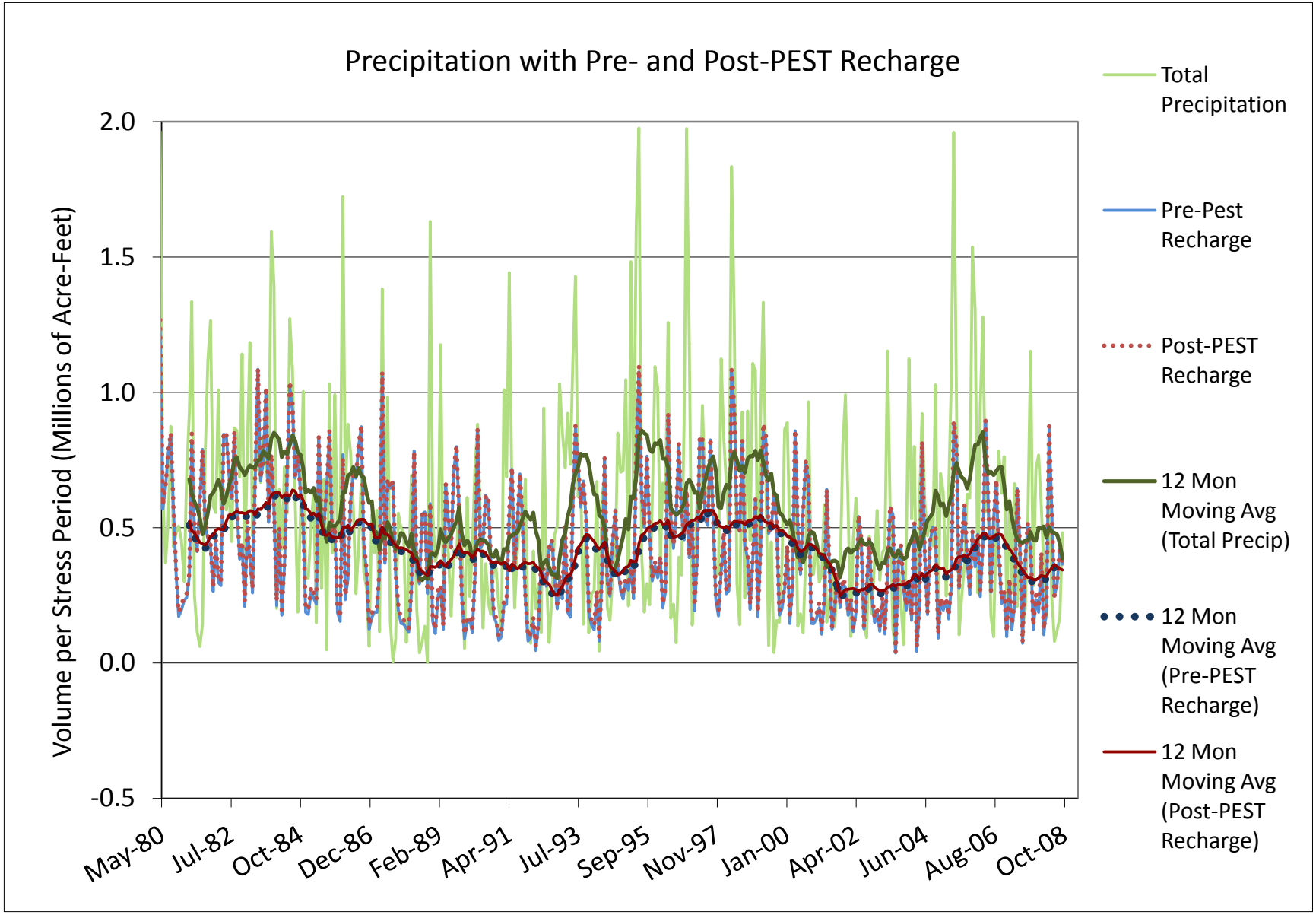

Figure 56. Pre-PEST and Post-PEST net recharge plotted over time in comparison with total precipitation for the transient ESPAM model.

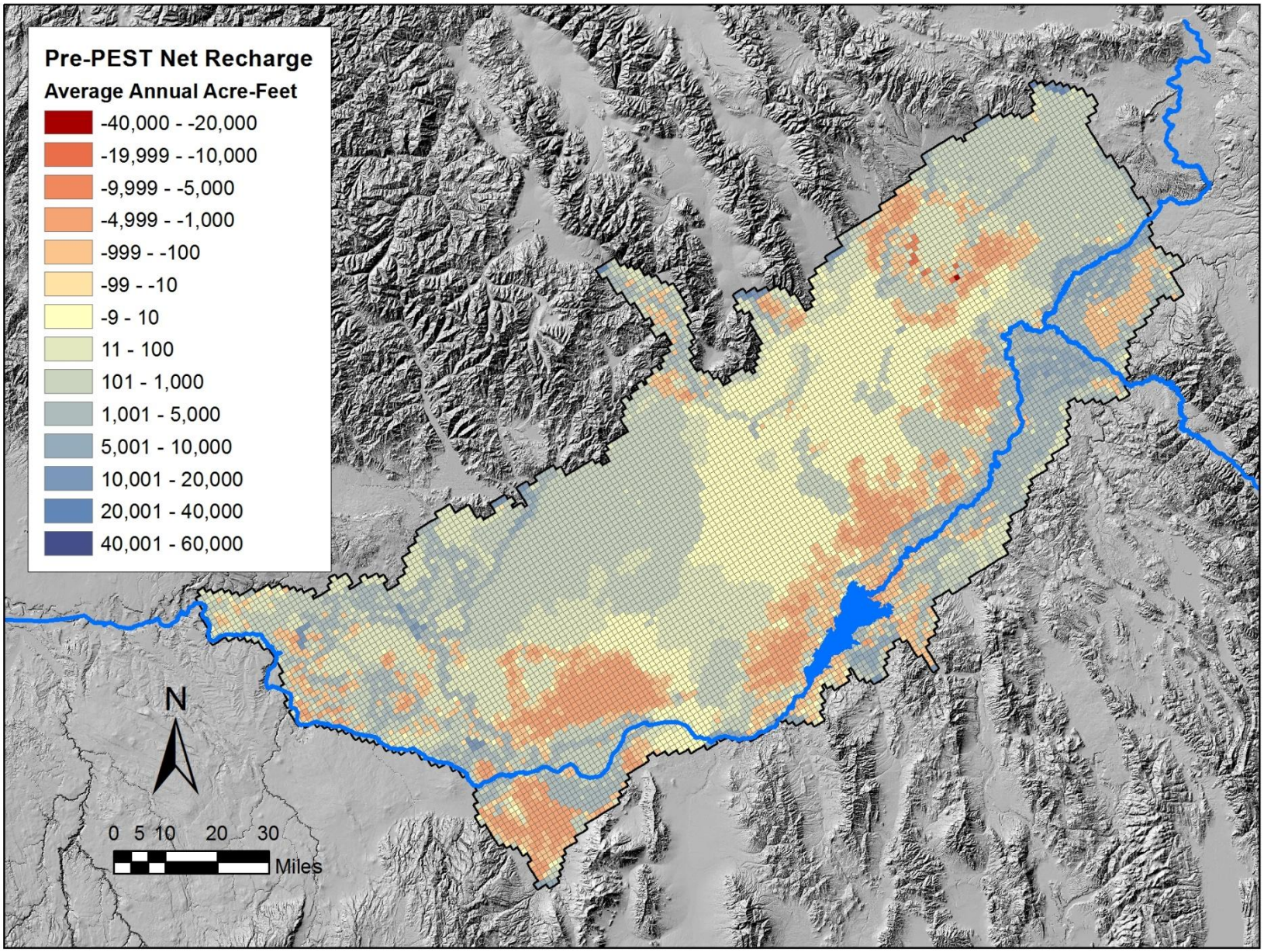

Figure 57. Pre-PEST areal distribution of net recharge (average annual water year values).

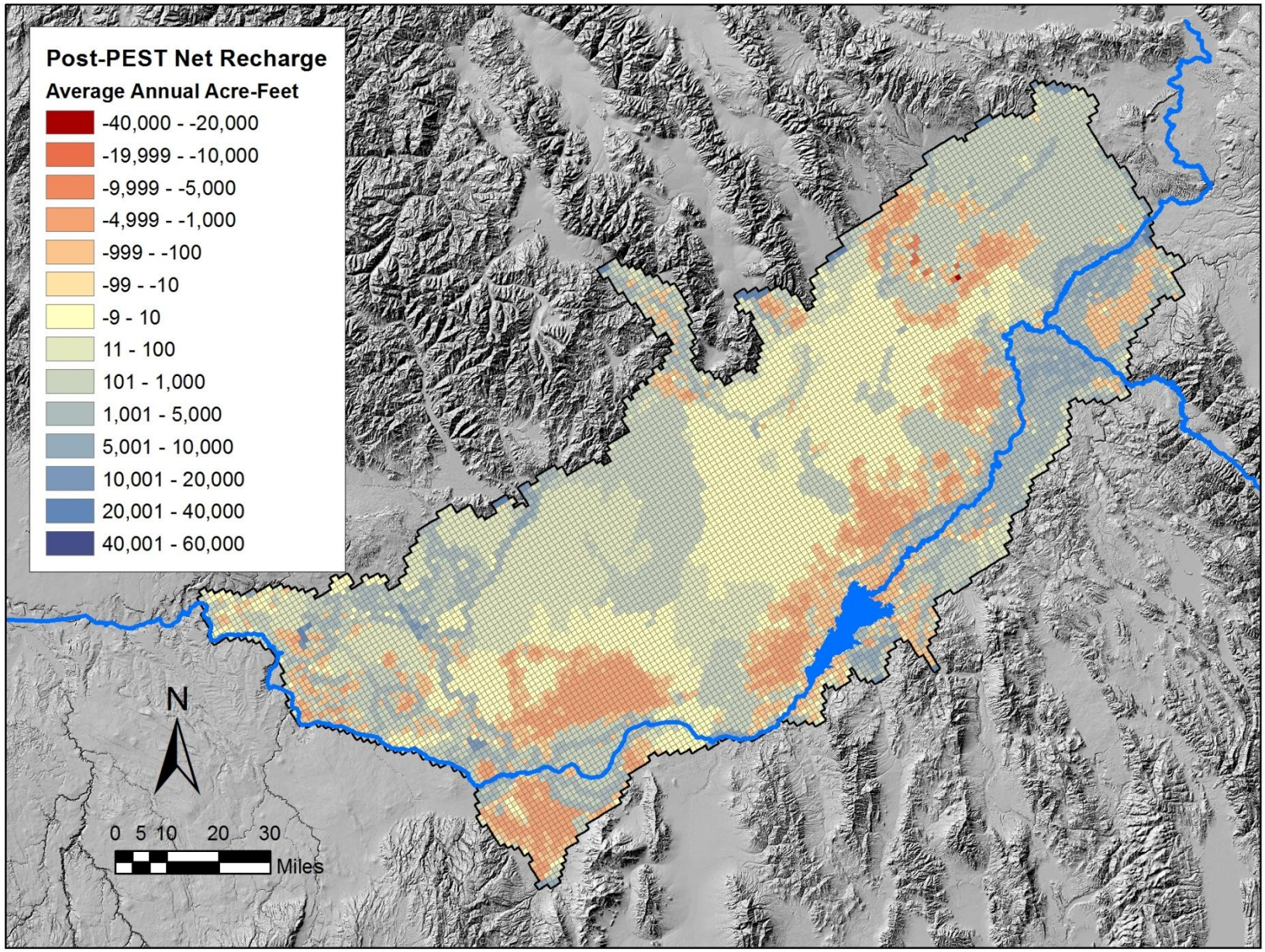

Figure 58. Post-PEST areal distribution of net recharge (average annual water year values).

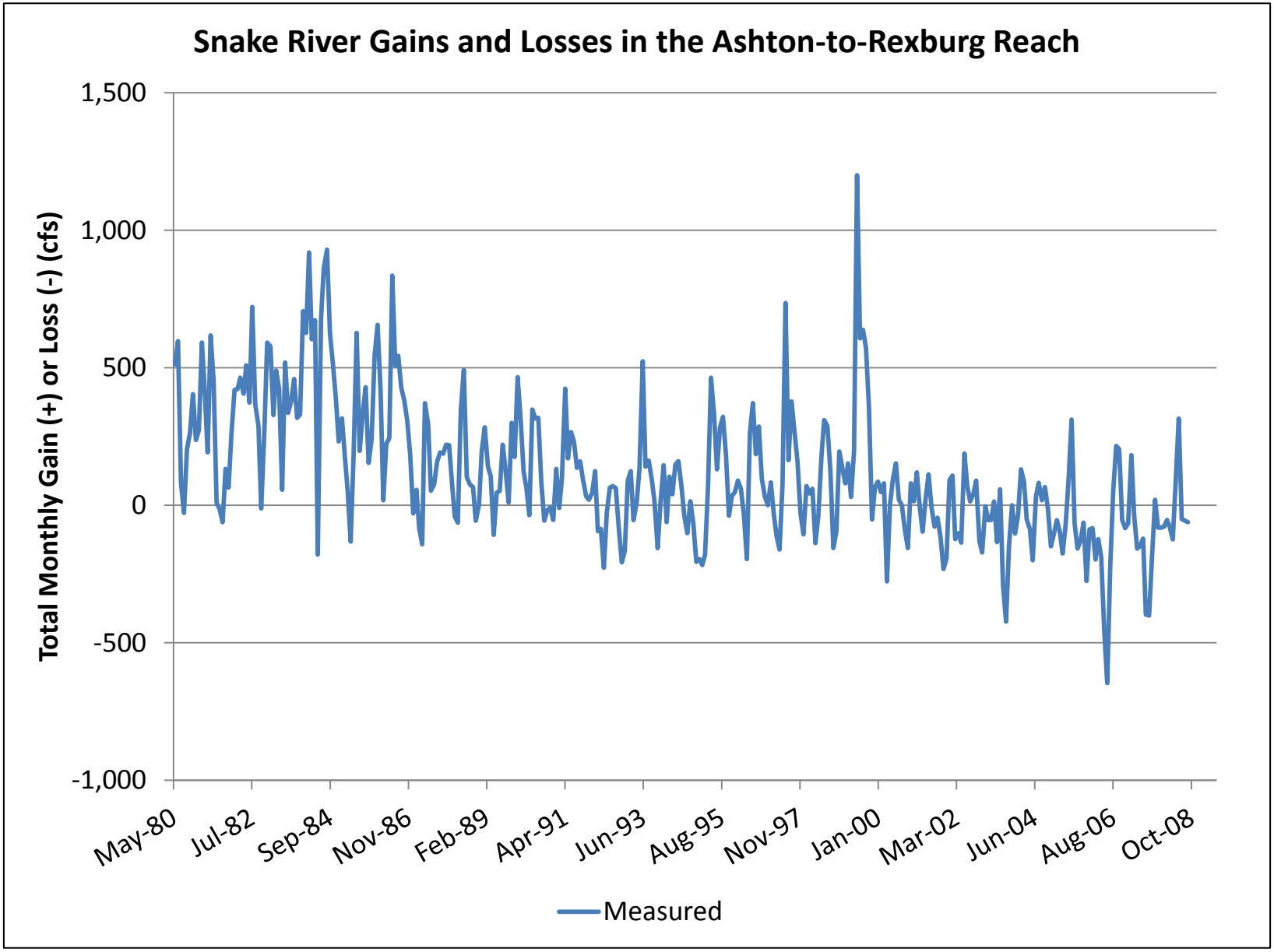

Figure 59. Monthly Snake River gains and losses in the Ashton-to-Rexburg reach.

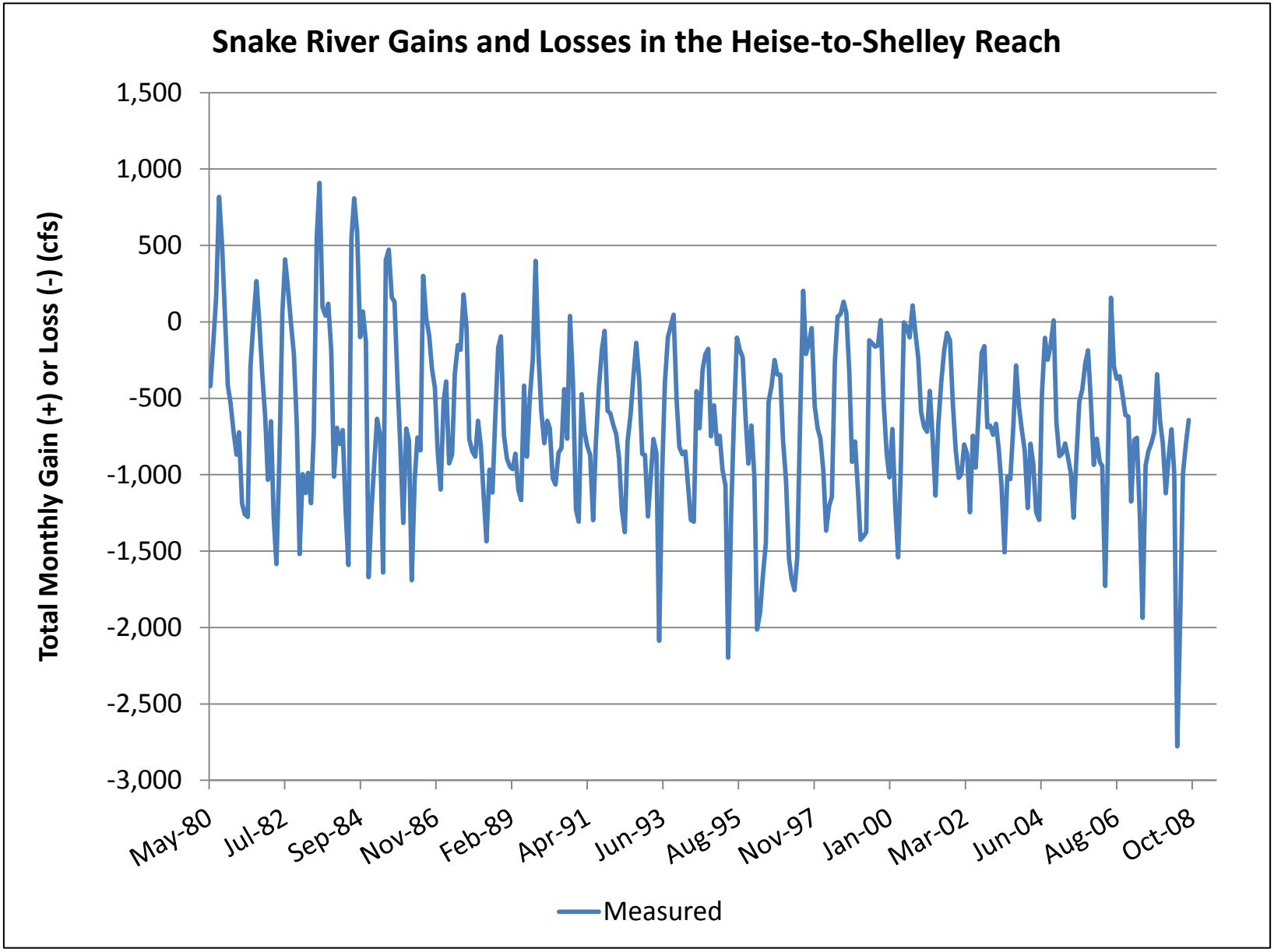

Figure 60. Monthly Snake River gains and losses in the Heise-to-Shelley reach.

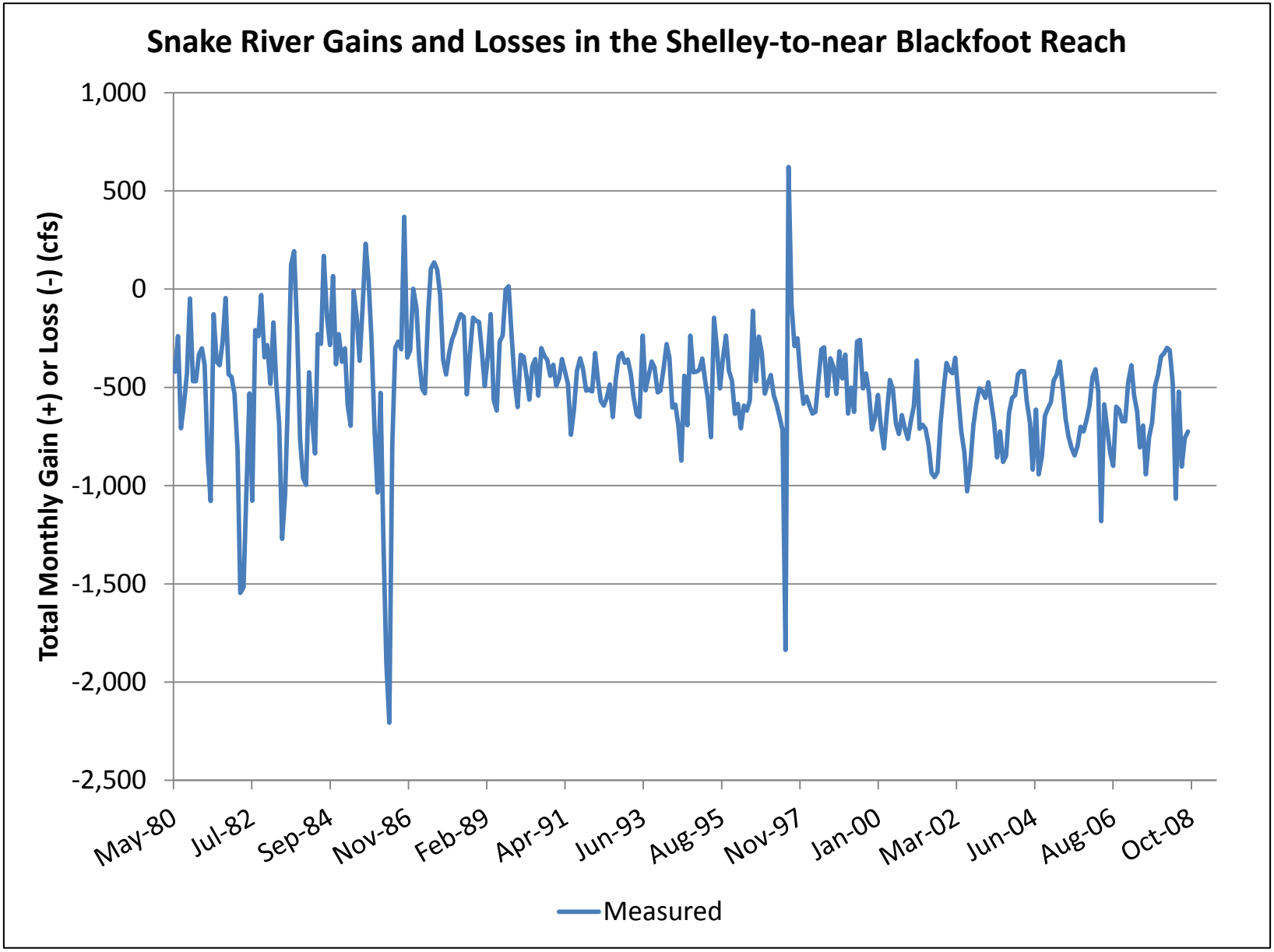

Figure 61. Monthly Snake River gains and losses in the Shelley-to-near Blackfoot reach.

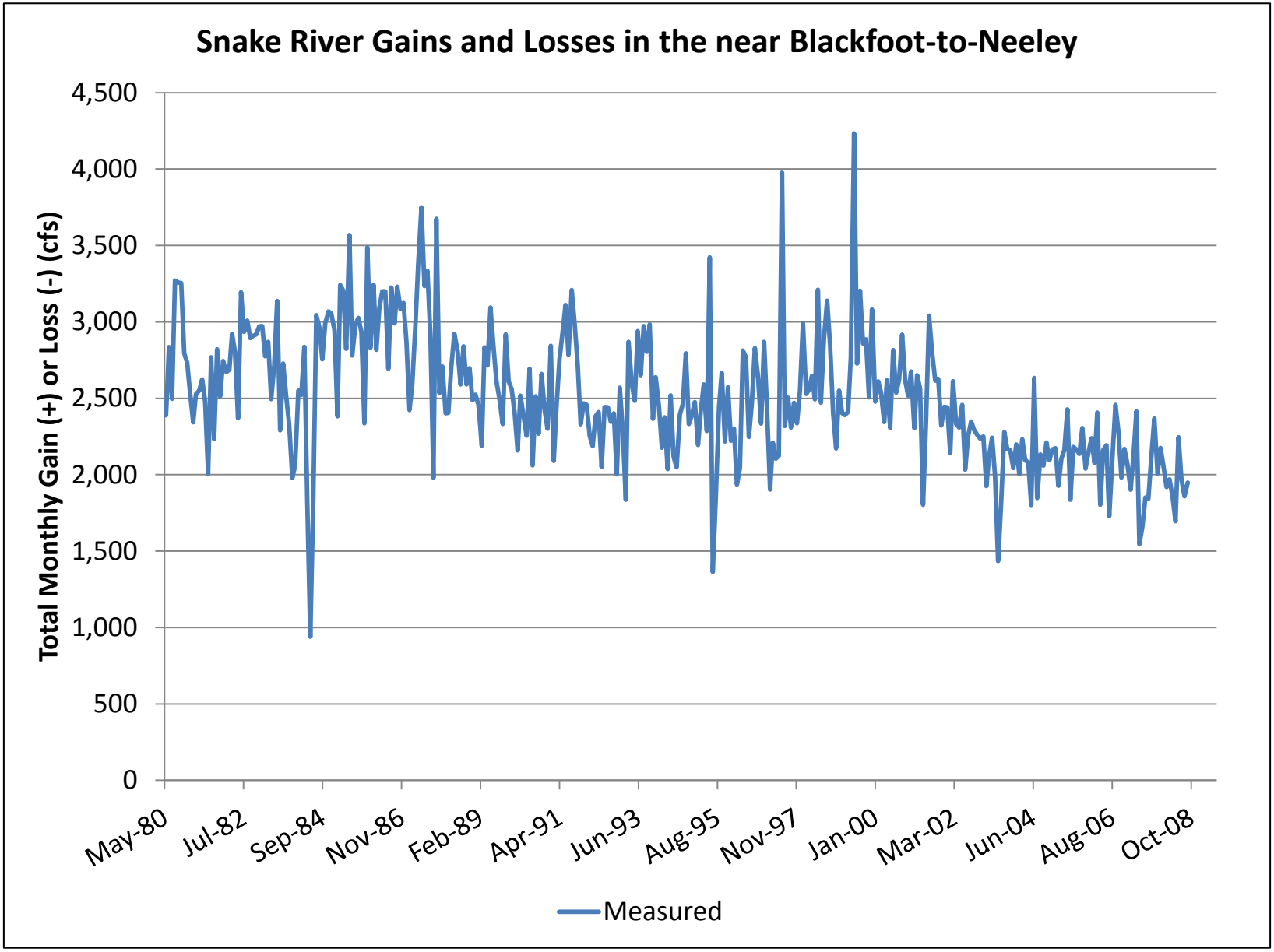

Figure 62. Monthly Snake River gains and losses in the near Blackfoot-to-Neeley reach.

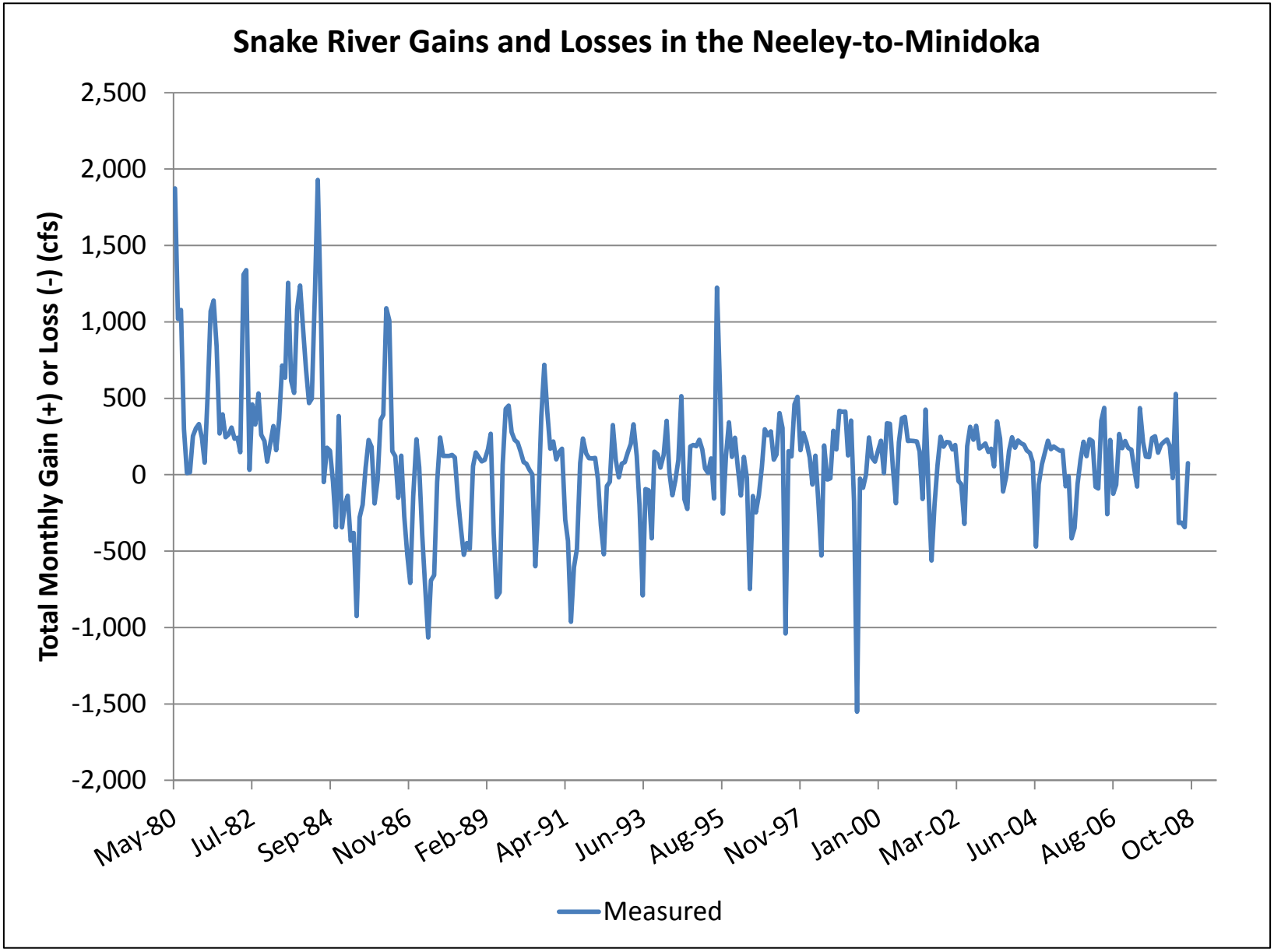

Figure 63. Monthly Snake River gains and losses in the Neeley-to-Minidoka reach.

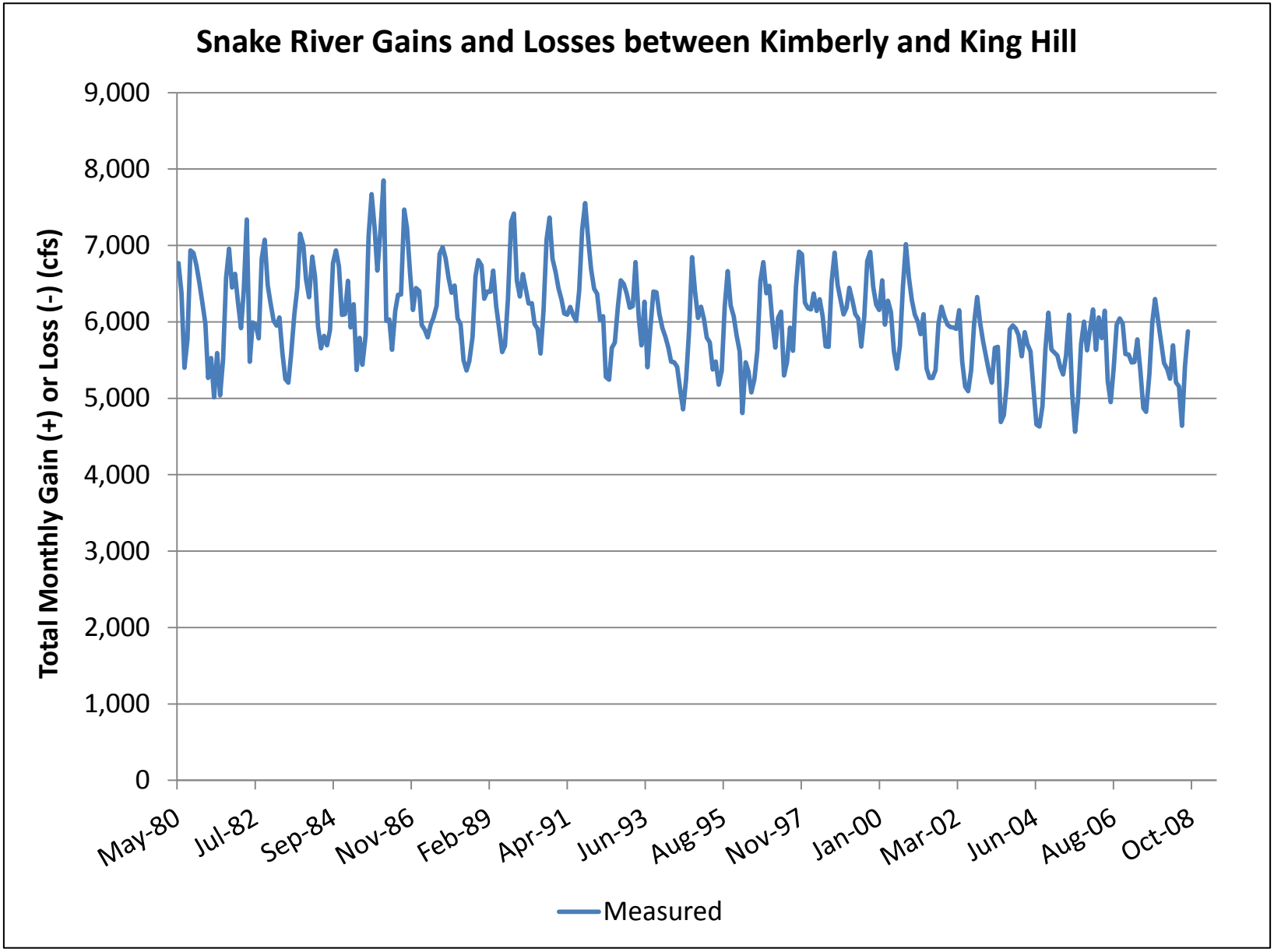

Figure 64. Monthly Snake River gains and losses between Kimberly and King Hill.

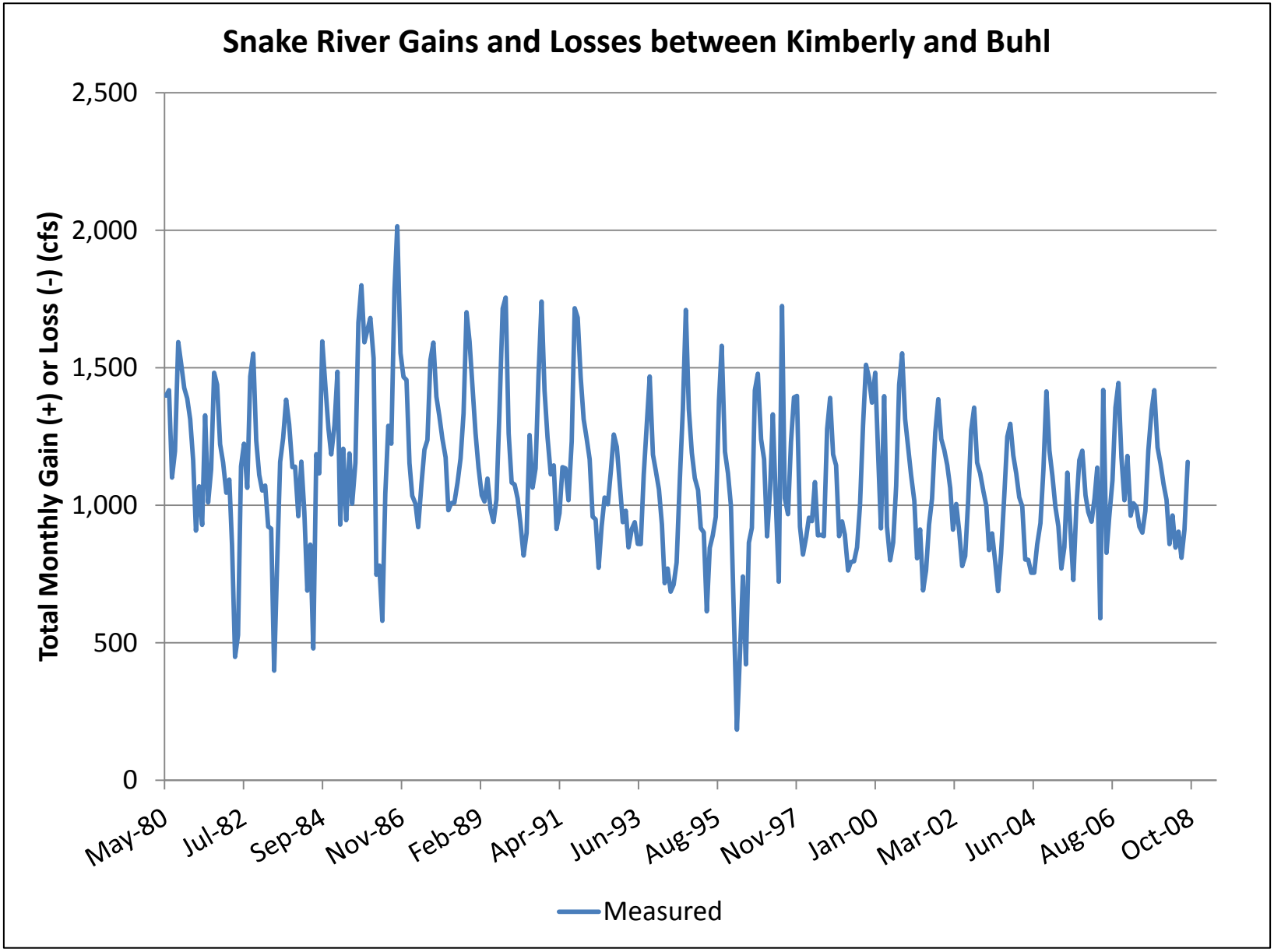

Figure 65. Monthly Snake River gains and losses between Kimberly and Buhl.

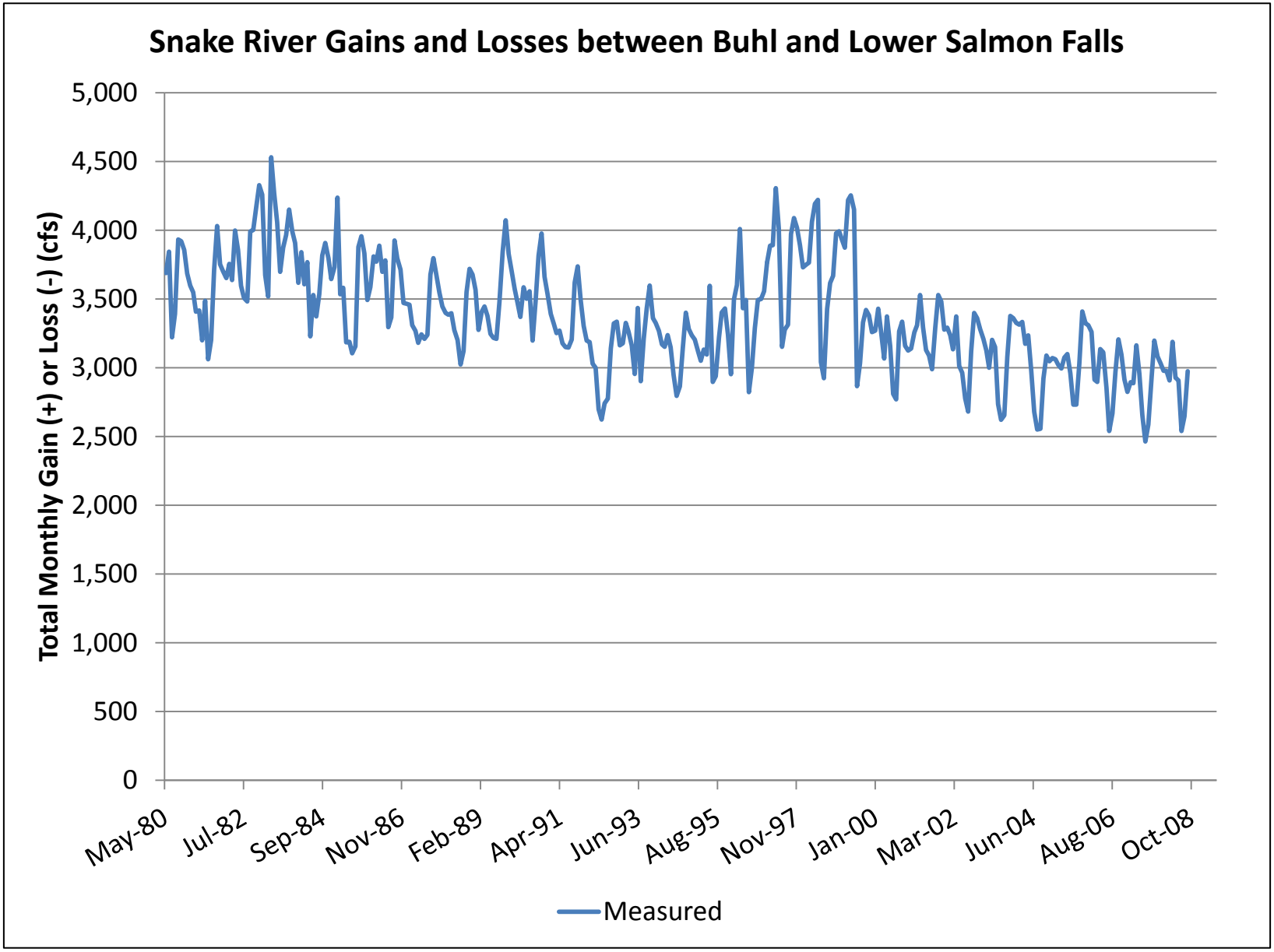

Figure 66. Monthly Snake River gains and losses between Buhl and Lower Salmon Falls.

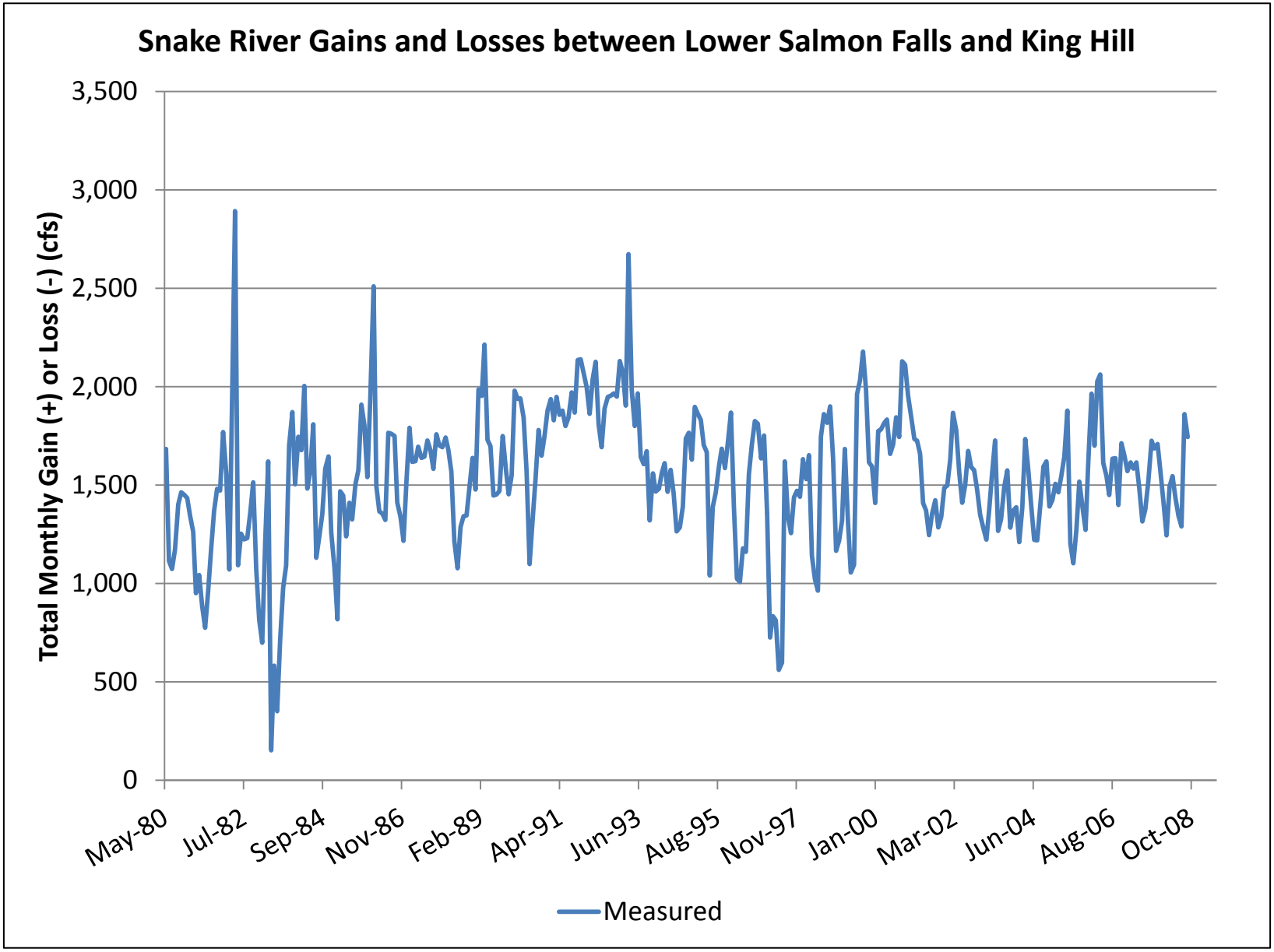

Figure 67. Monthly Snake River gains and losses between Lower Salmon Falls and King Hill.

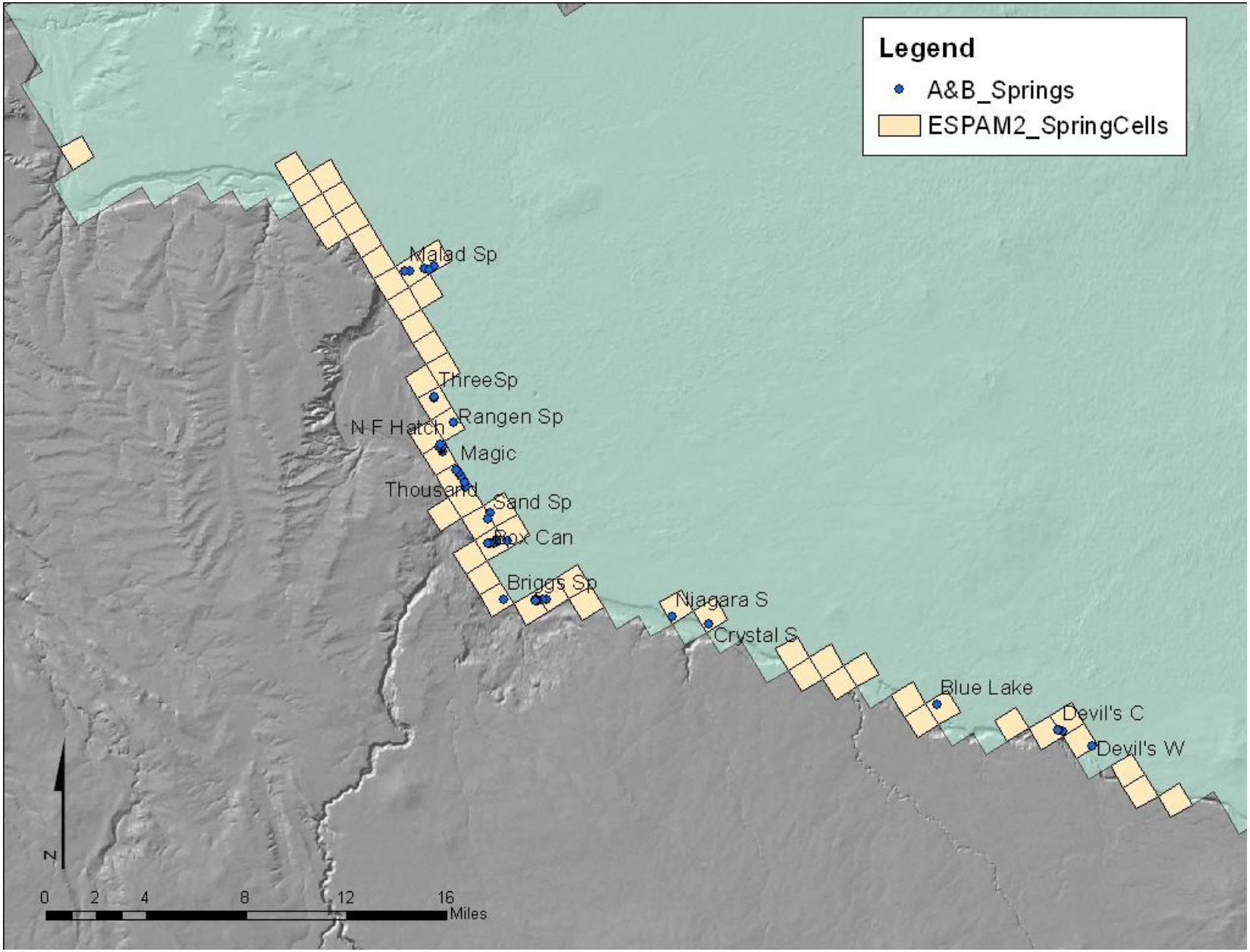

Figure 68. Location of Group A and B springs used as calibration targets.

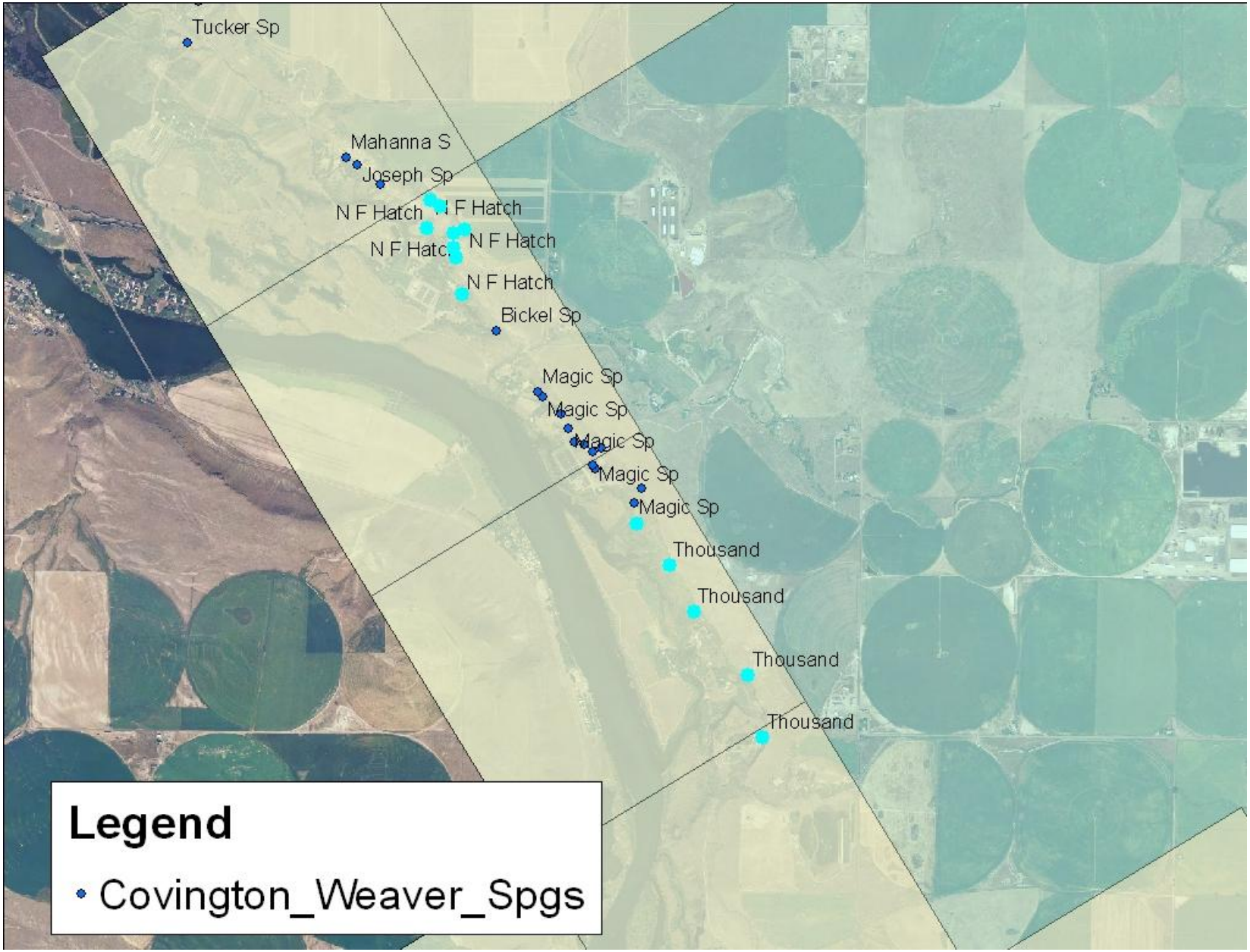

Figure 69. Magic Springs Complex.

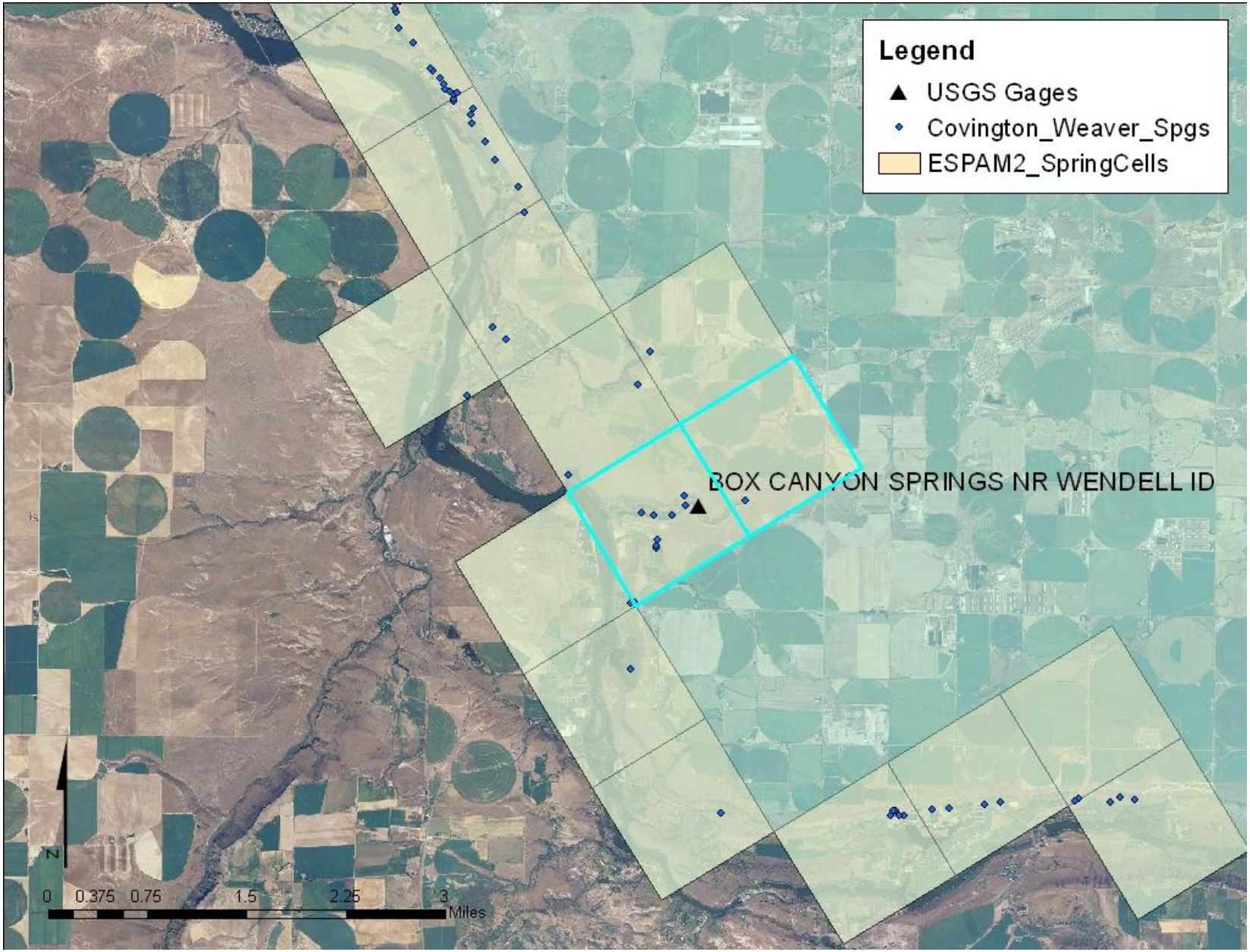

Figure 70. Box Canyon Springs location relative to the model drain cells.

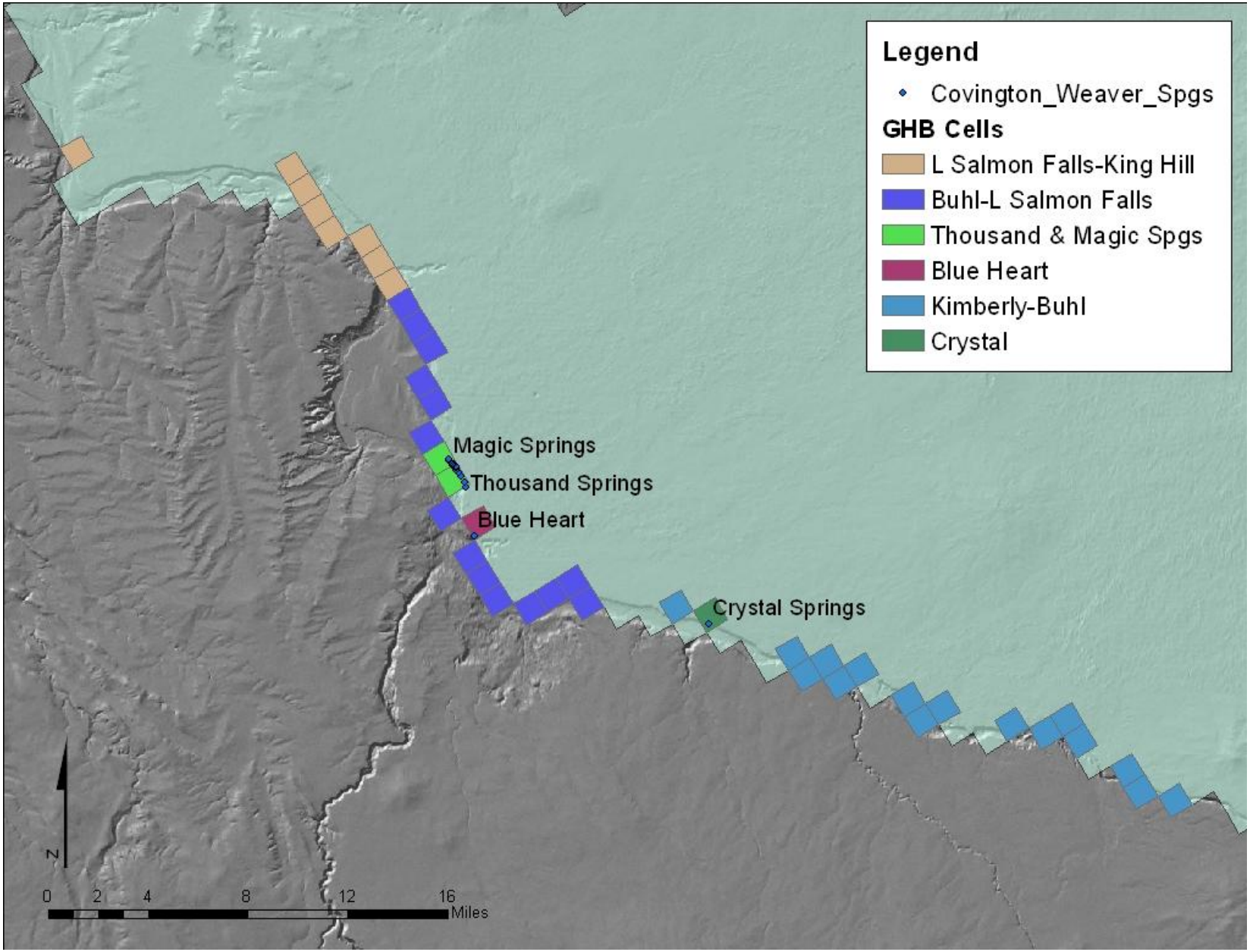

Figure 71. Location of General Head Boundary (GHB) targets in the Thousand Springs area.

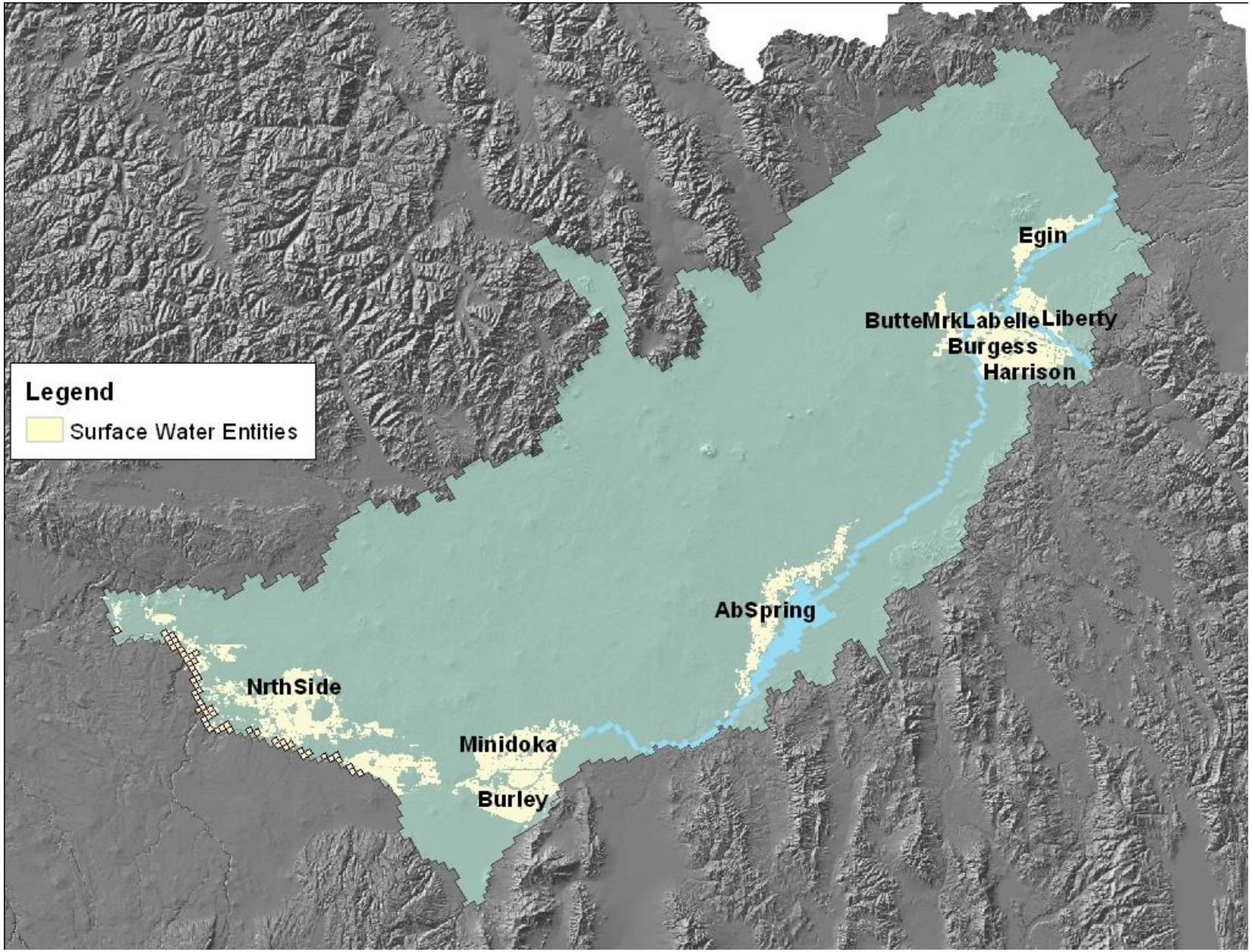

Figure 72. Location of entities with measured returns.

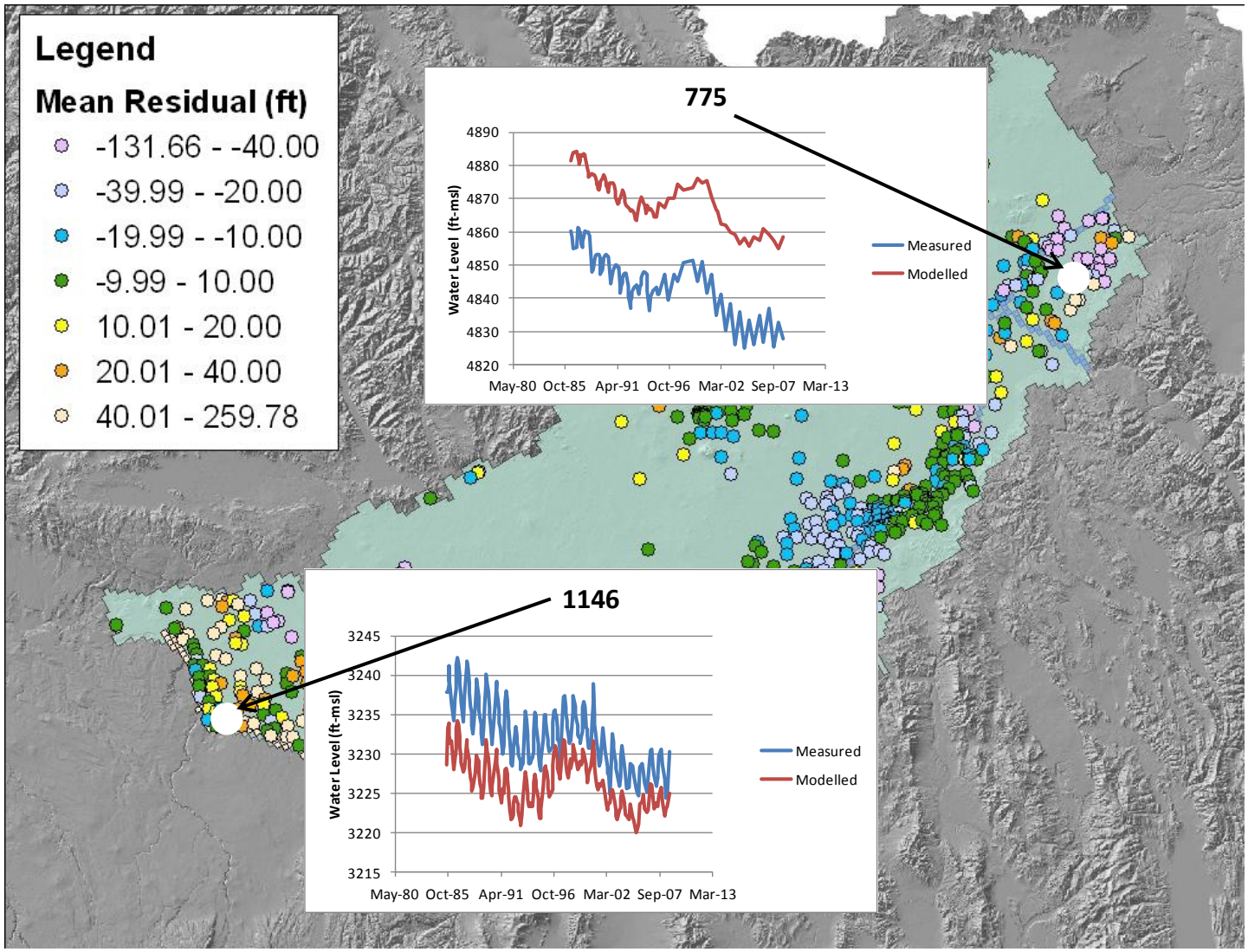

Figure 73. Simulated versus observed water levels for wells 775 and 1146.

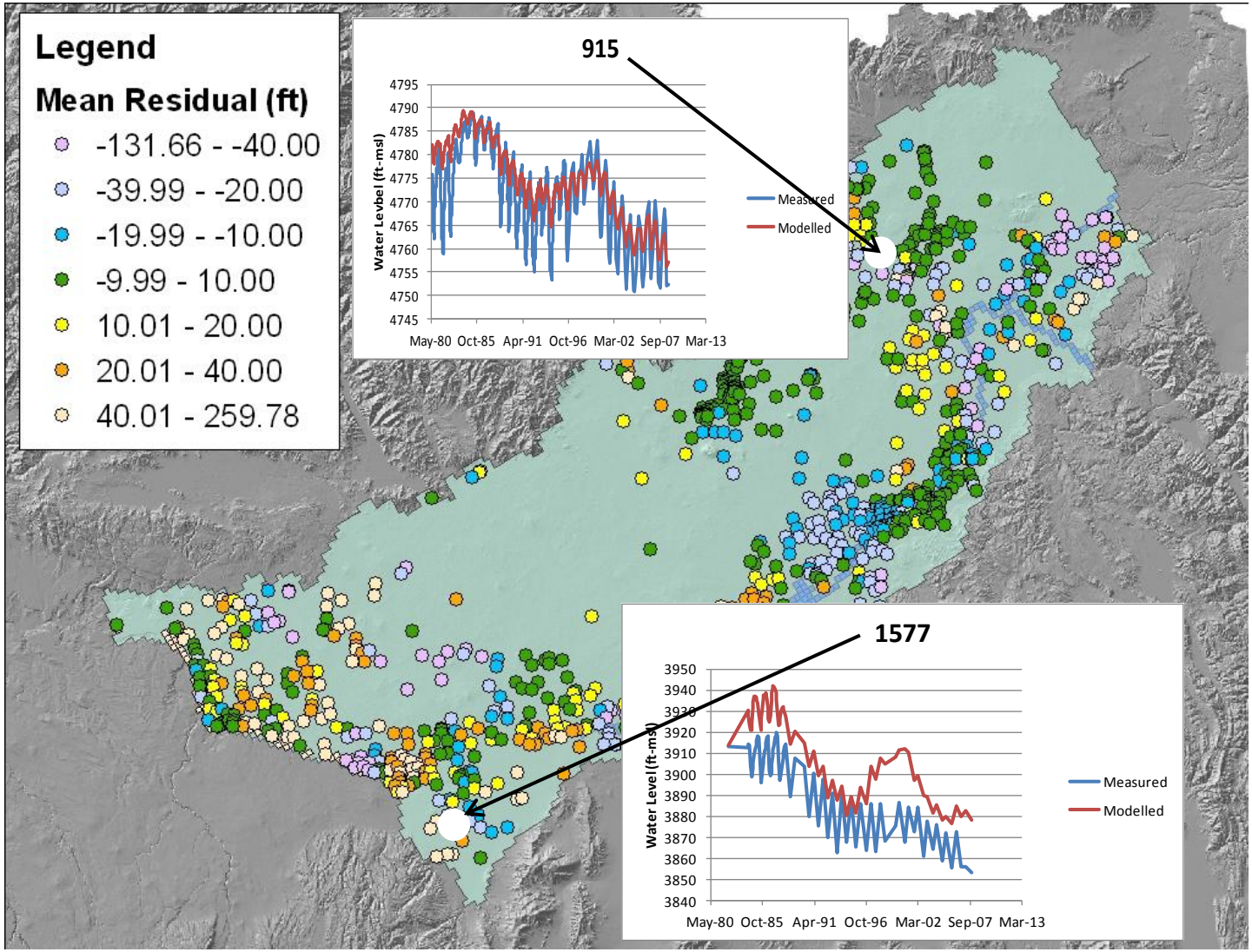

Figure 74. Simulated versus observed water levels for wells 915 and 1577.

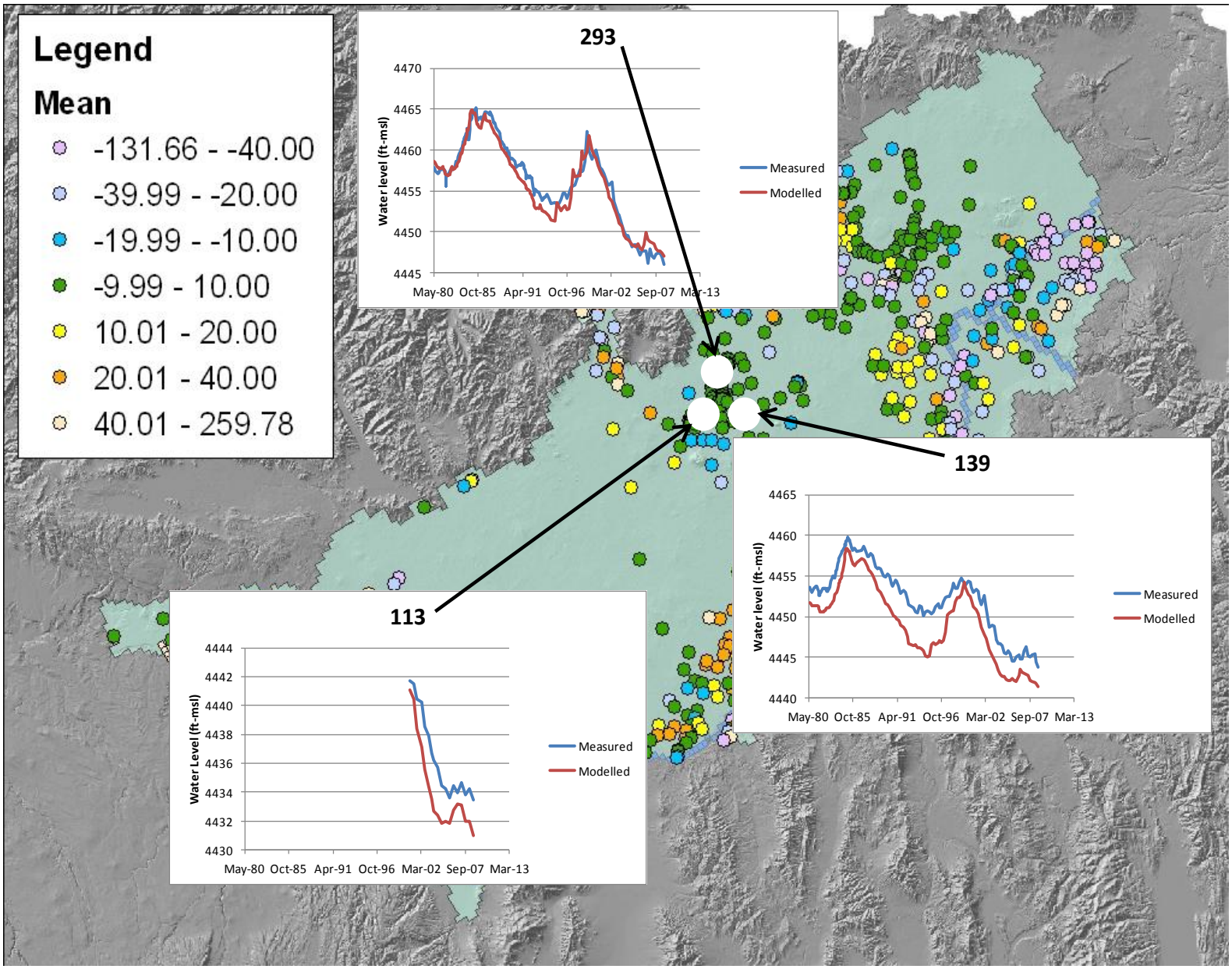

Figure 75. Simulated versus observed water levels for wells 113, 139, and 293.

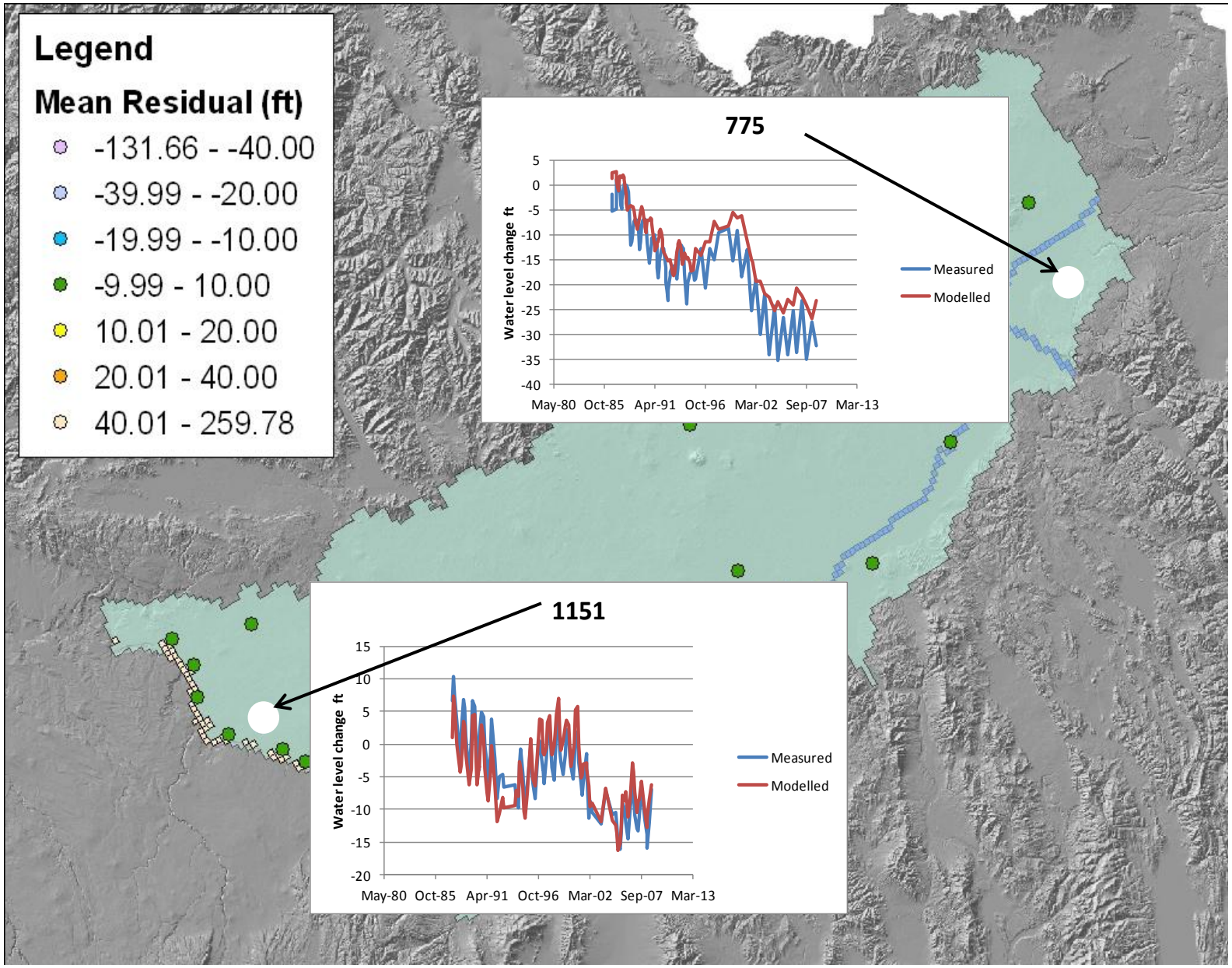

Figure 76. Simulated versus observed water level change for wells 775 and 1151.

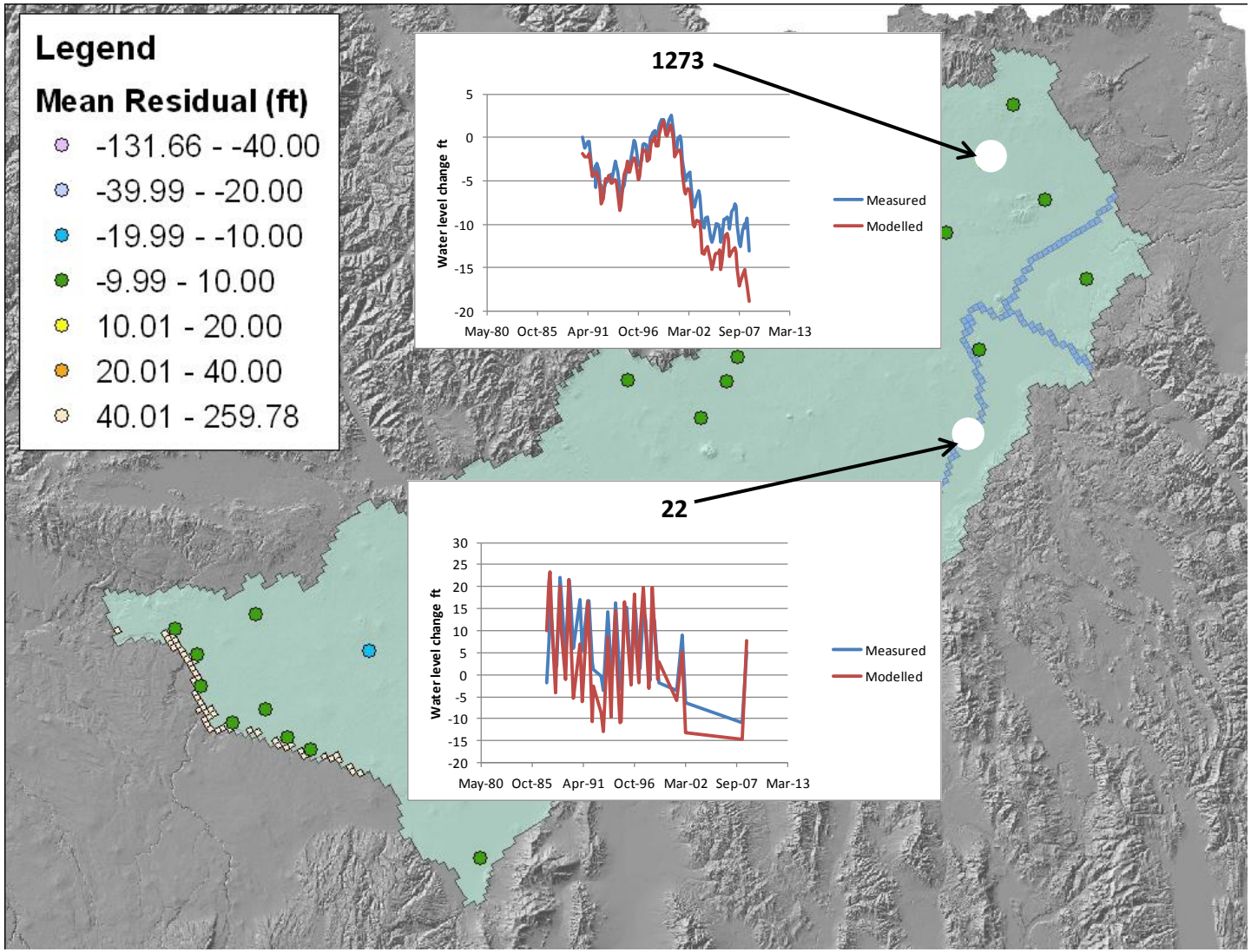

Figure 77. Simluated versus observed water level change for wells 22 and 1273.

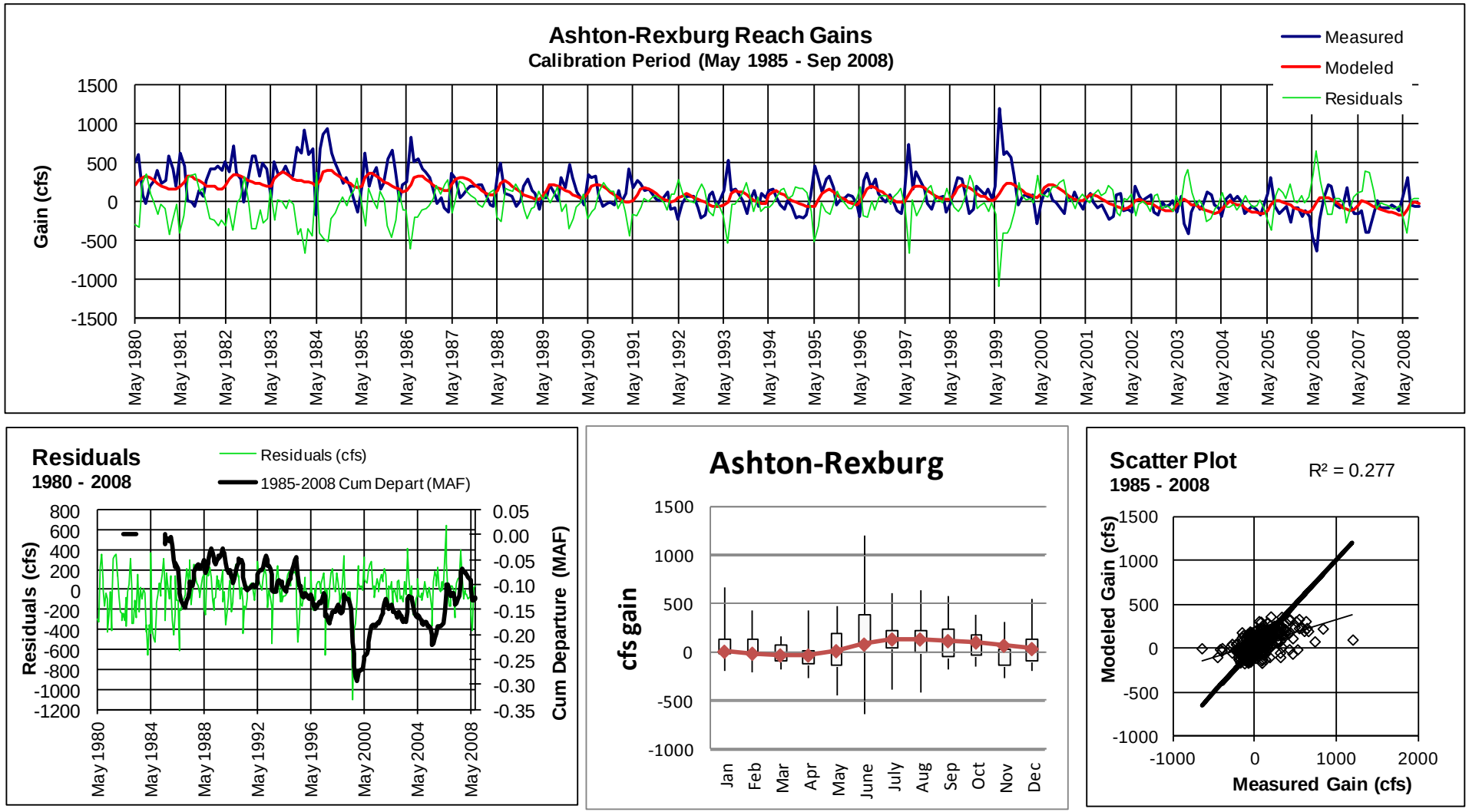

Figure 78. Reach gains in the Ashton-to-Rexburg reach. The top chart shows the measured gains, modeled gains, and residual over the calibration period. The lower chart figure shows the cumulative departures. The lower middle chart is a Box-and-Whisker plot of the gains. The lower right chart is a scatter plot of modeled gains against measured gains.

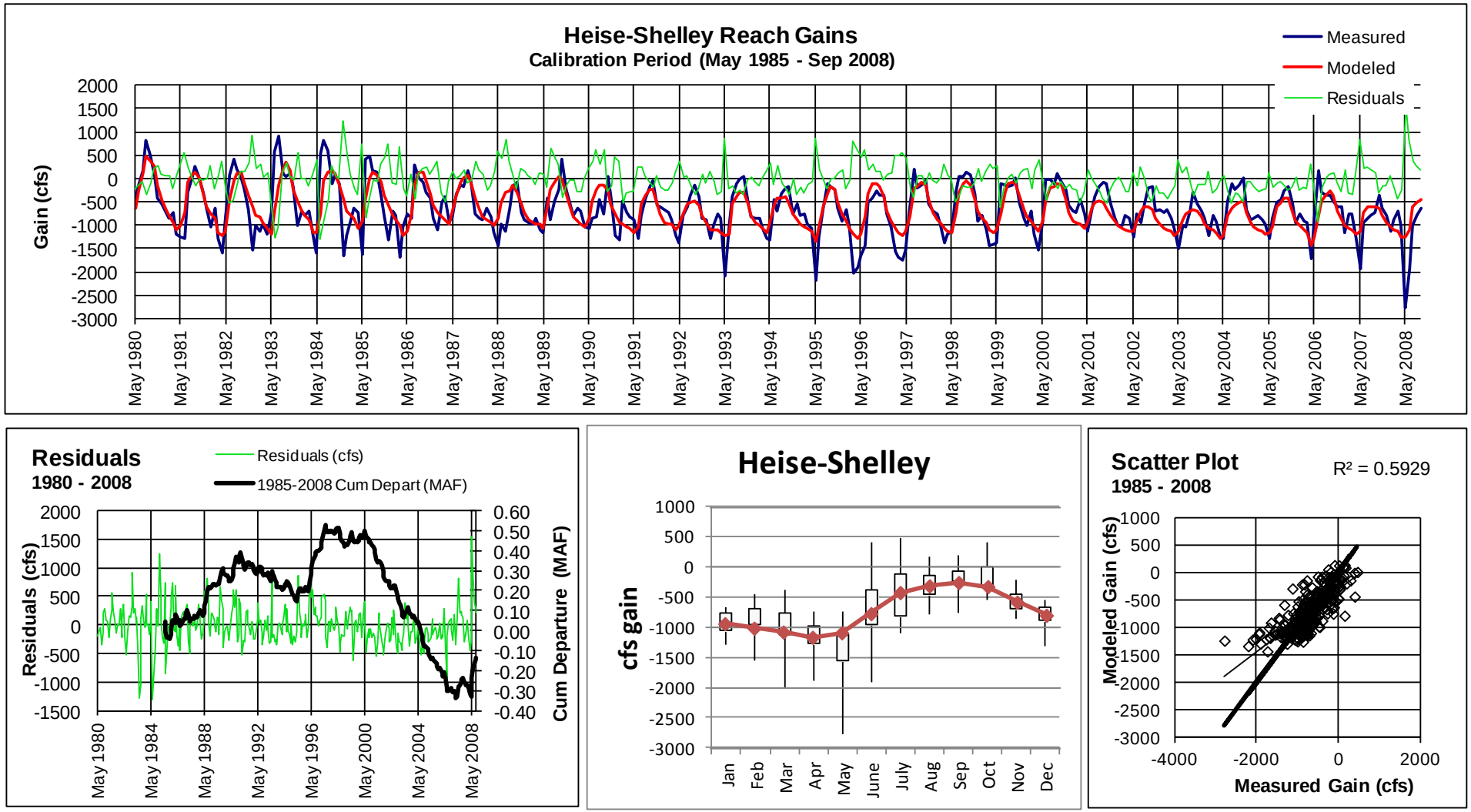

Figure 79. Reach gains in the Heise-to-Shelley reach. The top chart shows the measured gains, modeled gains, and residual over the calibration period. The lower chart figure shows the cumulative departures. The lower middle chart is a Box-and-Whisker plot of the gains. The lower right chart is a scatter plot of modeled gains against measured gains.

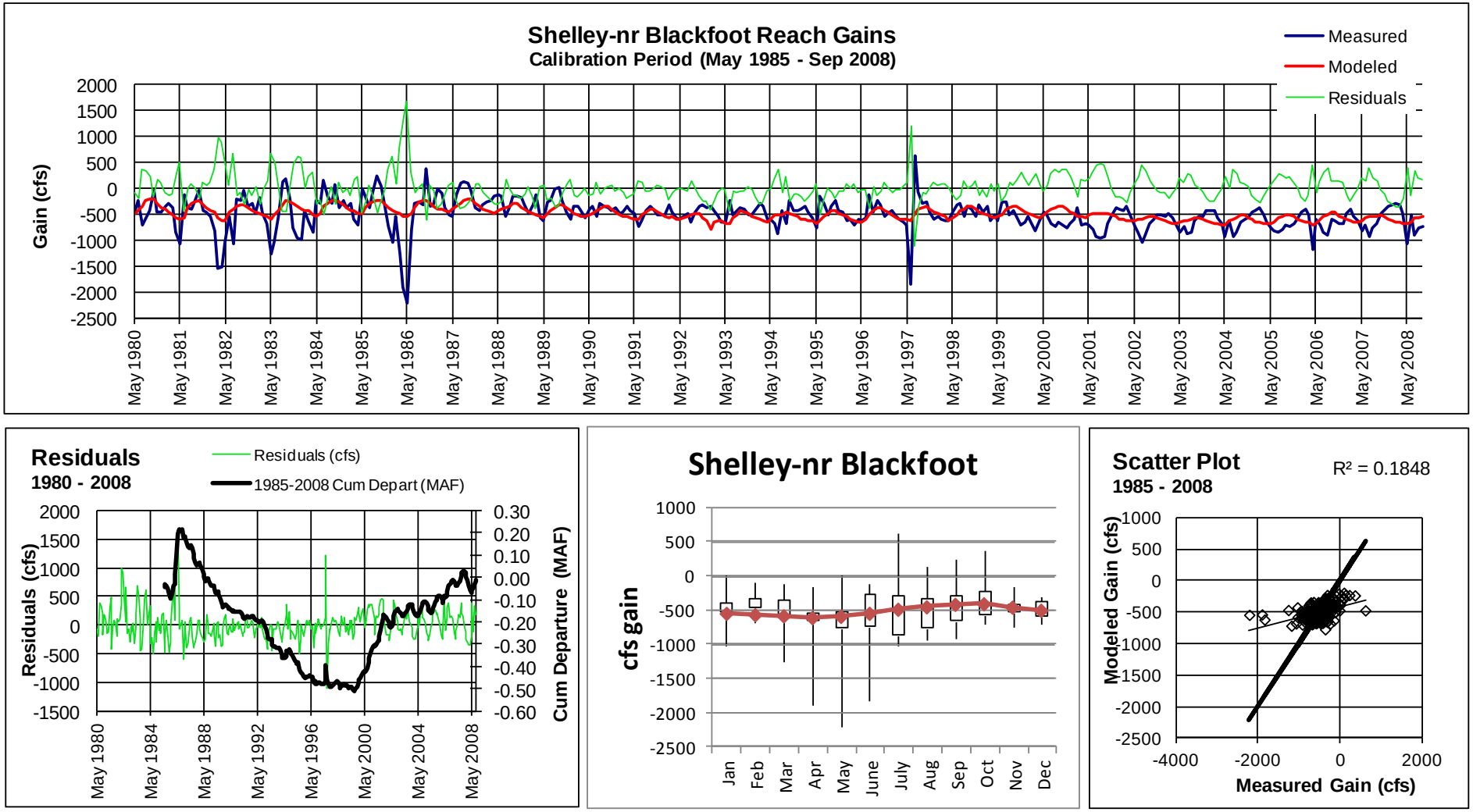

Figure 80. Reach gains in the Shelley-to-near Blackfoot reach. The top chart shows the measured gains, modeled gains, and residual over the calibration period. The lower chart figure shows the cumulative departures. The lower middle chart is a Box-and-Whisker plot of the gains. The lower right chart is a scatter plot of modeled gains against measured gains.

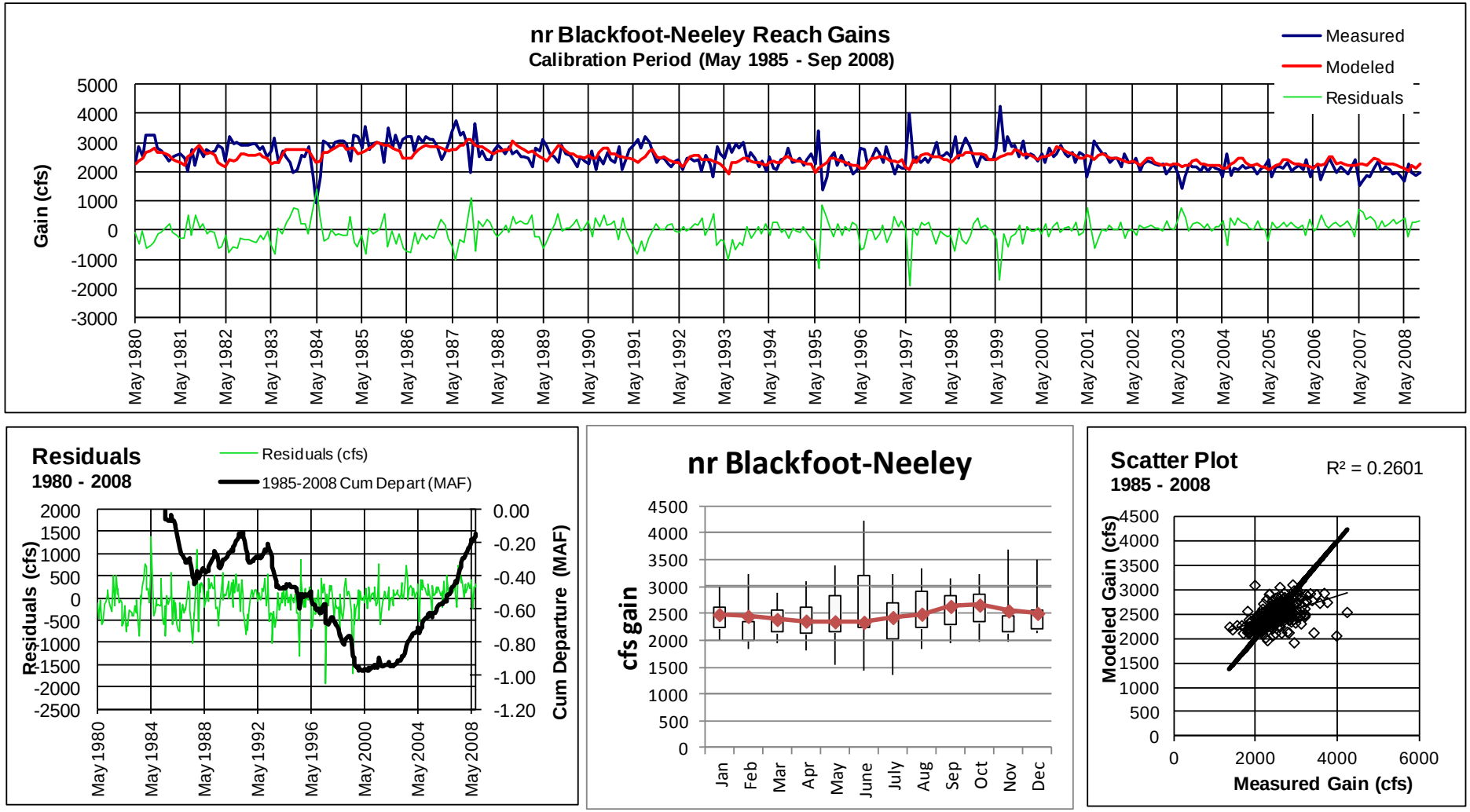

Figure 81. Reach gains in the near Blackfoot-to-Neeley reach. The top chart shows the measured gains, modeled gains, and residual over the calibration period. The lower chart figure shows the cumulative departures. The lower middle chart is a Box-and-Whisker plot of the gains. The lower right chart is a scatter plot of modeled gains against measured gains.

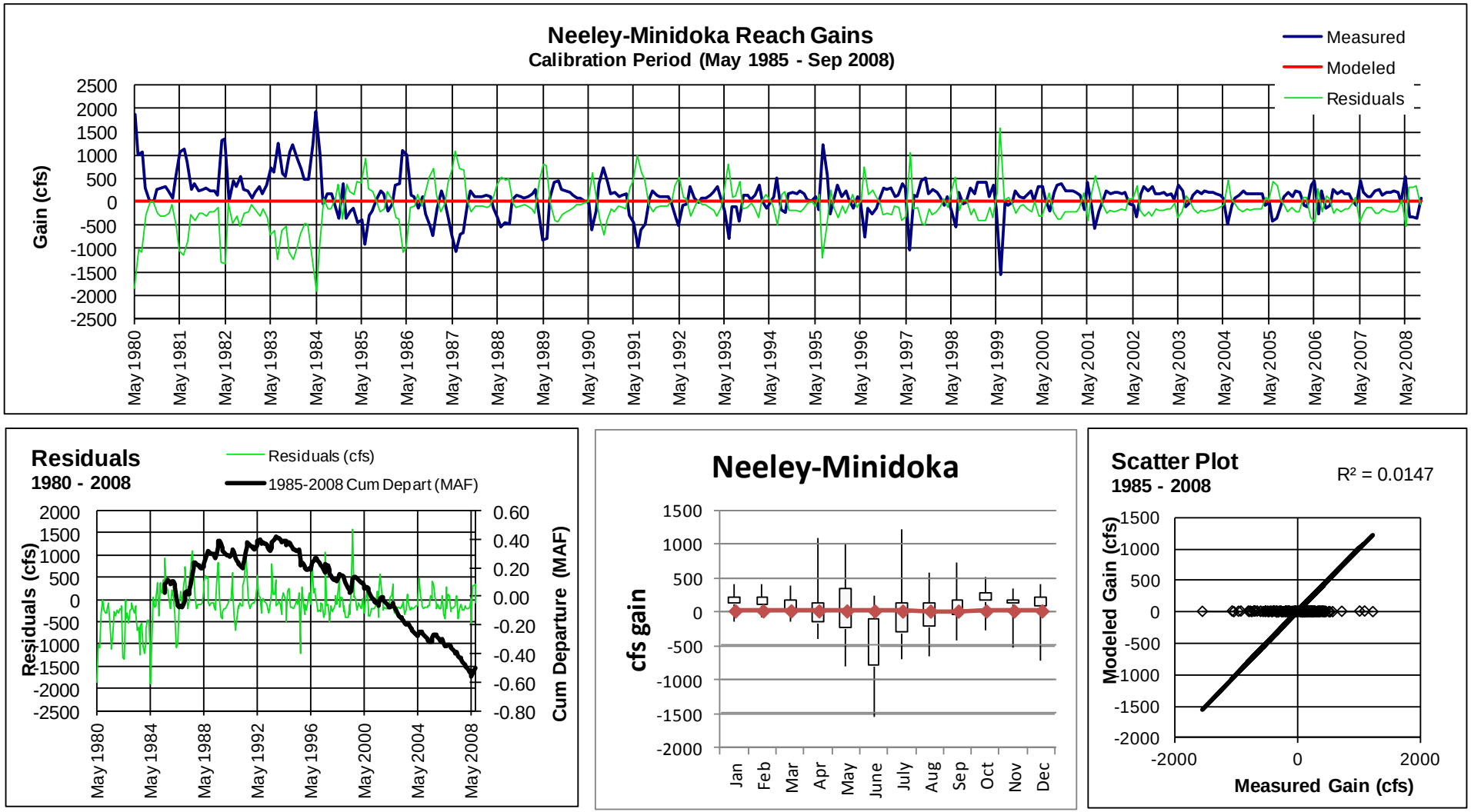

Figure 82. Reach gains in the Neeley-to-Minidoka reach. The top chart shows the measured gains, modeled gains, and residual over the calibration period. The lower chart figure shows the cumulative departures. The lower middle chart is a Box-and-Whisker plot of the gains. The lower right chart is a scatter plot of modeled gains against measured gains.

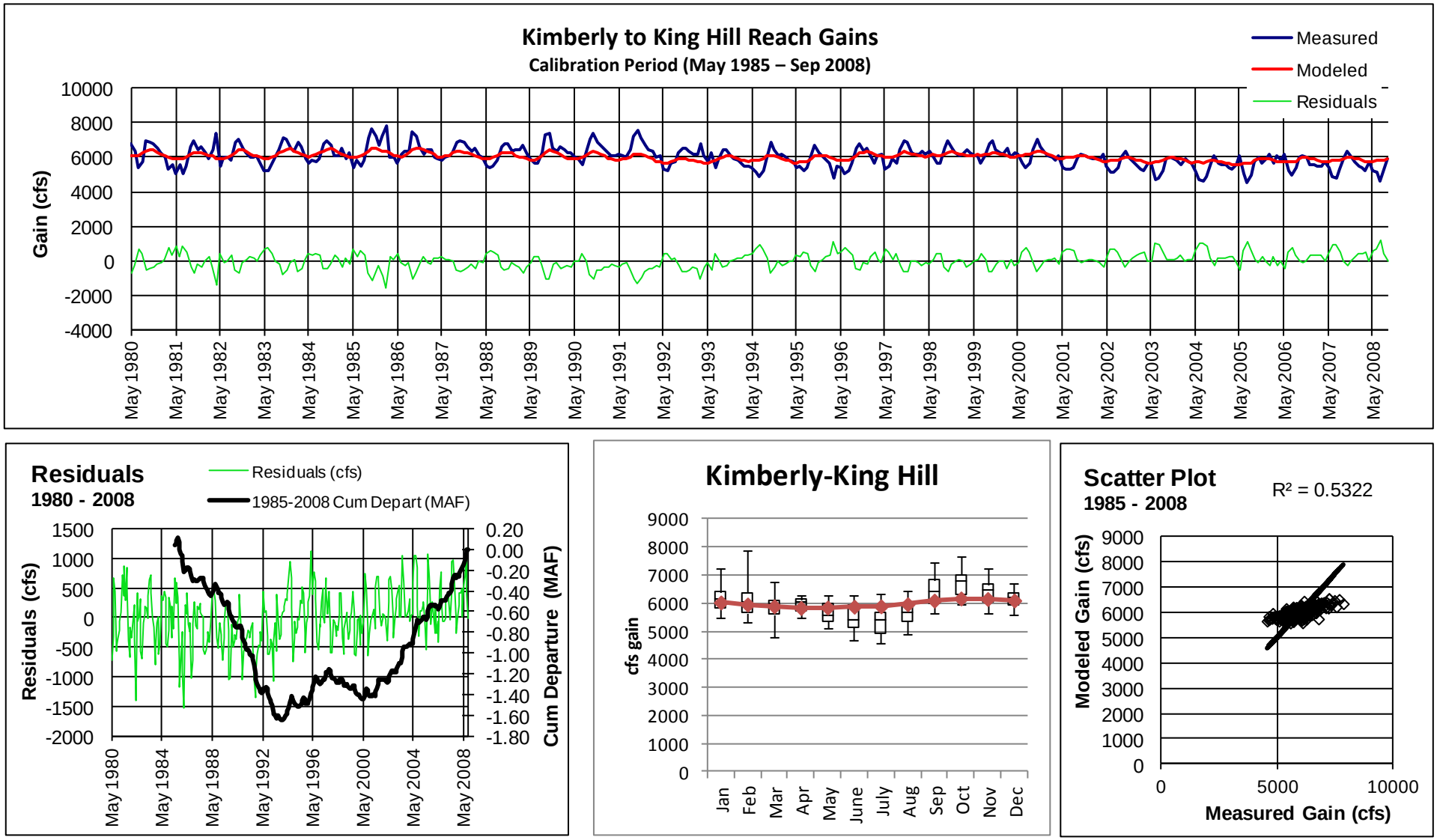

Figure 83. Reach gains in the Kimberly-to-King Hill reach. The top chart shows the measured gains, modeled gains, and residual over the calibration period. The lower chart figure shows the cumulative departures. The lower middle chart is a Box-and-Whisker plot of the gains. The lower right chart is a scatter plot of modeled gains against measured gains.

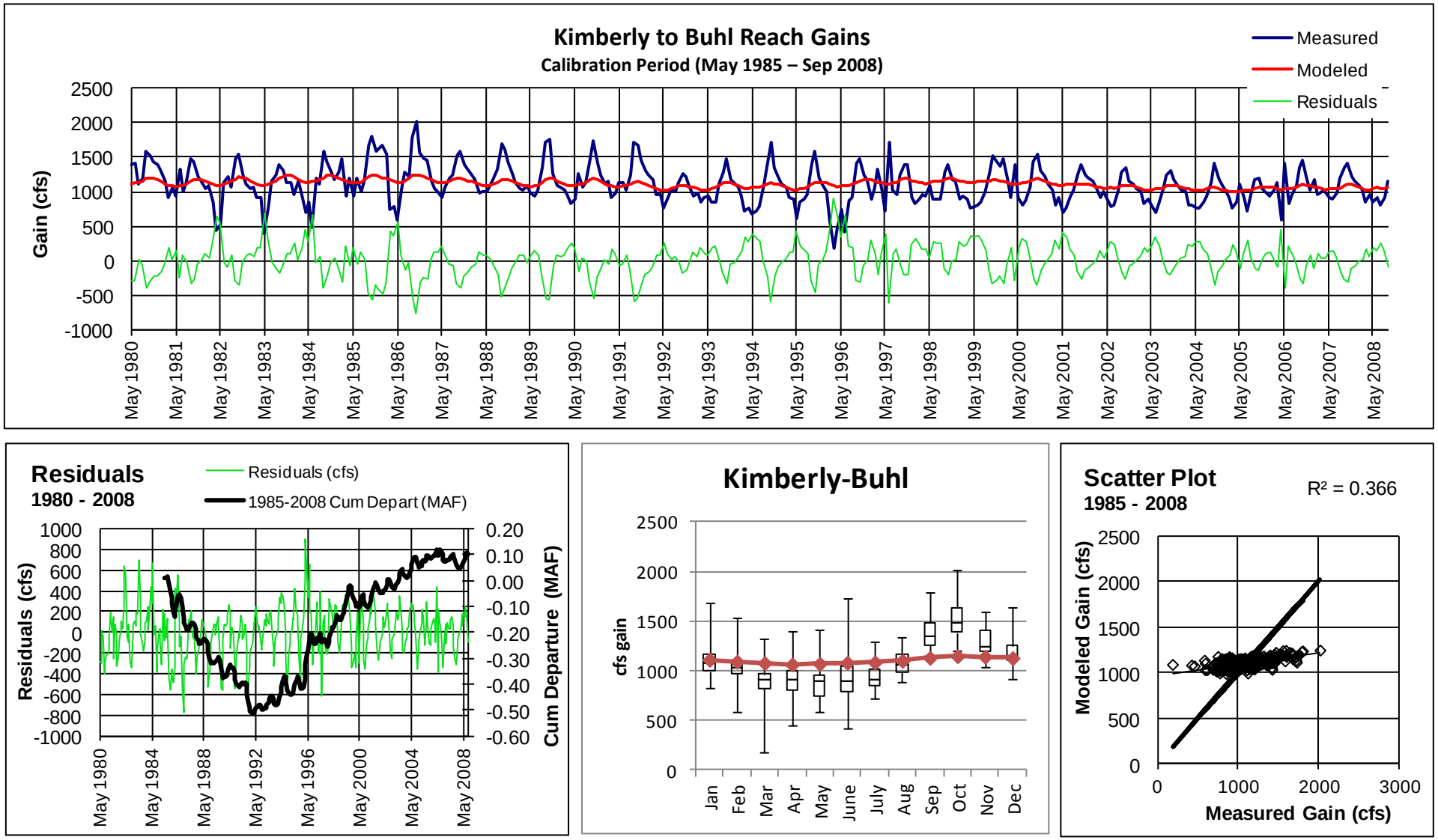

Figure 84. Reach gains in the Kimberly-to-Buhl reach. The top chart shows the measured gains, modeled gains, and residual over the calibration period. The lower chart figure shows the cumulative departures. The lower middle chart is a Box-and-Whisker plot of the gains. The lower right chart is a scatter plot of modeled gains against measured gains.

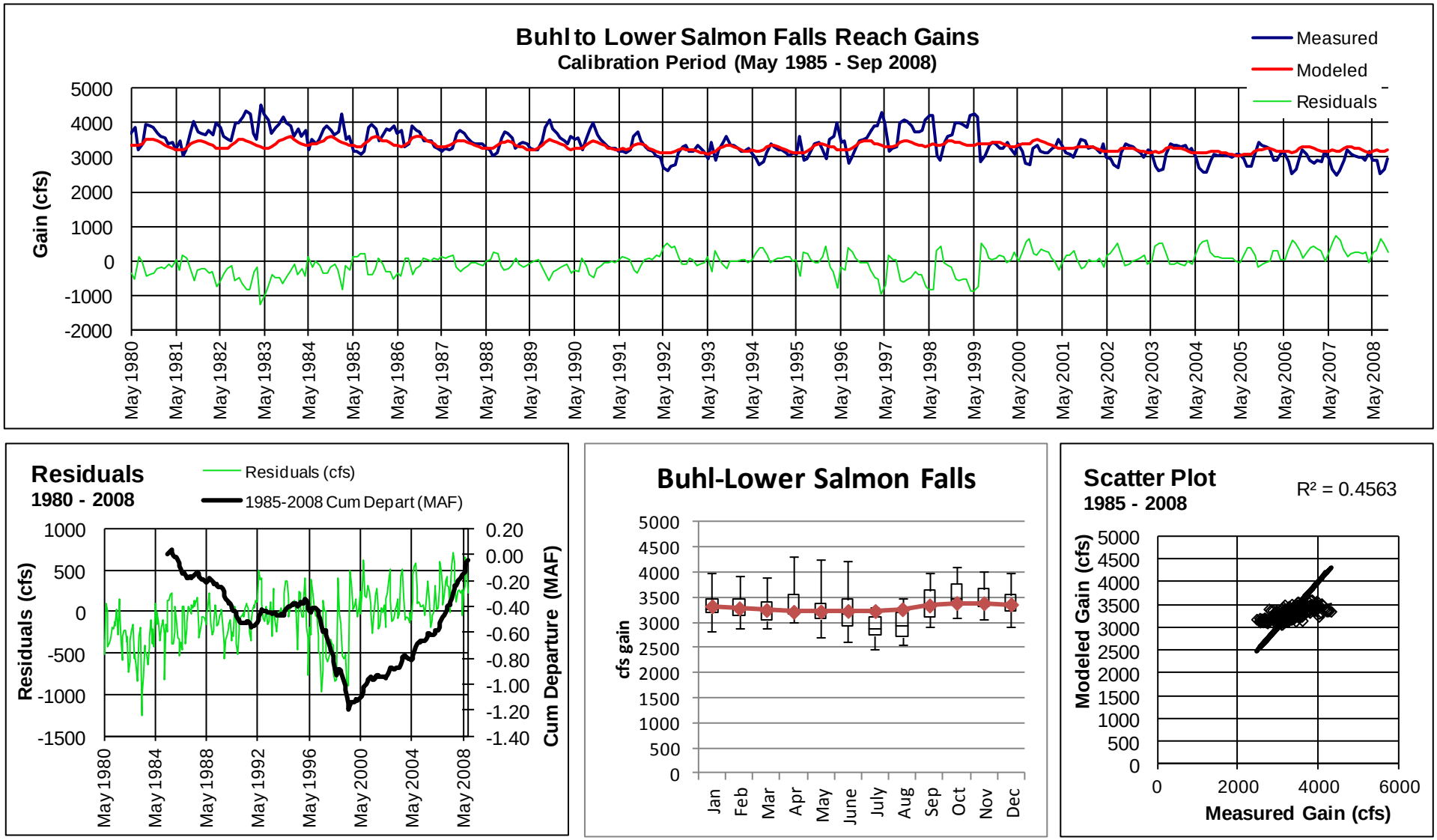

Figure 85. Reach gains in the Buhl-to-Lower Salmon Falls reach. The top chart shows the measured gains, modeled gains, and residual over the calibration period. The lower chart figure shows the cumulative departures. The lower middle chart is a Box-and-Whisker plot of the gains. The lower right chart is a scatter plot of modeled gains against measured gains.

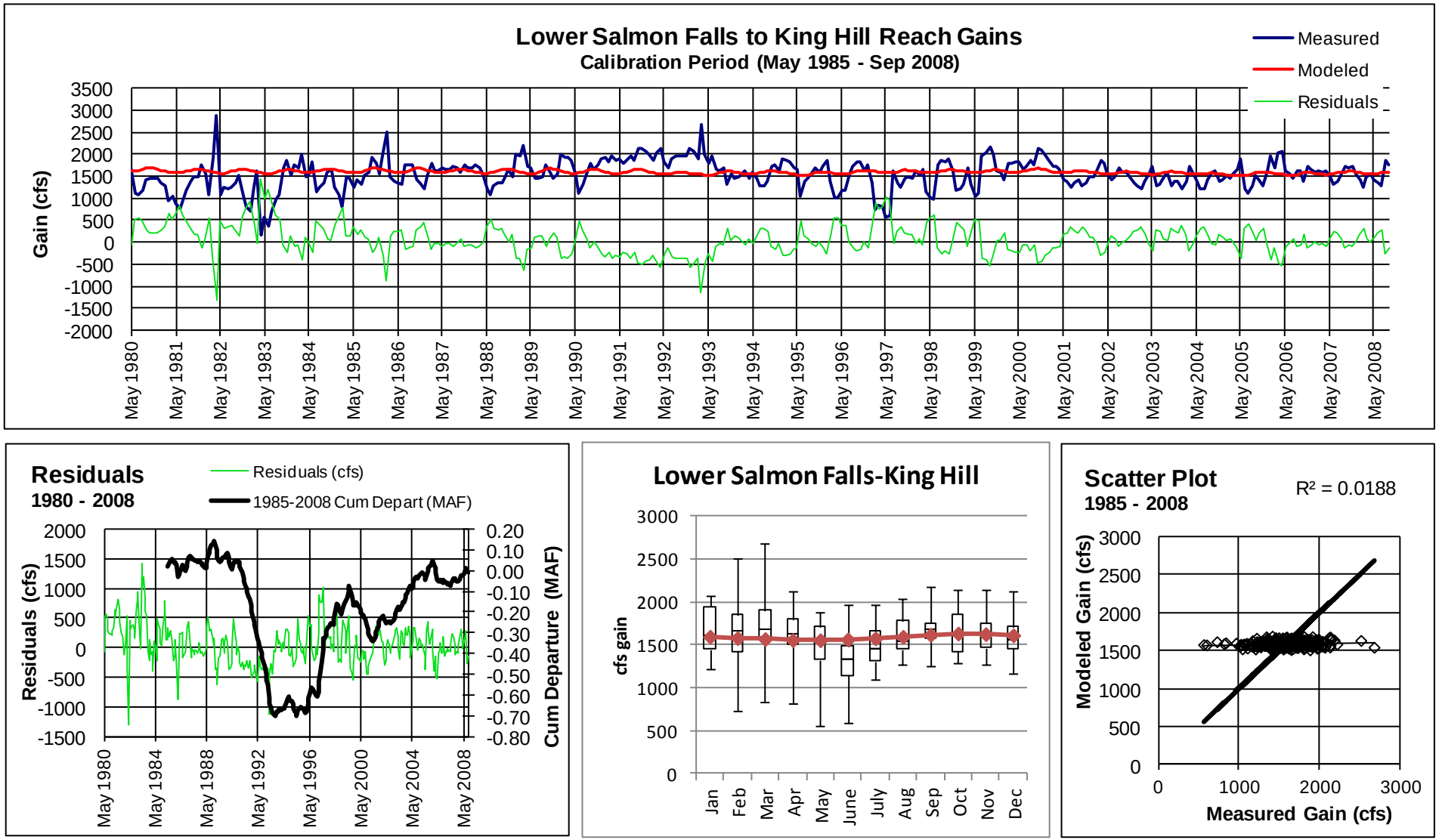

Figure 86. Reach gains in the Lower Salmon Falls-to-King Hill reach. The top chart shows the measured gains, modeled gains, and residual over the calibration period. The lower chart figure shows the cumulative departures. The lower middle chart is a Box-and-Whisker plot of the gains. The lower right chart is a scatter plot of modeled gains against measured gains.

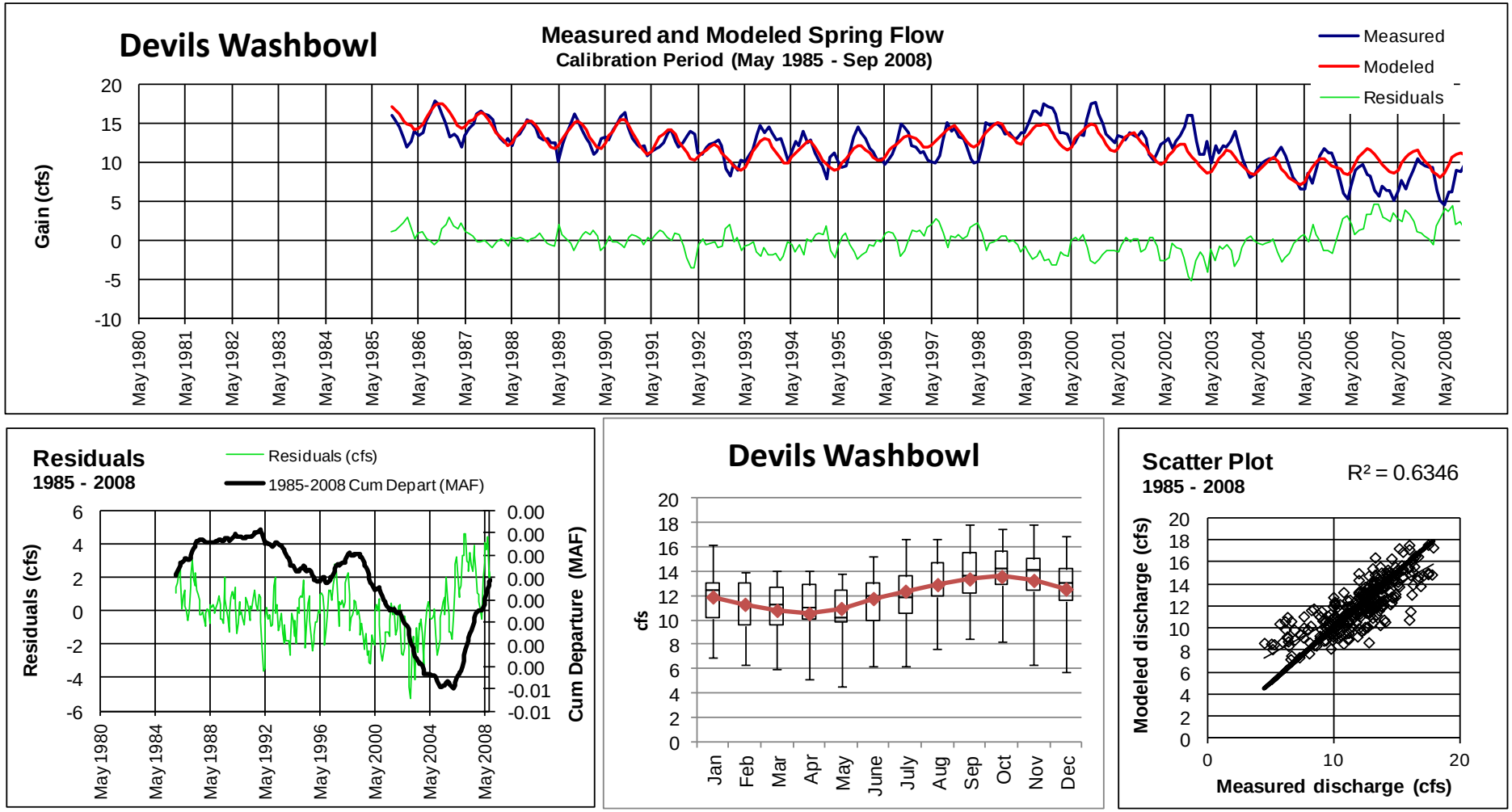

Figure 87. Spring flow for Devils Washbowl. The top chart shows the measured gains, modeled gains, and residual over the calibration period. The lower chart figure shows the cumulative departures. The lower middle chart is a Box-and-Whisker plot of the gains. The lower right chart is a scatter plot of modeled gains against measured gains.

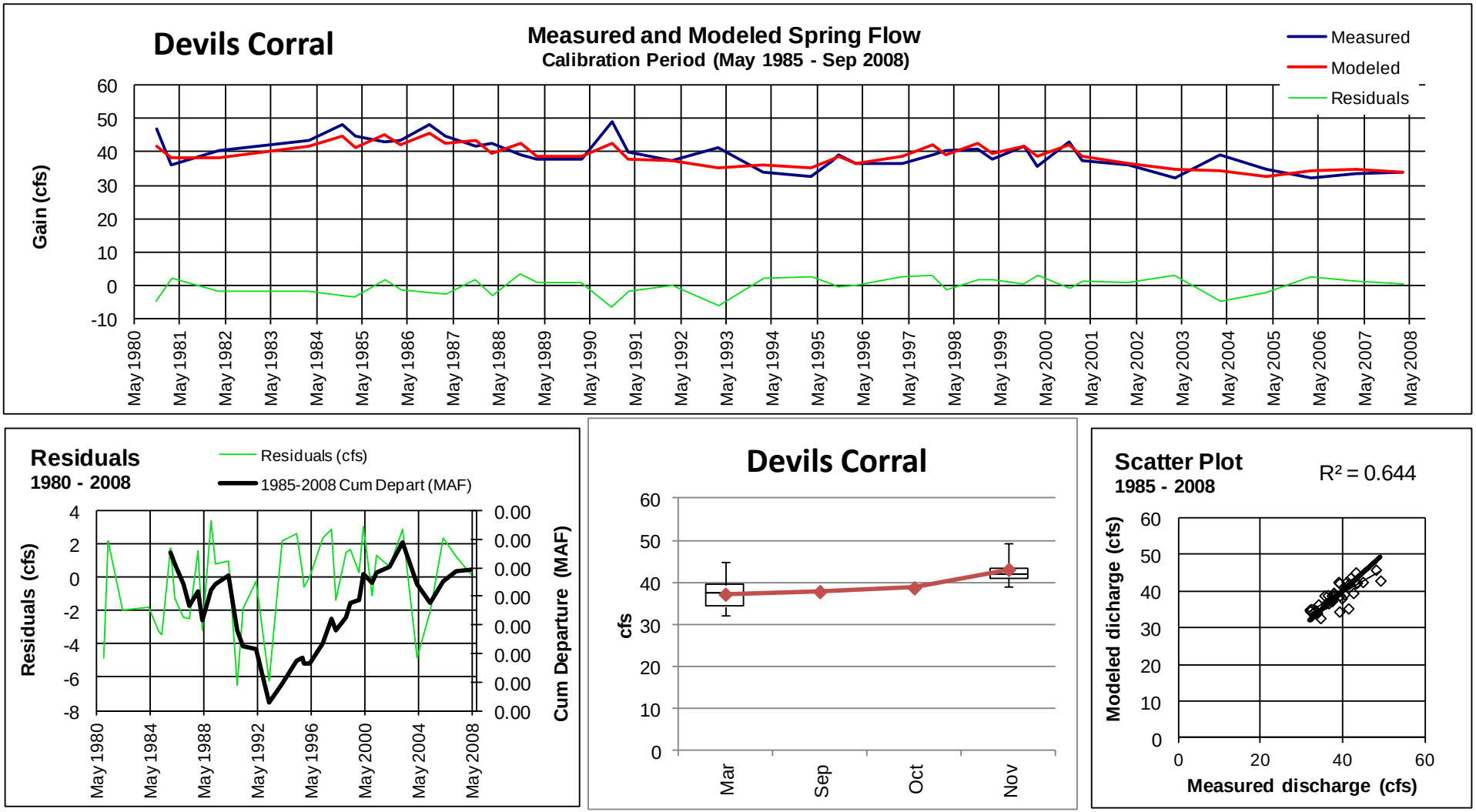

Figure 88. Spring flow for Devils Corral. The top chart shows the measured gains, modeled gains, and residual over the calibration period. The lower chart figure shows the cumulative departures. The lower middle chart is a Box-and-Whisker plot of the gains. The lower right chart is a scatter plot of modeled gains against measured gains.

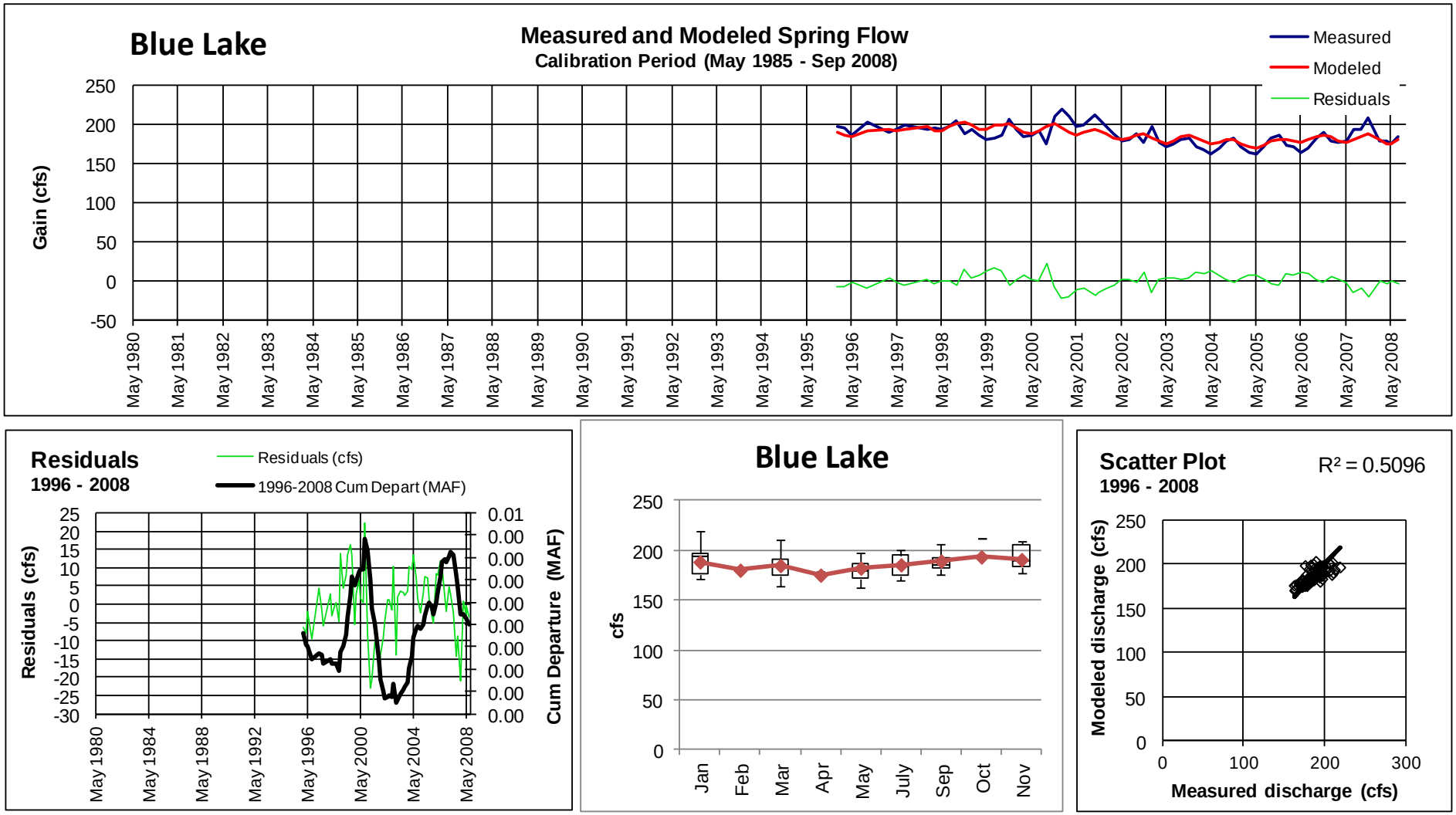

Figure 89. Spring flow for Blue Lake. The top chart shows the measured gains, modeled gains, and residual over the calibration period. The lower chart figure shows the cumulative departures. The lower middle chart is a Box-and-Whisker plot of the gains. The lower right chart is a scatter plot of modeled gains against measured gains.

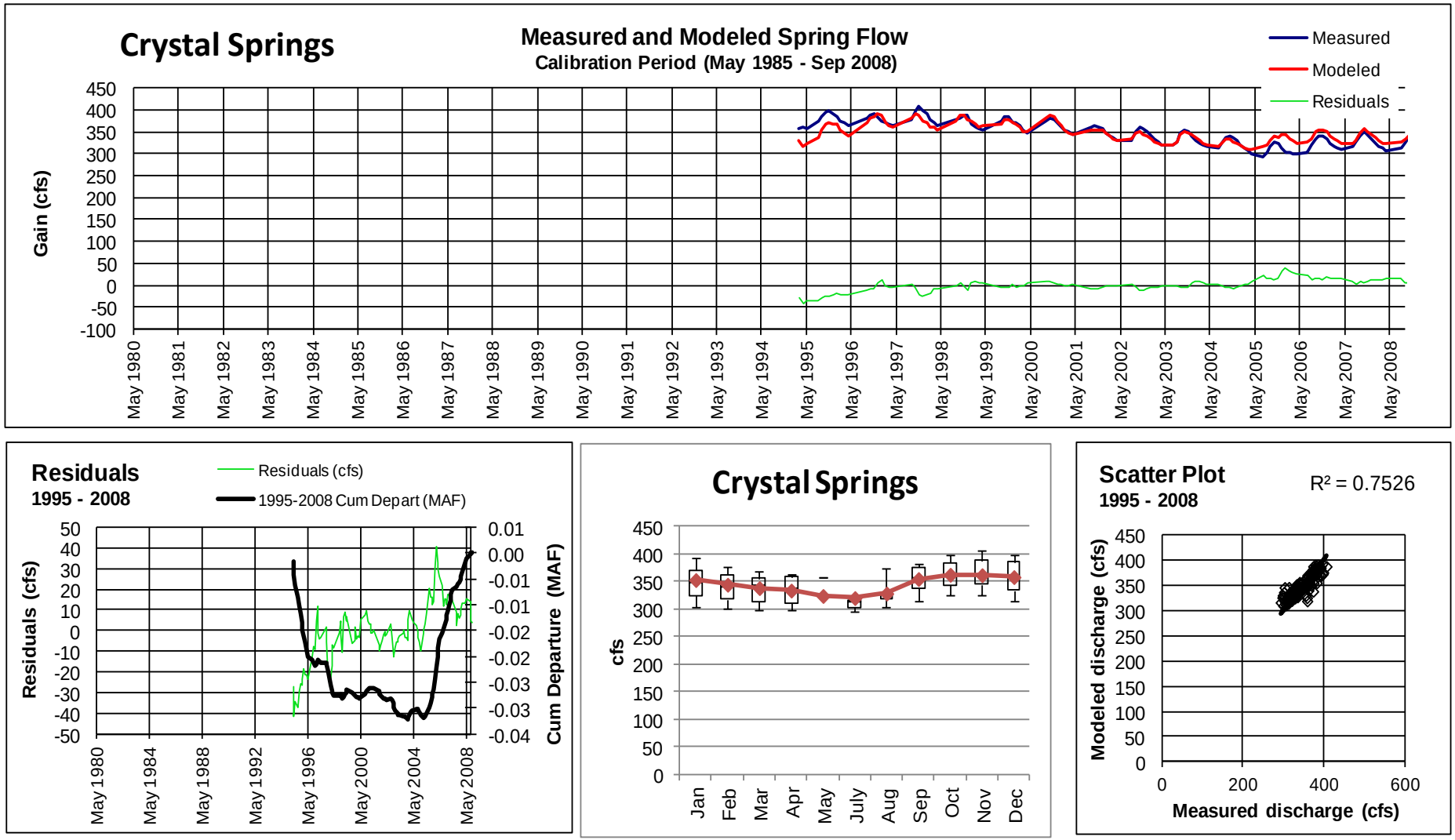

Figure 90. Spring flow for Crystal Springs. The top chart shows the measured gains, modeled gains, and residual over the calibration period. The lower chart figure shows the cumulative departures. The lower middle chart is a Box-and-Whisker plot of the gains. The lower right chart is a scatter plot of modeled gains against measured gains.

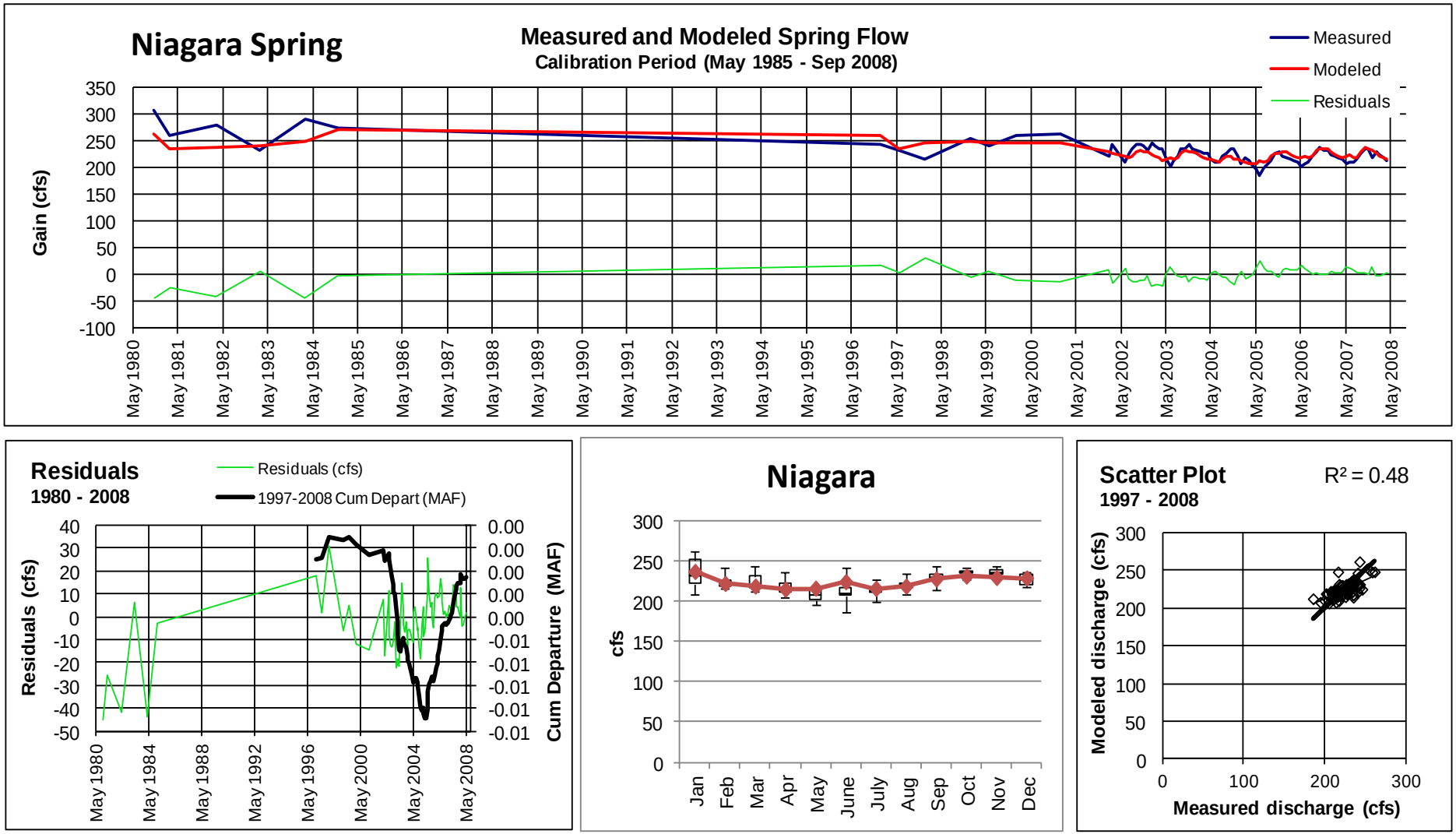

Figure 91. Spring flow for Niagara Spring. The top chart shows the measured gains, modeled gains, and residual over the calibration period. The lower chart figure shows the cumulative departures. The lower middle chart is a Box-and-Whisker plot of the gains. The lower right chart is a scatter plot of modeled gains against measured gains.

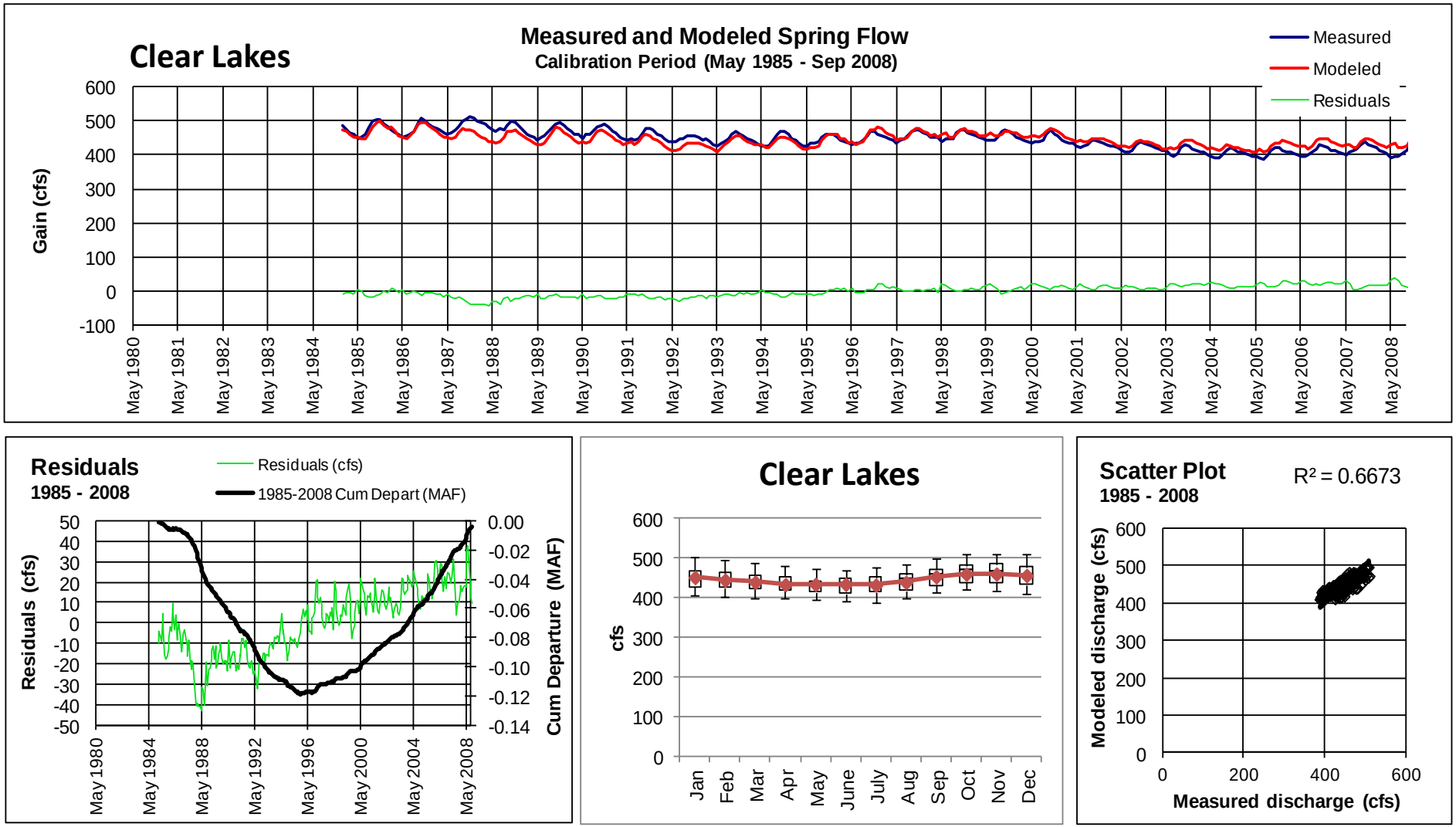

Figure 92. Spring flow for Clear Lakes Spring. The top chart shows the measured gains, modeled gains, and residual over the calibration period. The lower chart figure shows the cumulative departures. The lower middle chart is a Box-and-Whisker plot of the gains. The lower right chart is a scatter plot of modeled gains against measured gains.

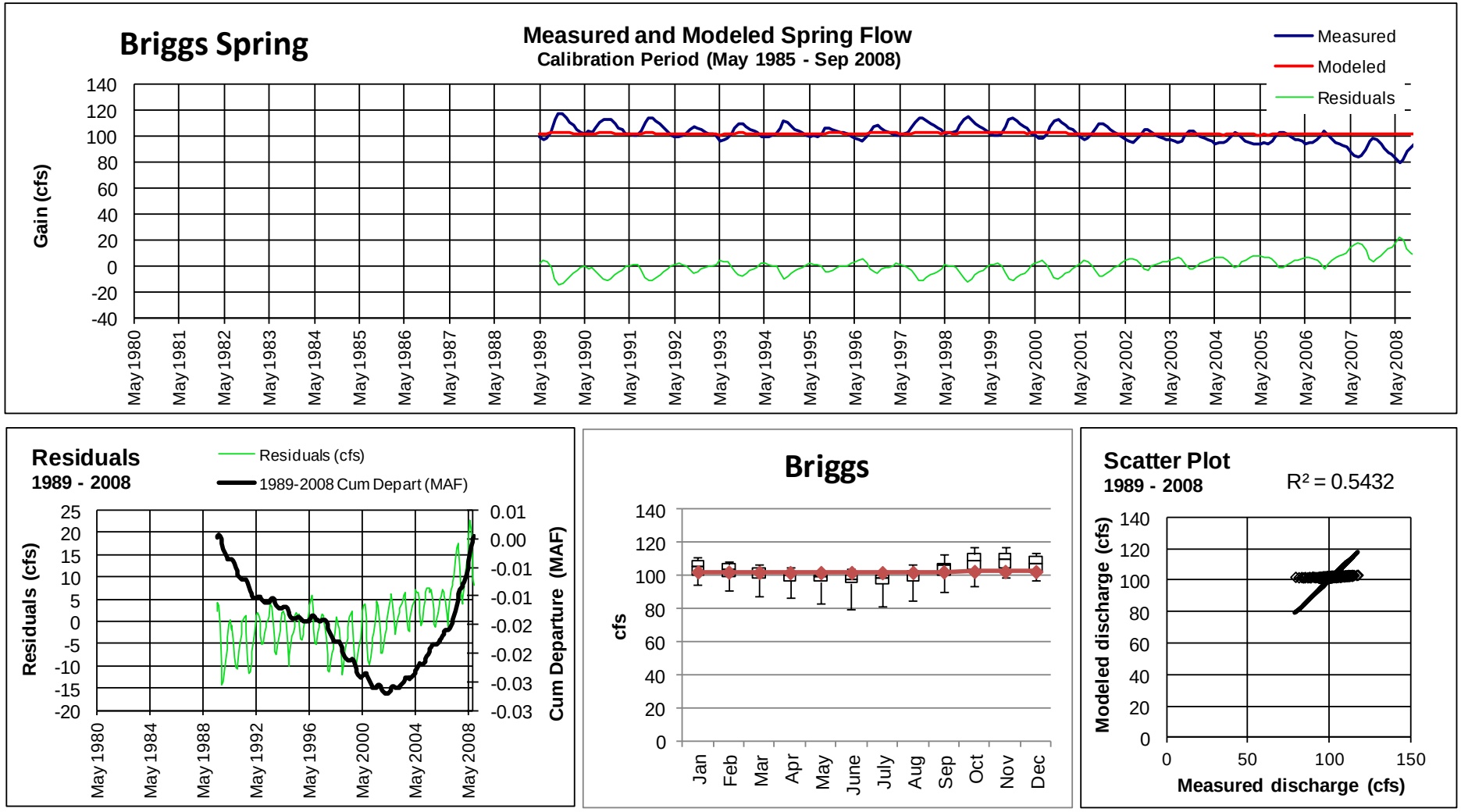

Figure 93. Spring flow for Briggs Spring. The top chart shows the measured gains, modeled gains, and residual over the calibration period. The lower chart figure shows the cumulative departures. The lower middle chart is a Box-and-Whisker plot of the gains. The lower right chart is a scatter plot of modeled gains against measured gains.

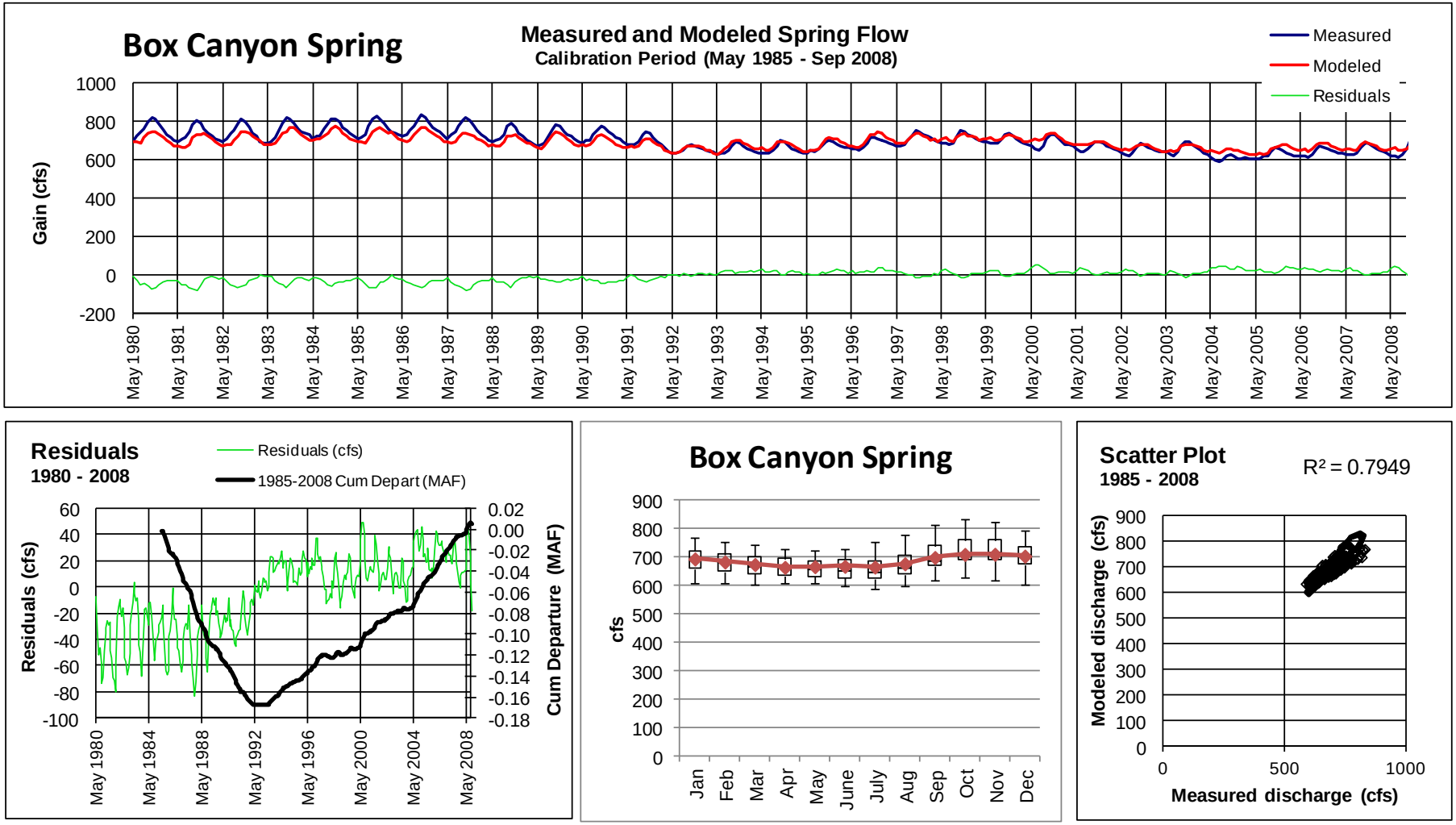

Figure 94. Spring flow for Box Canyon Spring. The top chart shows the measured gains, modeled gains, and residual over the calibration period. The lower chart figure shows the cumulative departures. The lower middle chart is a Box-and-Whisker plot of the gains. The lower right chart is a scatter plot of modeled gains against measured gains.

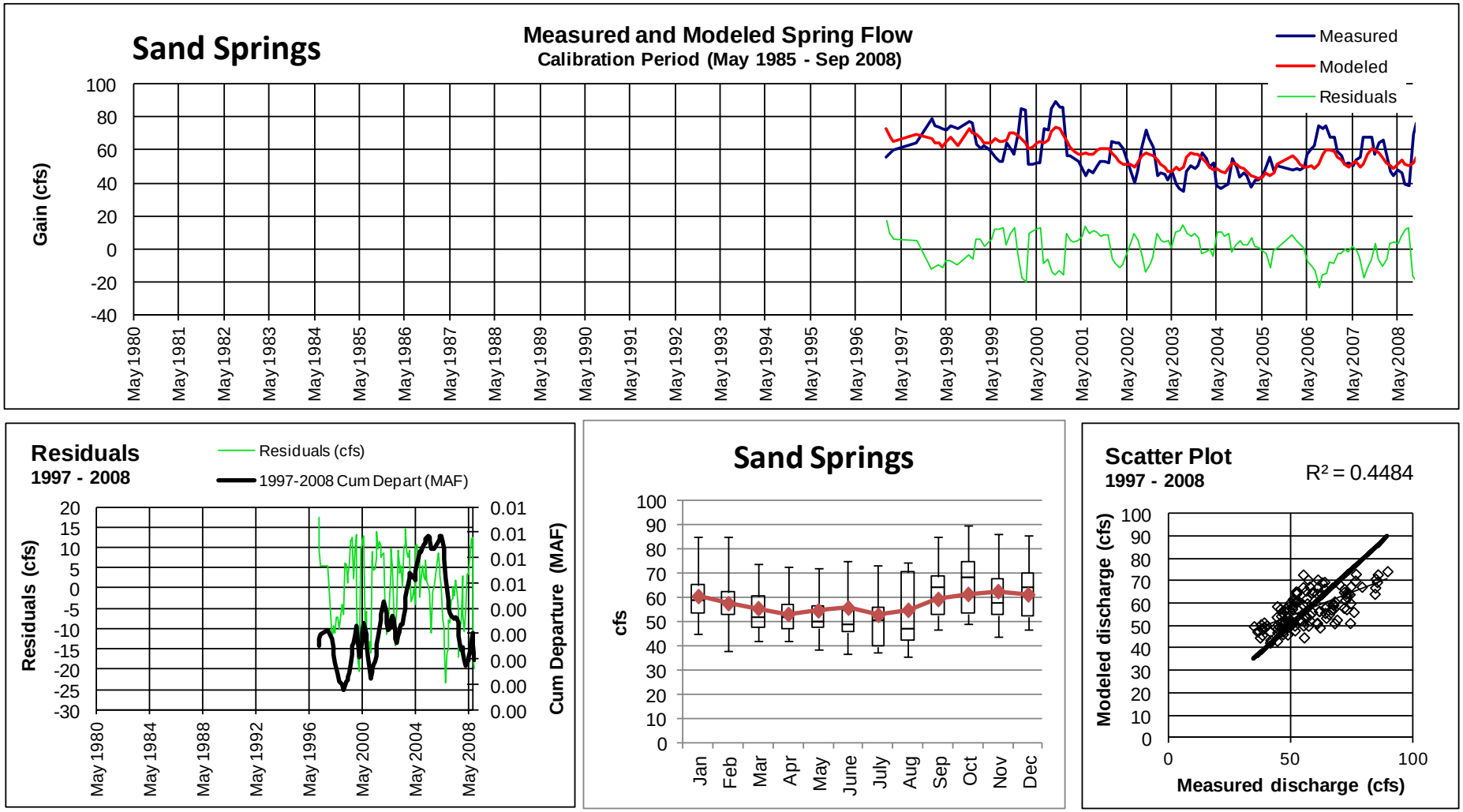

Figure 95. Spring flow for Sand Springs. The top chart shows the measured gains, modeled gains, and residual over the calibration period. The lower chart figure shows the cumulative departures. The lower middle chart is a Box-and-Whisker plot of the gains. The lower right chart is a scatter plot of modeled gains against measured gains.

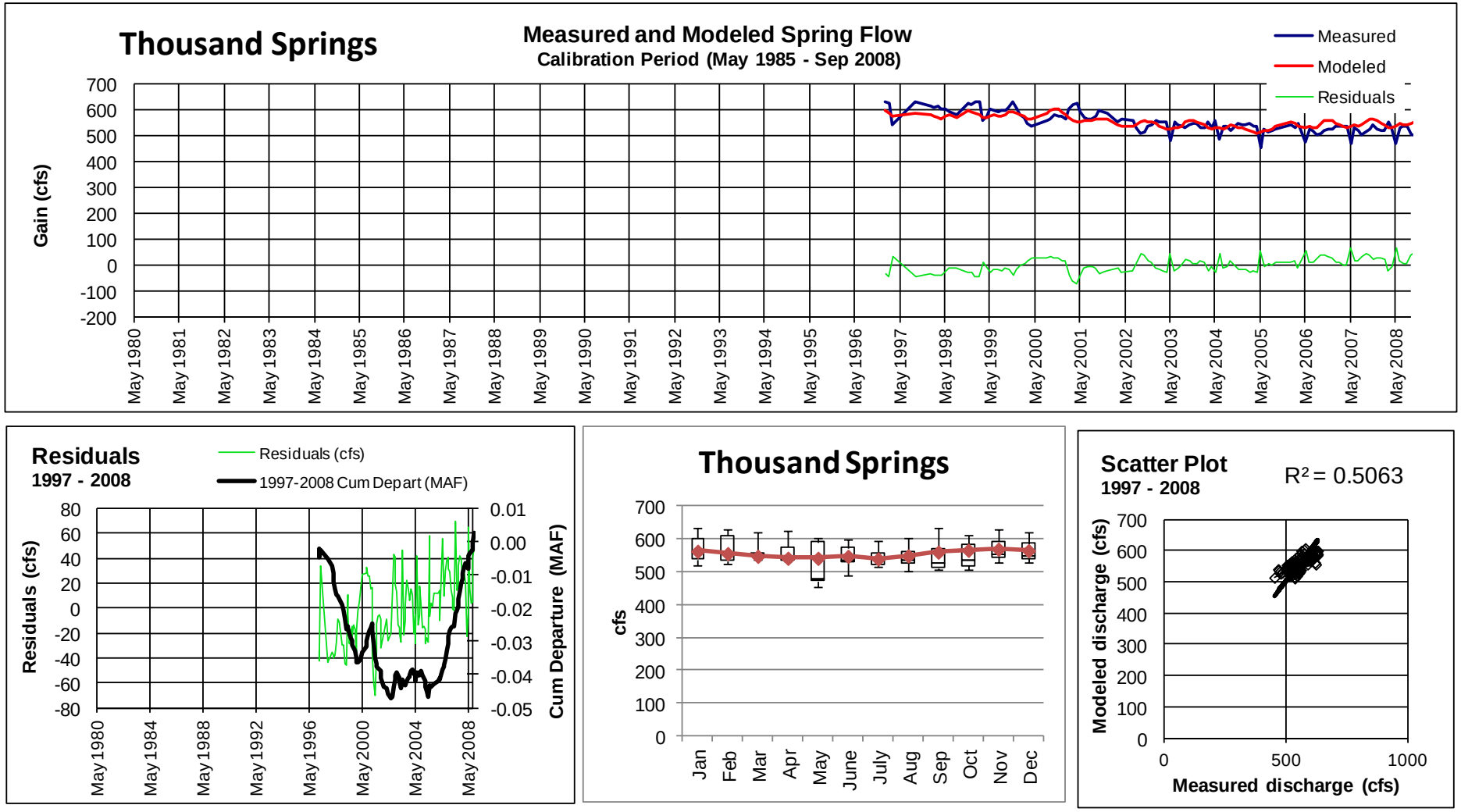

Figure 96. Spring flow for Thousand Springs. The top chart shows the measured gains, modeled gains, and residual over the calibration period. The lower chart figure shows the cumulative departures. The lower middle chart is a Box-and-Whisker plot of the gains. The lower right chart is a scatter plot of modeled gains against measured gains.

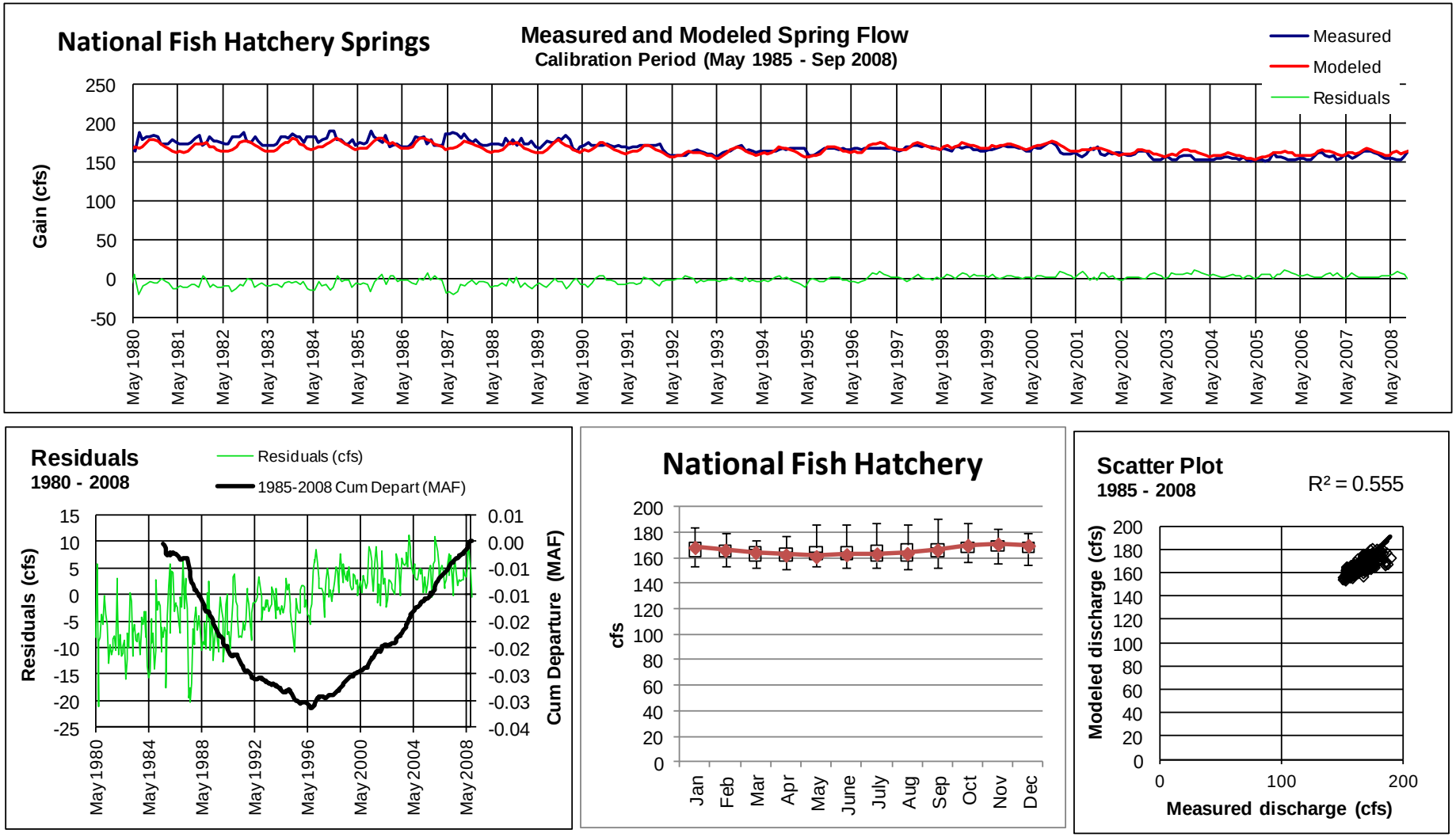

Figure 97. Spring flow for the National Fish Hatchery Springs. The top chart shows the measured gains, modeled gains, and residual over the calibration period. The lower chart figure shows the cumulative departures. The lower middle chart is a Box-and-Whisker plot of the gains. The lower right chart is a scatter plot of modeled gains against measured gains.

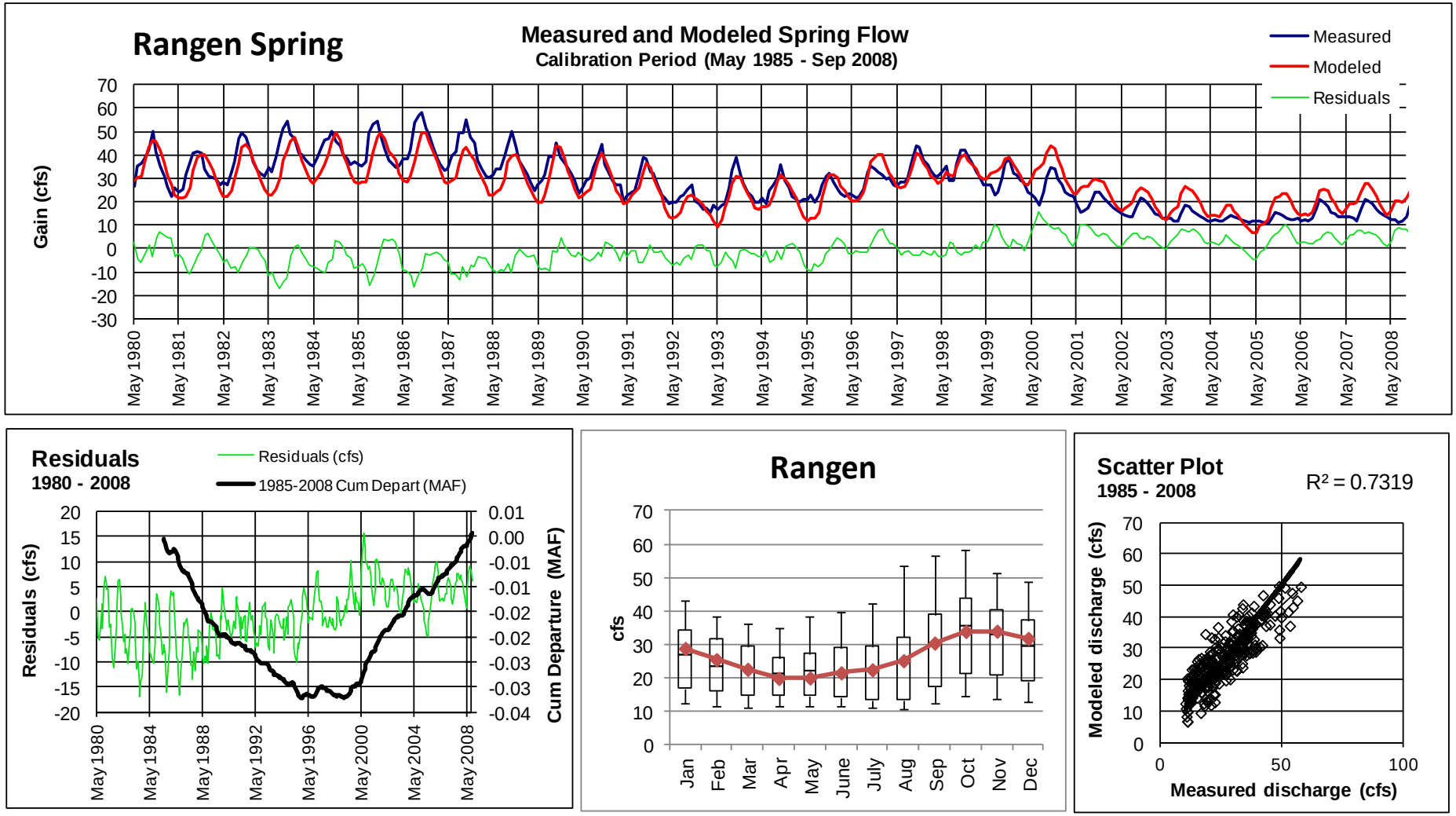

Figure 98. Spring flow for Rangen Spring. The top chart shows the measured gains, modeled gains, and residual over the calibration period. The lower chart figure shows the cumulative departures. The lower middle chart is a Box-and-Whisker plot of the gains. The lower right chart is a scatter plot of modeled gains against measured gains.

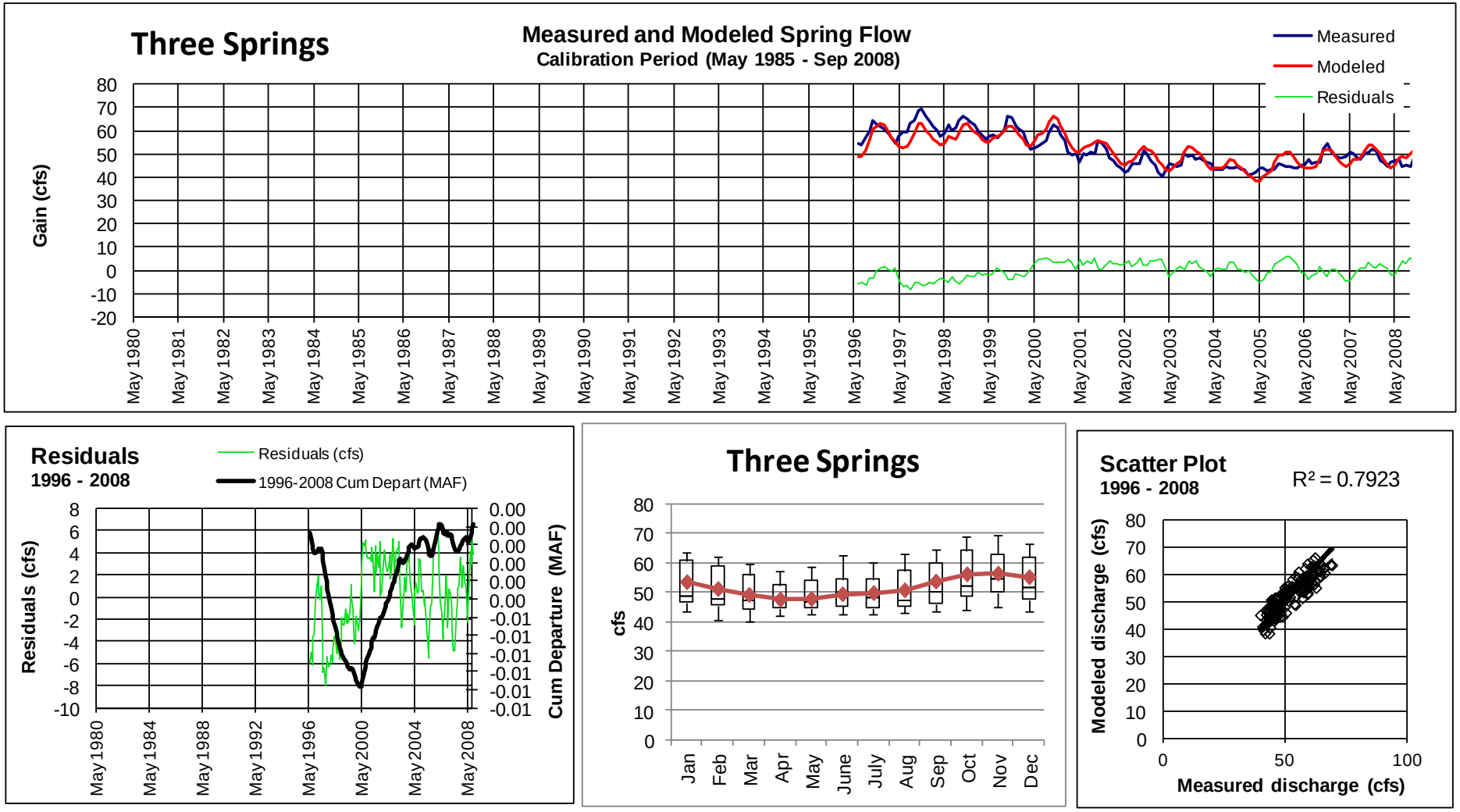

Figure 99. Spring flow for Three Springs. The top chart shows the measured gains, modeled gains, and residual over the calibration period. The lower chart figure shows the cumulative departures. The lower middle chart is a Box-and-Whisker plot of the gains. The lower right chart is a scatter plot of modeled gains against measured gains.

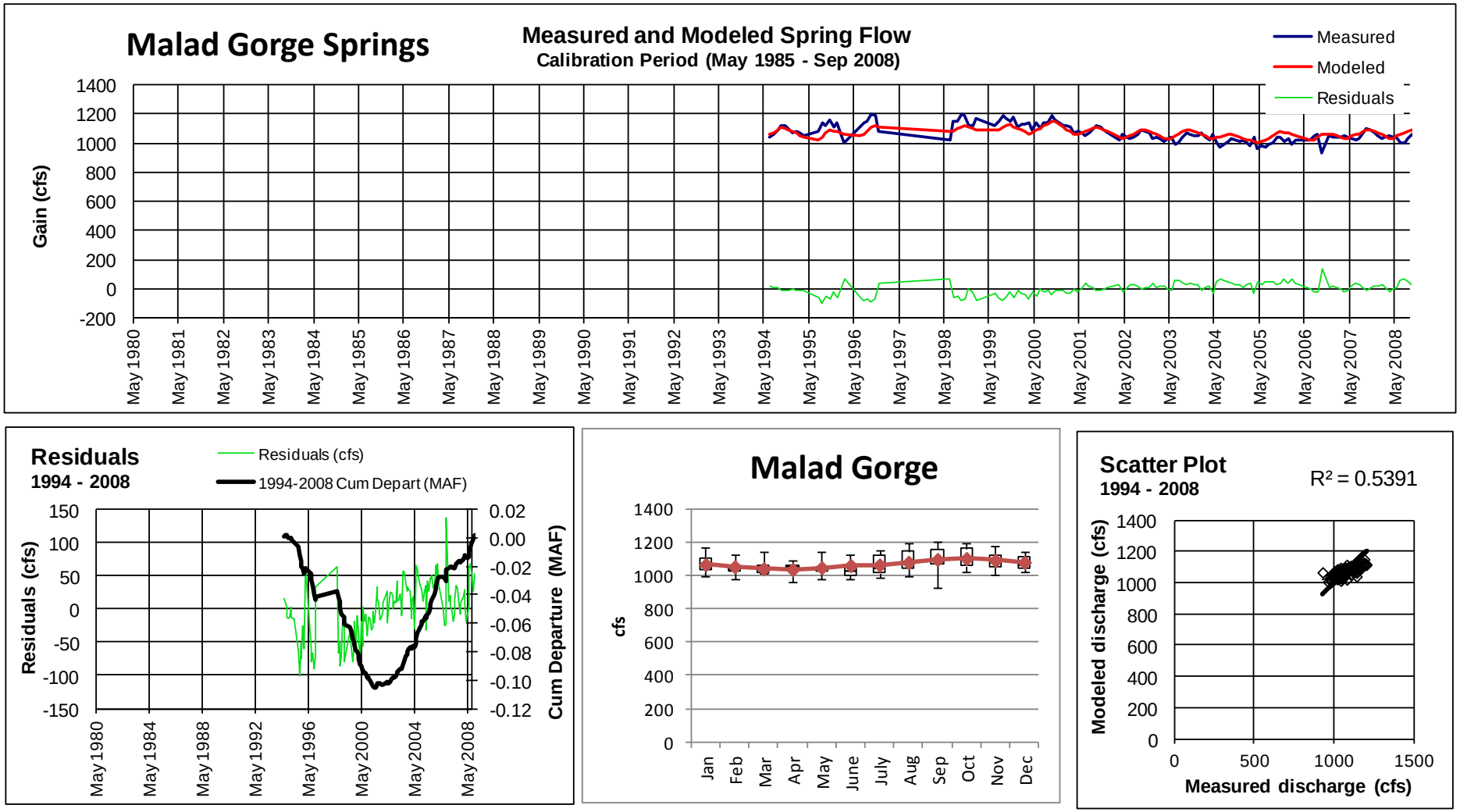

Figure 100. Spring flow for Malad Gorge Springs. The top chart shows the measured gains, modeled gains, and residual over the calibration period. The lower chart figure shows the cumulative departures. The lower middle chart is a Box-and-Whisker plot of the gains. The lower right chart is a scatter plot of modeled gains against measured gains.

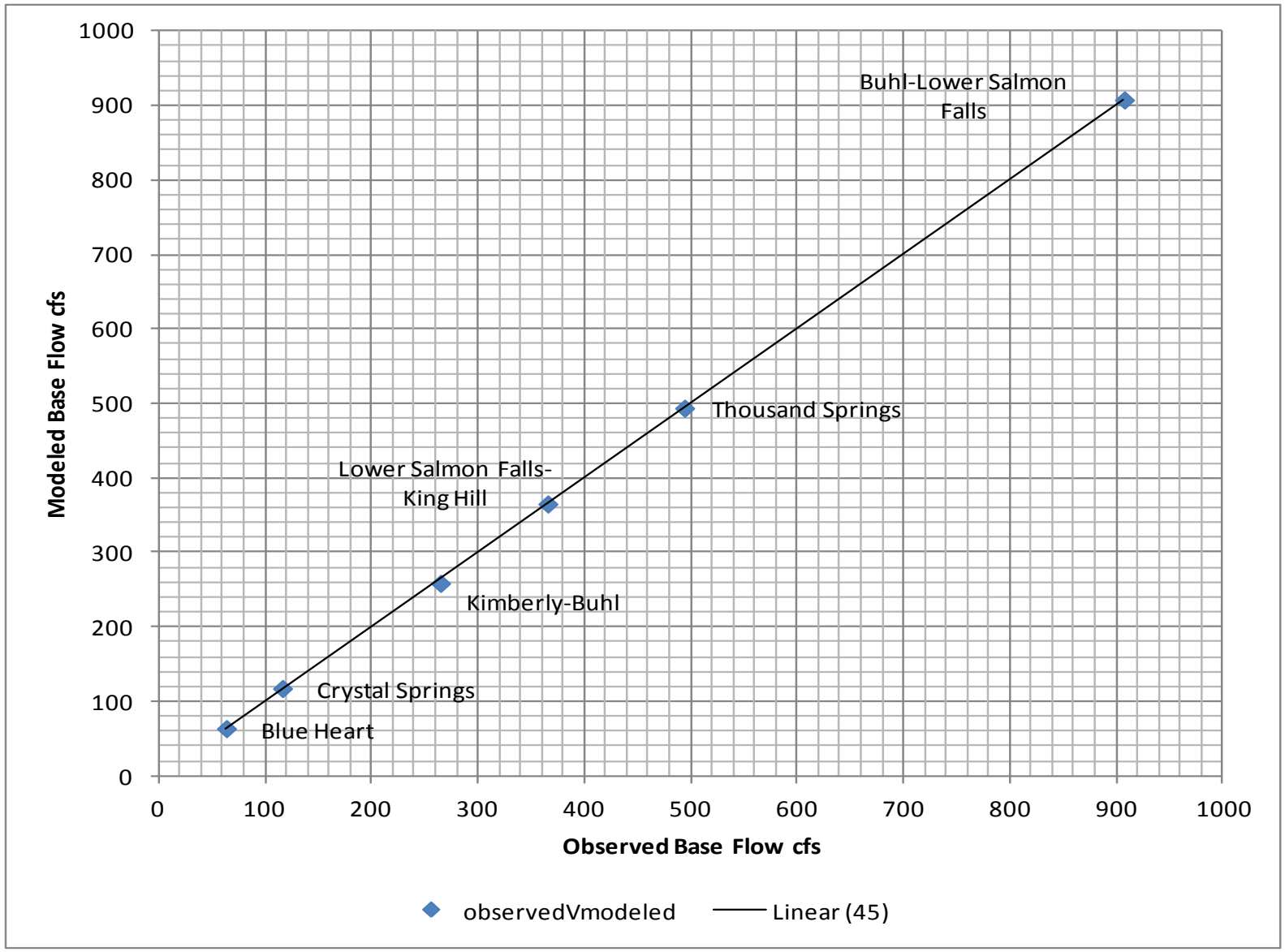

Figure 101. Plot of modeled base flow versus observed base flow for Kimberly-to-Buhl, Buhl-to-Lower Salmon Falls, Lower Salmon Falls reaches, and the local sites of Crystal Springs, Blue Heart Spring, and Thousand Springs.

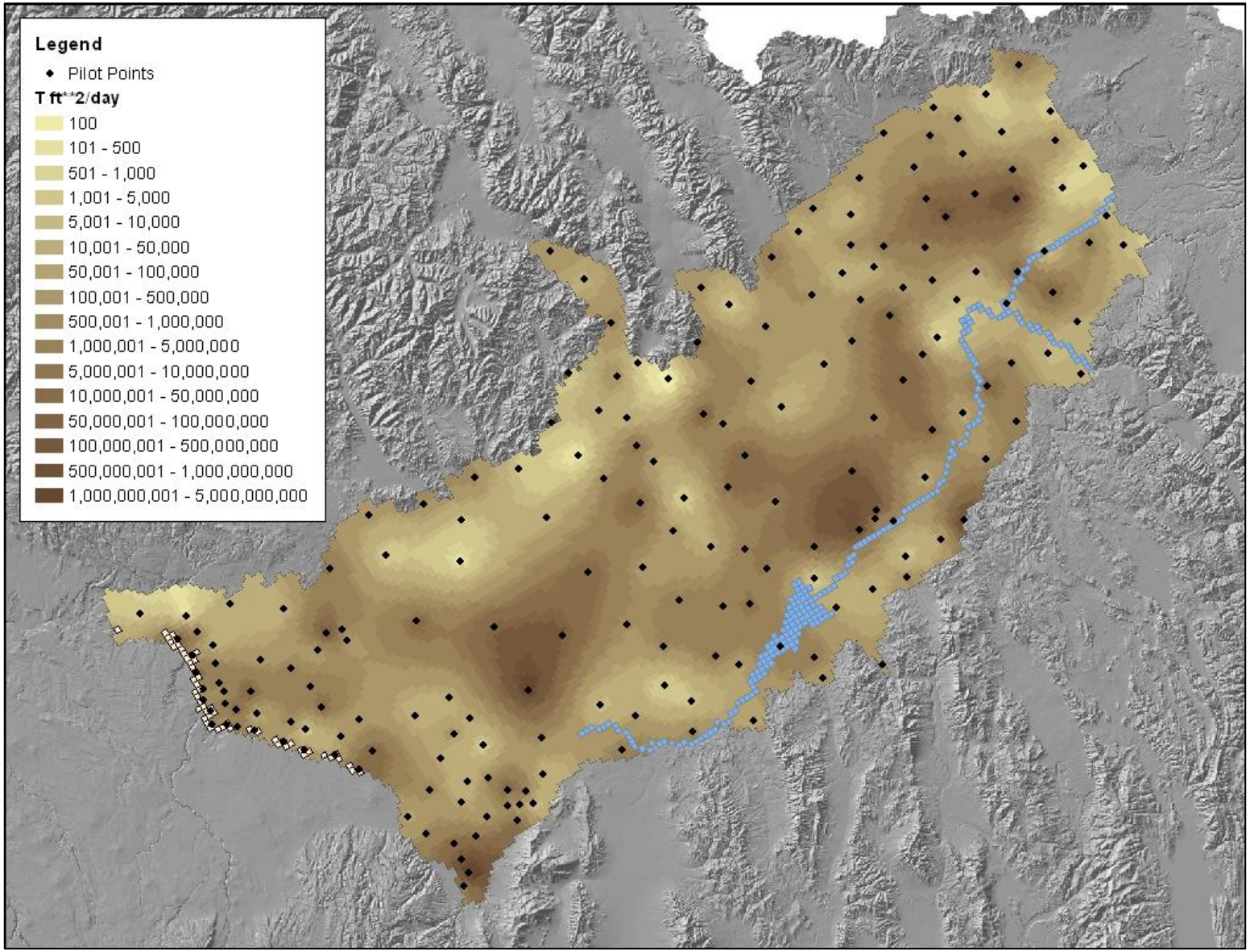

Figure 102. Map of the calibrated aquifer transmissivity (ft^2/day) in the Enhanced Snake Plain Aquifer Model Version 2.1.

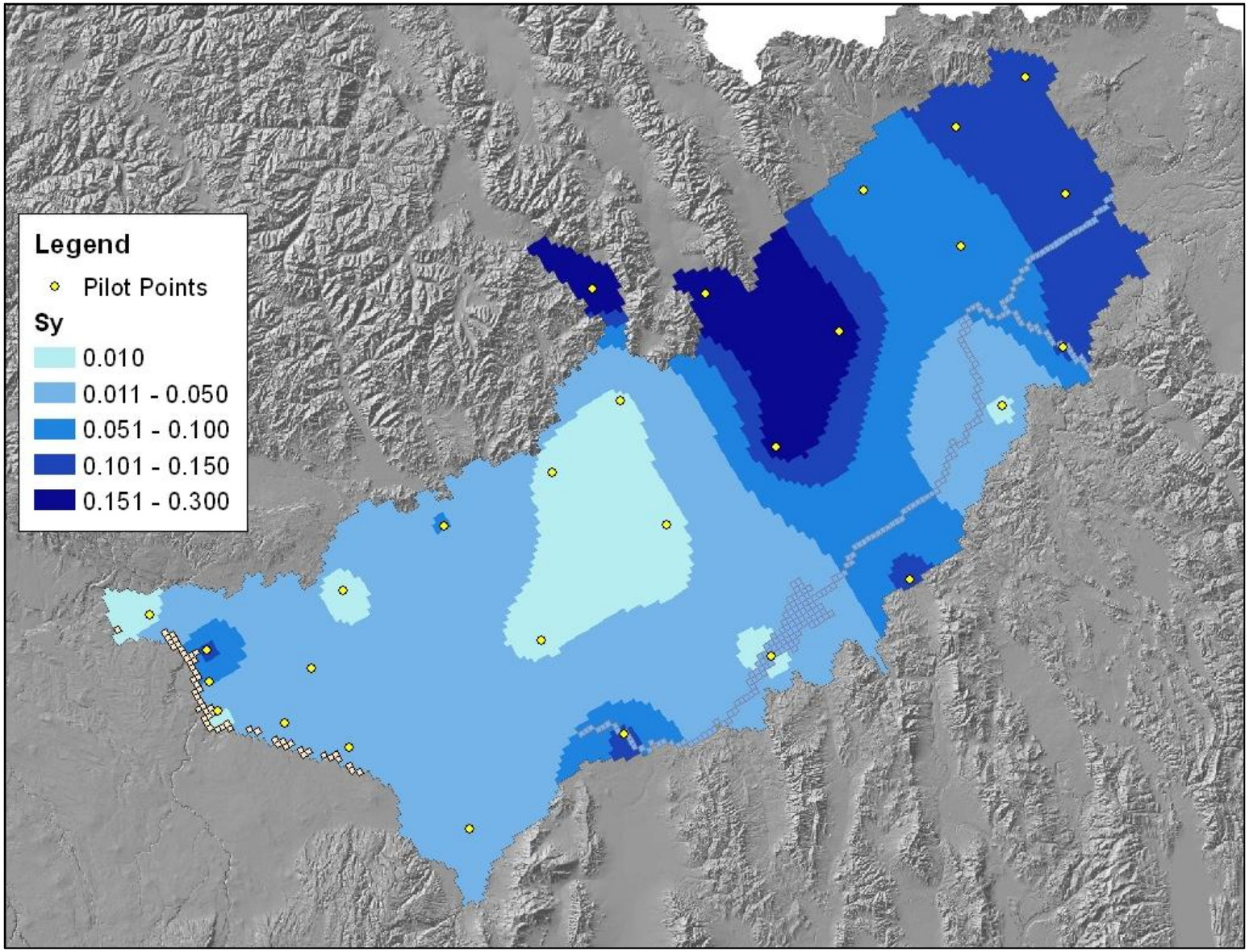

Figure 103. Map of the calibrated aquifer storage (S_y) and pilot points (yellow circles) used to adjust the values.

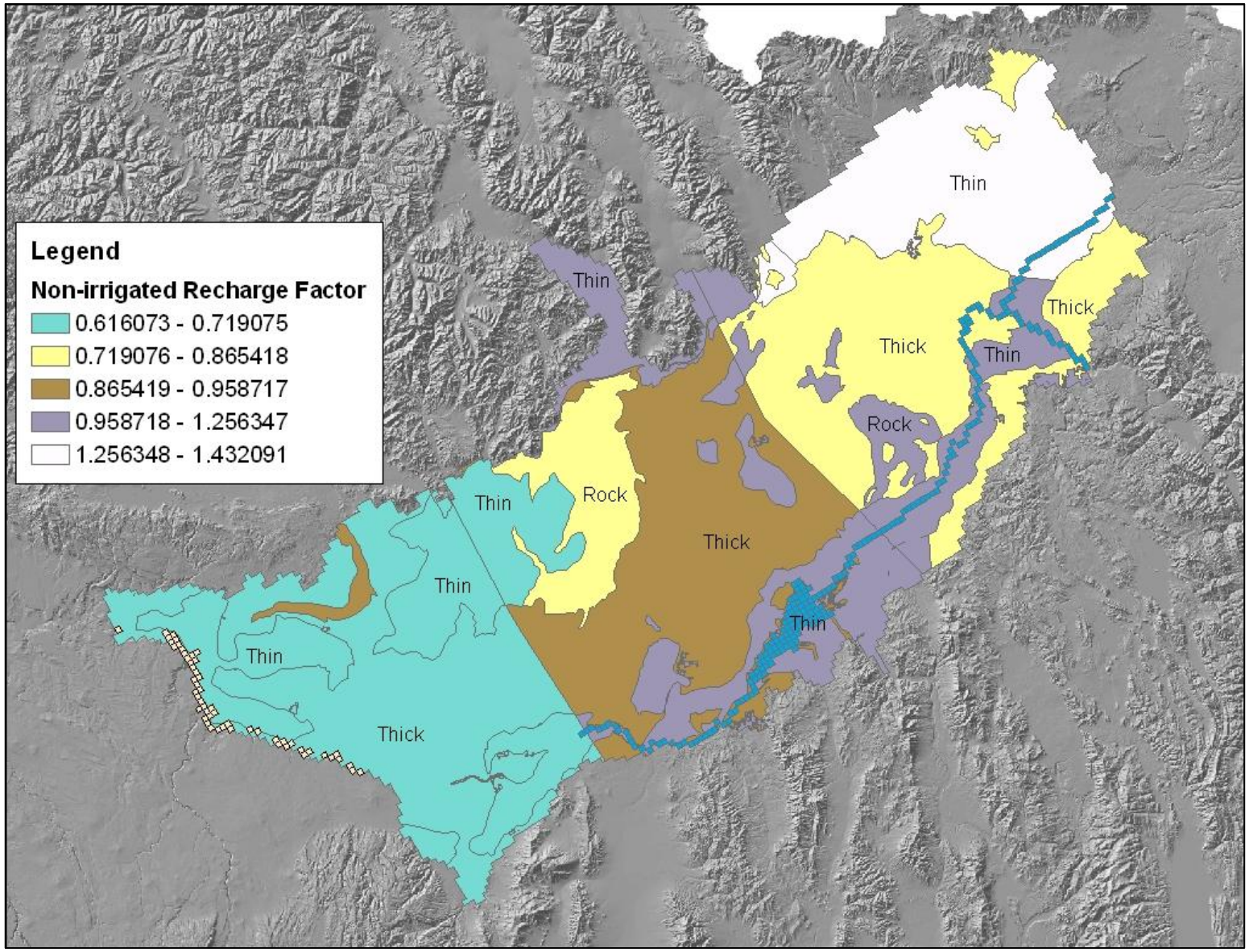

Figure 104. Calibrated non-irrigated recharge adjustment factors.

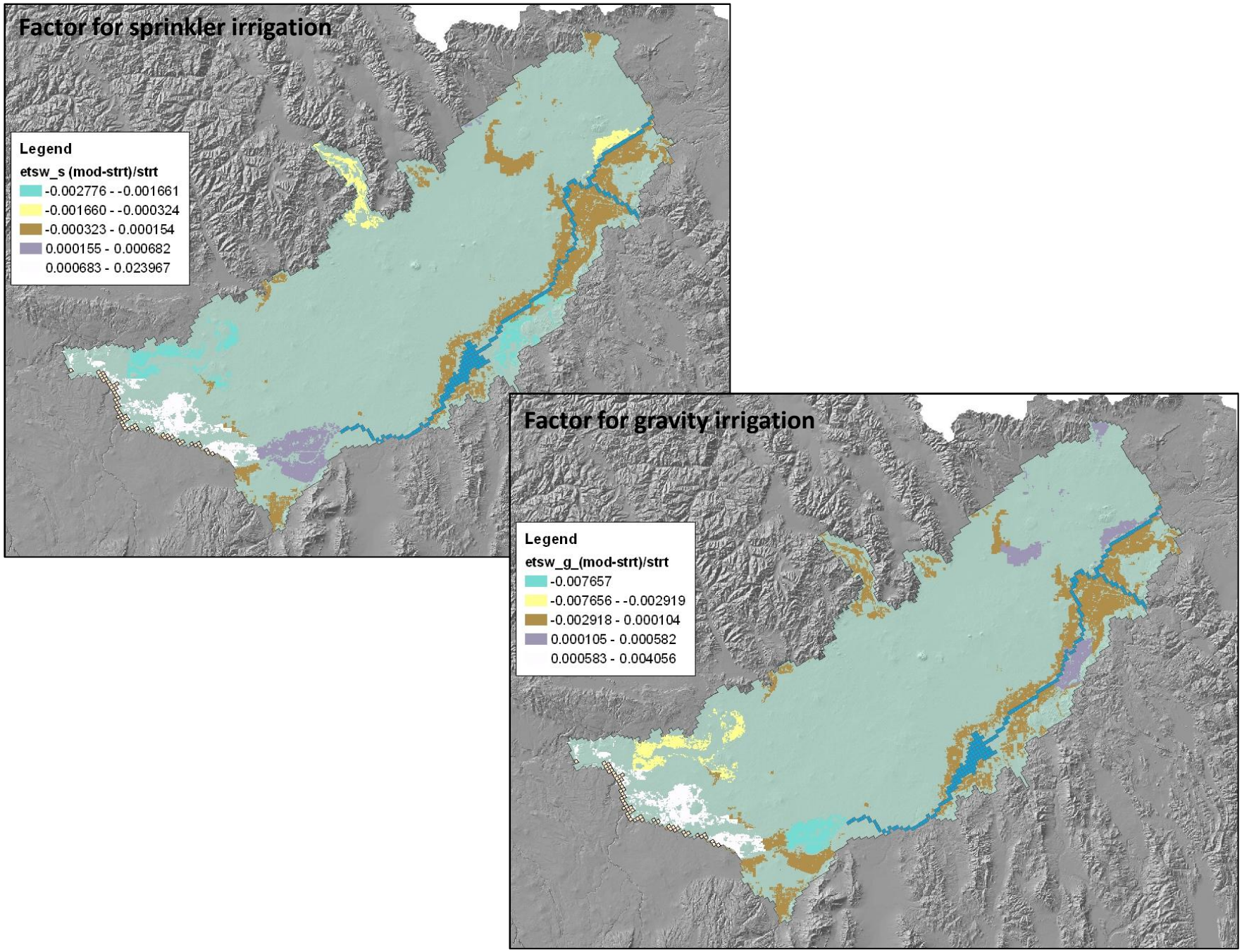

Figure 105. ET adjustment on surface-water irrigated lands.

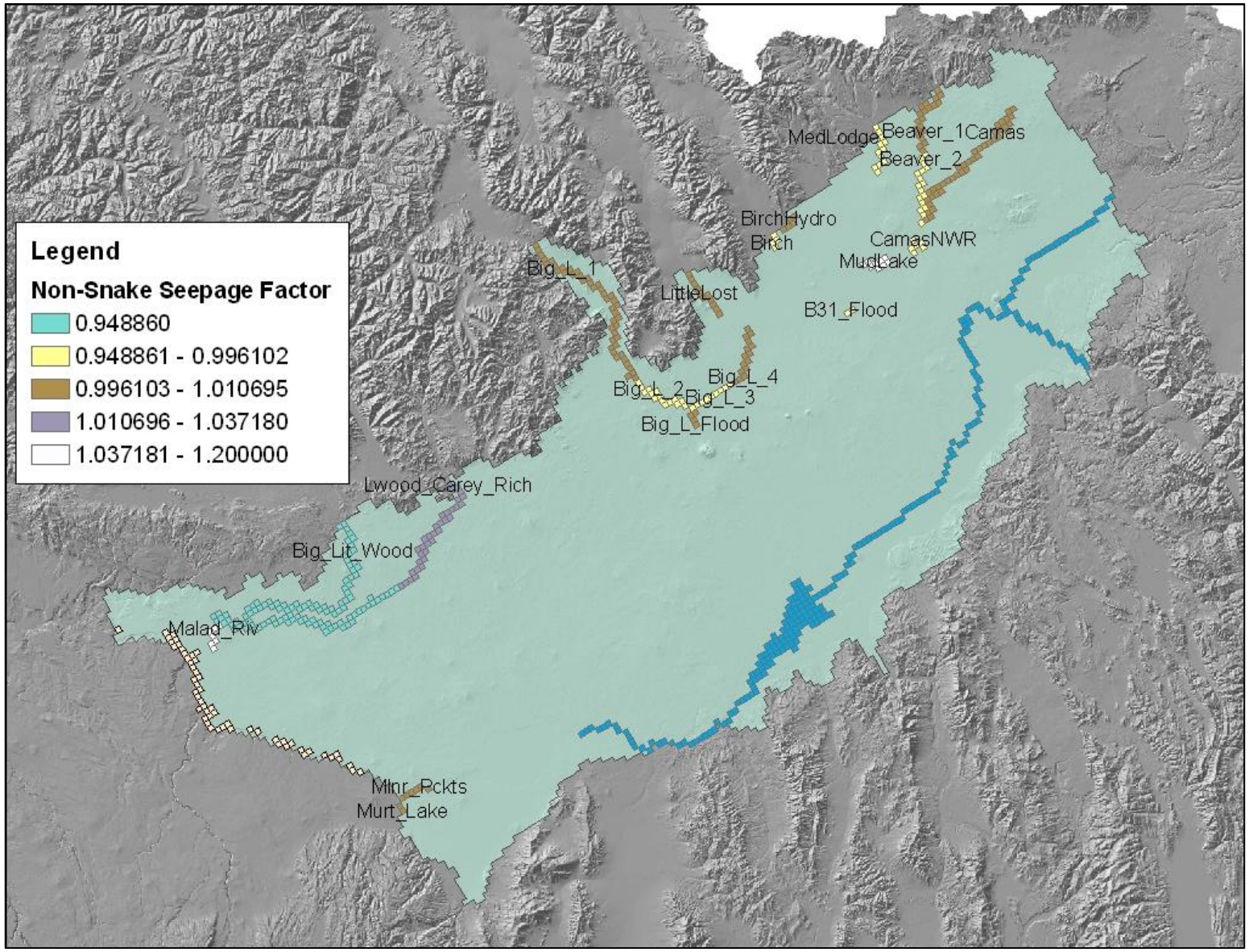

Figure 106. Adjustment factors for non-Snake River seepage sources.

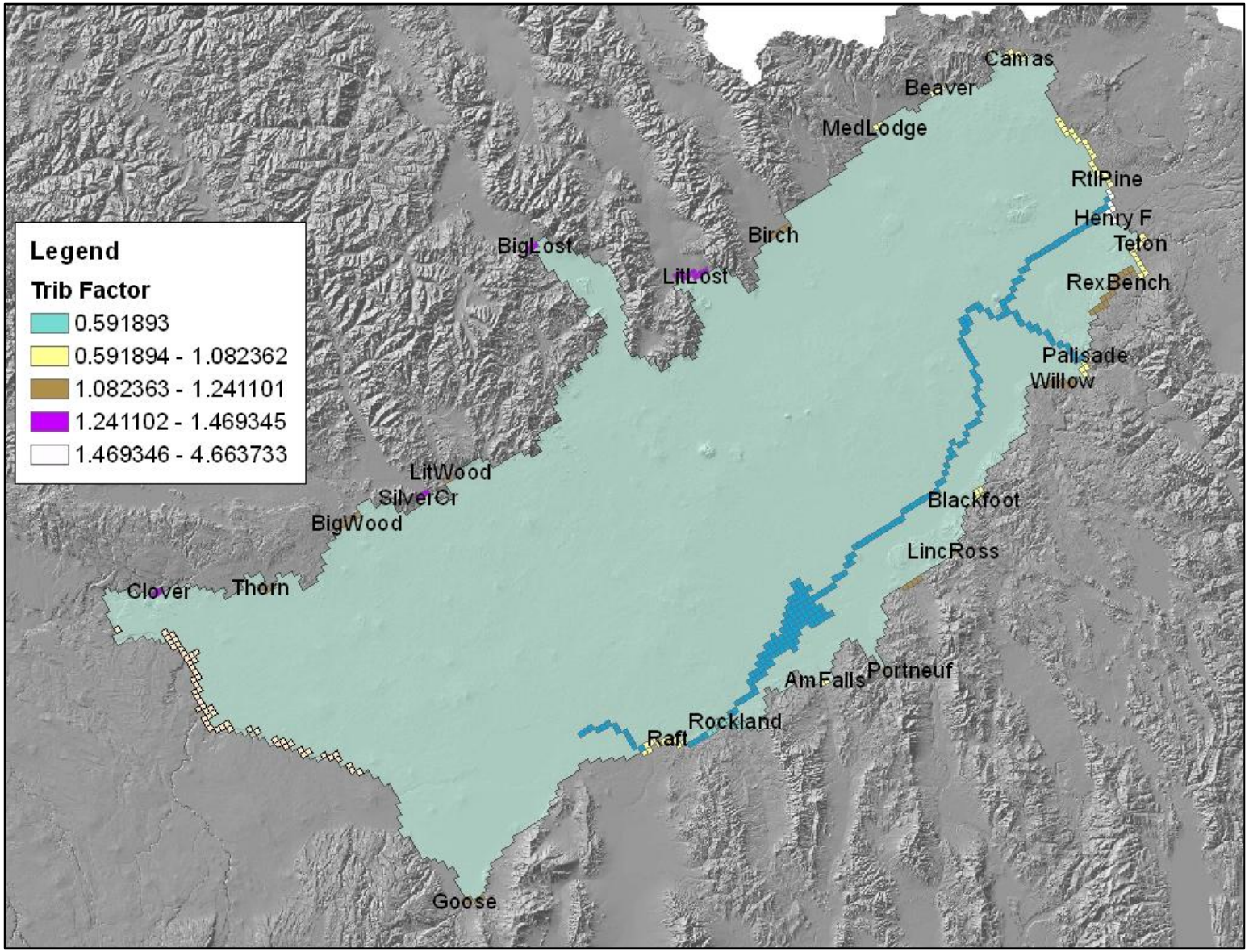

Figure 107. Adjustments factors for tributary underflow.

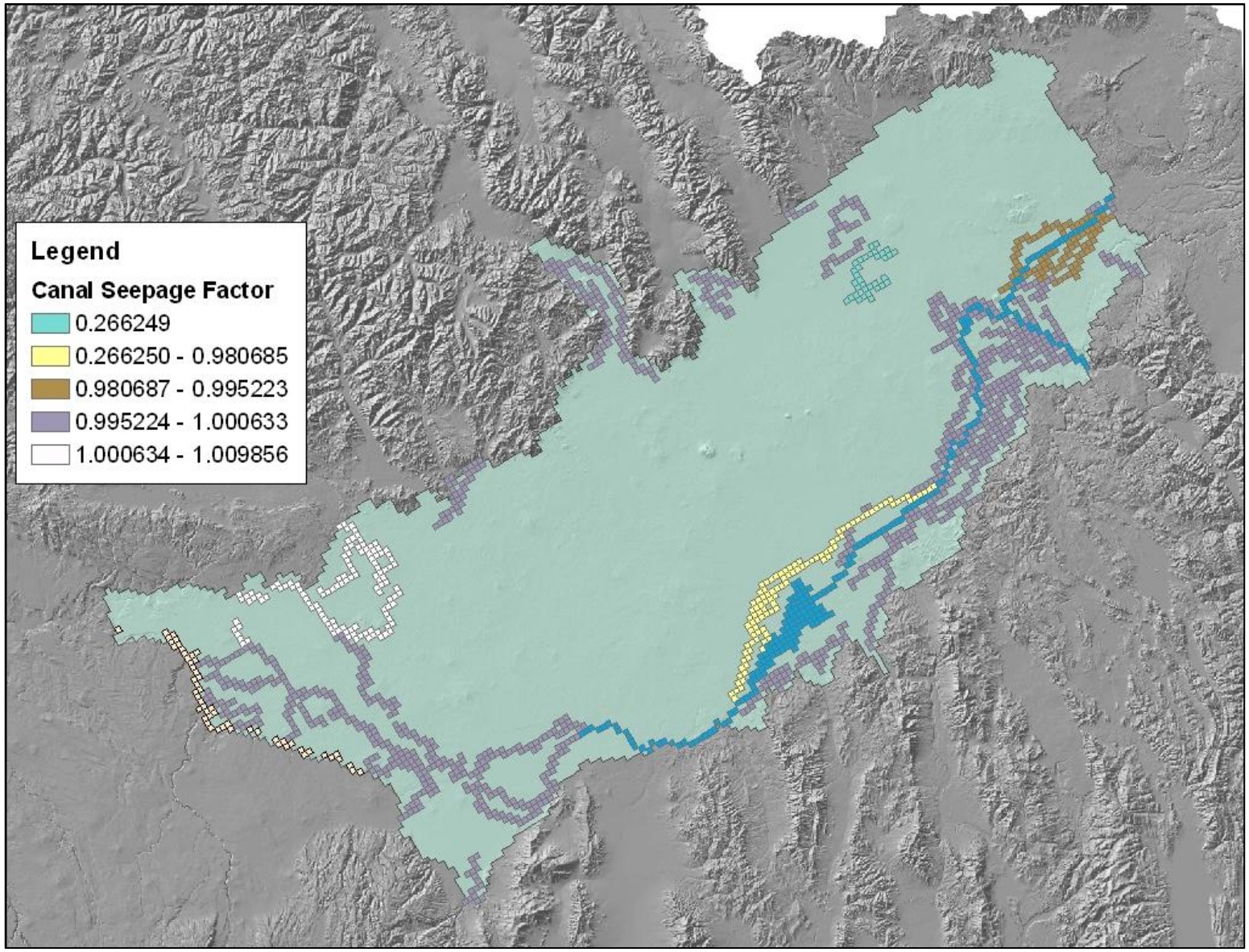

Figure 108. Adjustments factors for canal seepage.

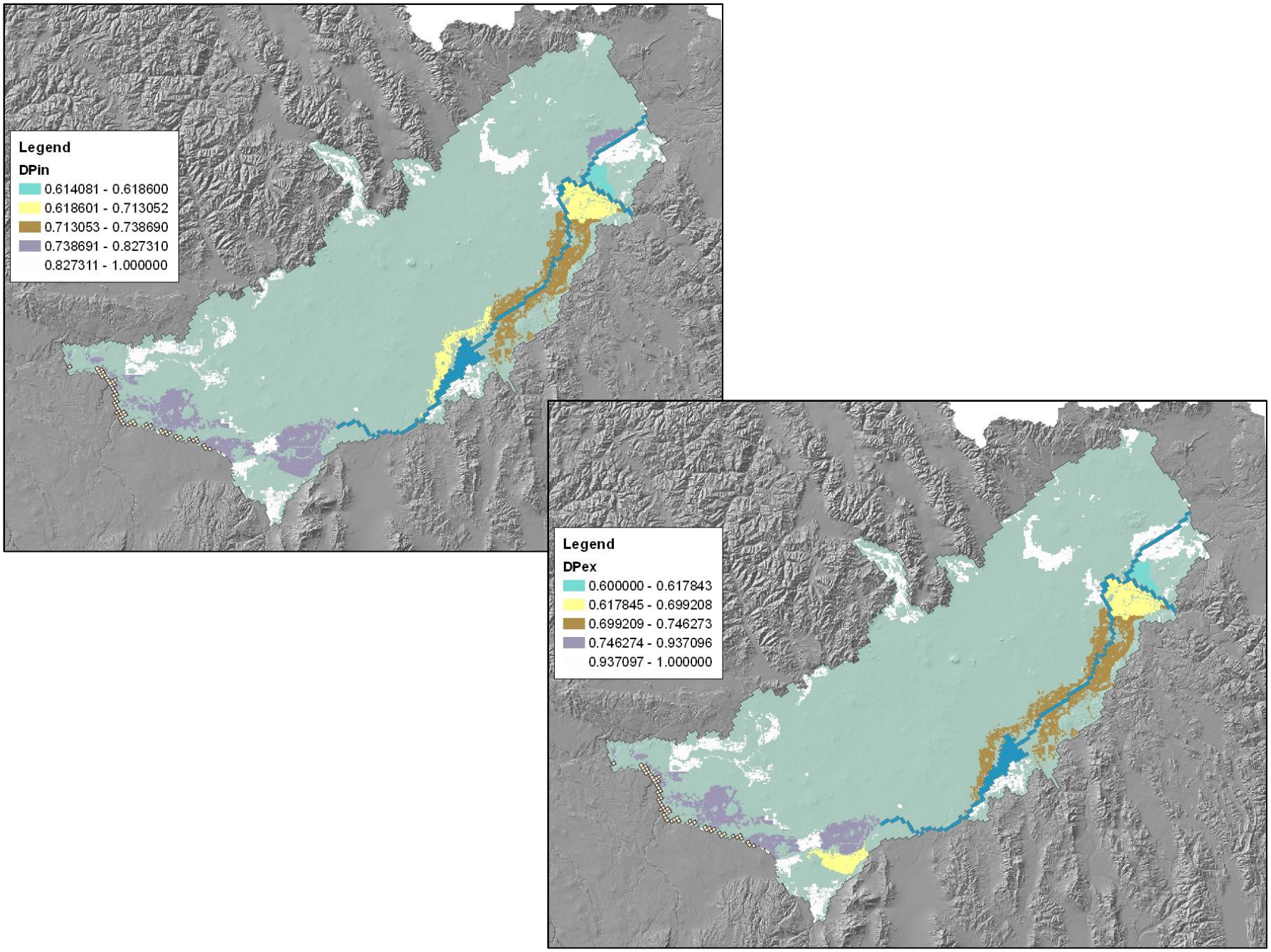

Figure 109. Distribution of the parameters DPin and DPex.

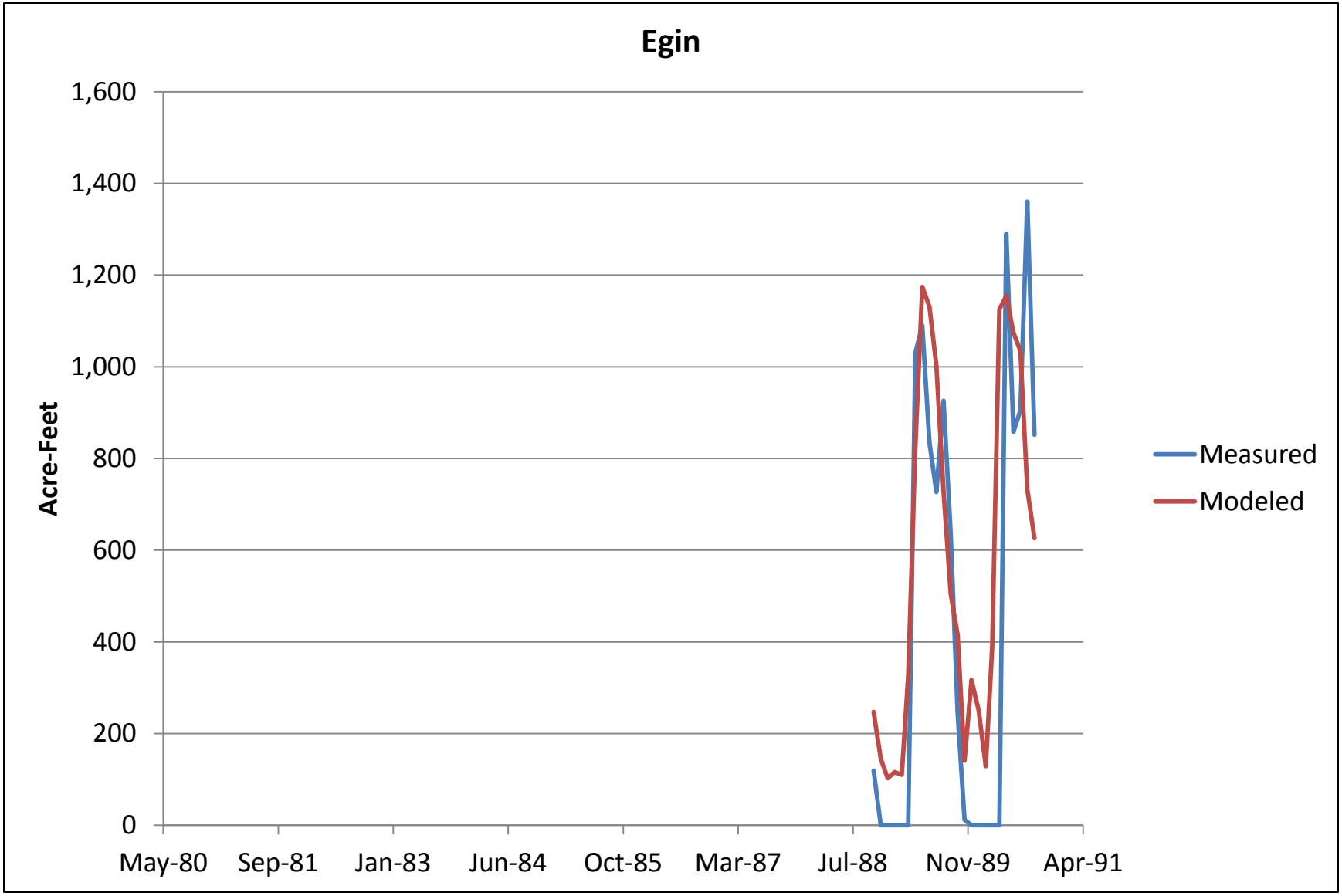

Figure 110. Measured and modeled return flows at Egin.

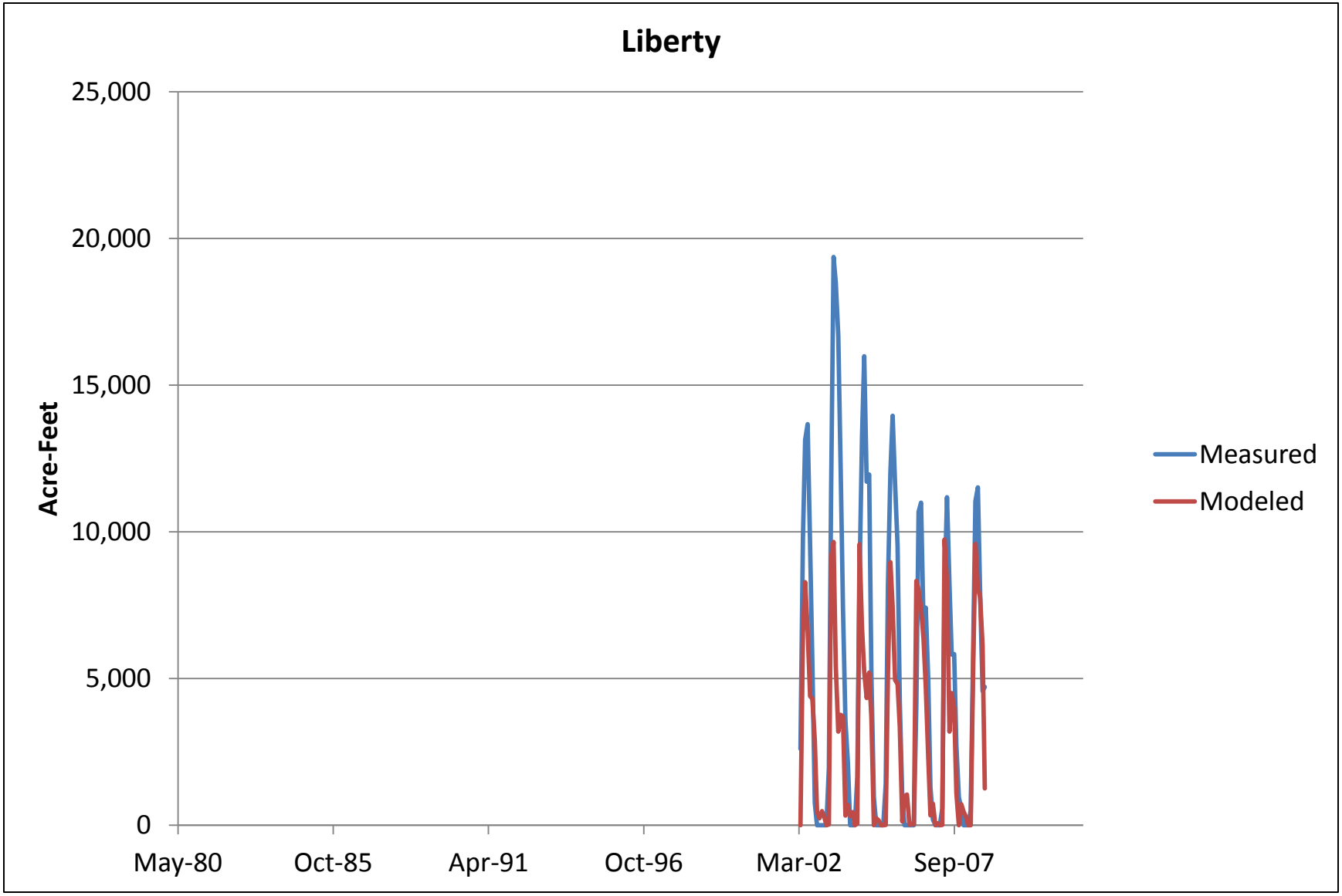

Figure 111. Measured and modeled return flows at Liberty.

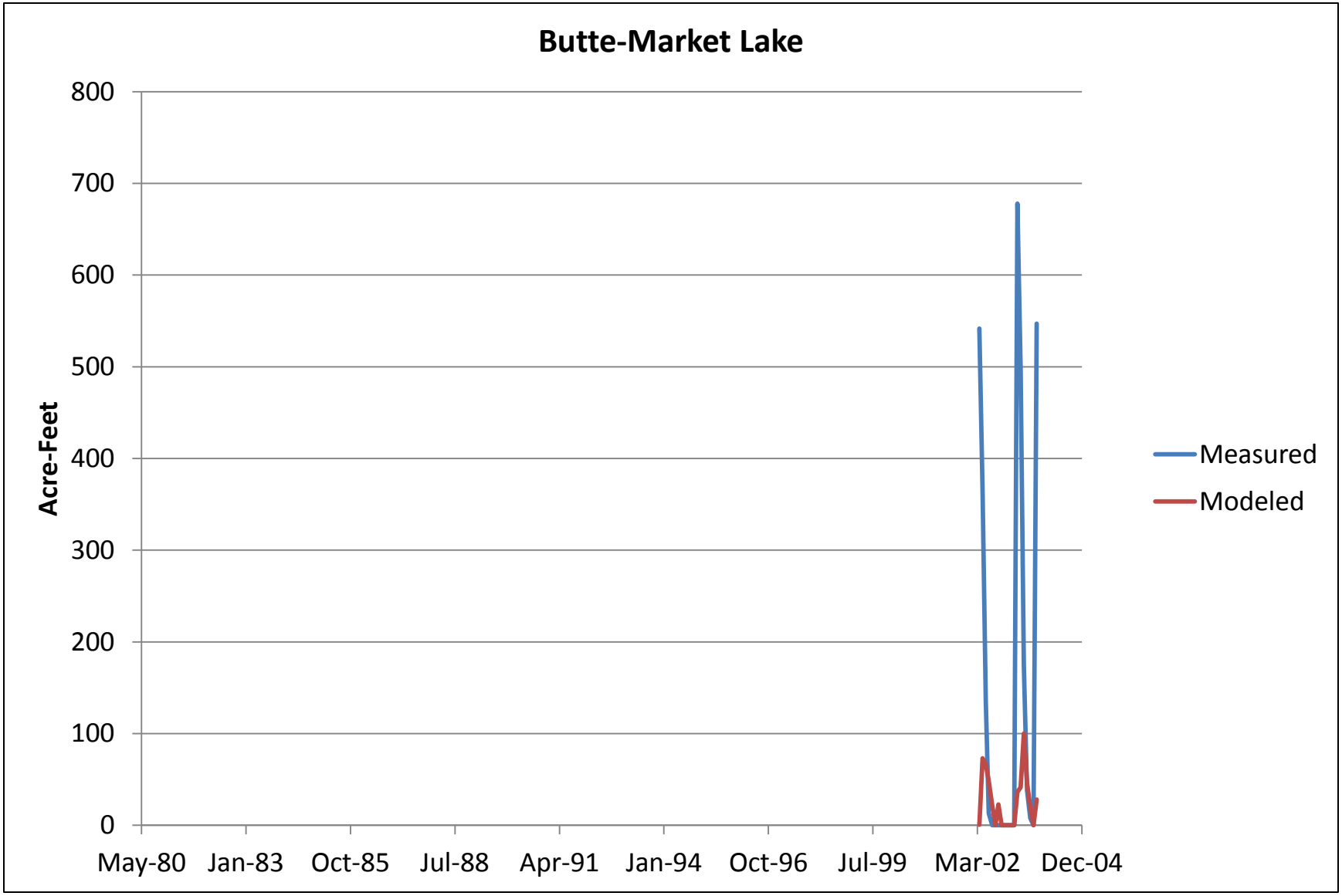

Figure 112. Measured and modeled return flows at Butte-Market Lake.

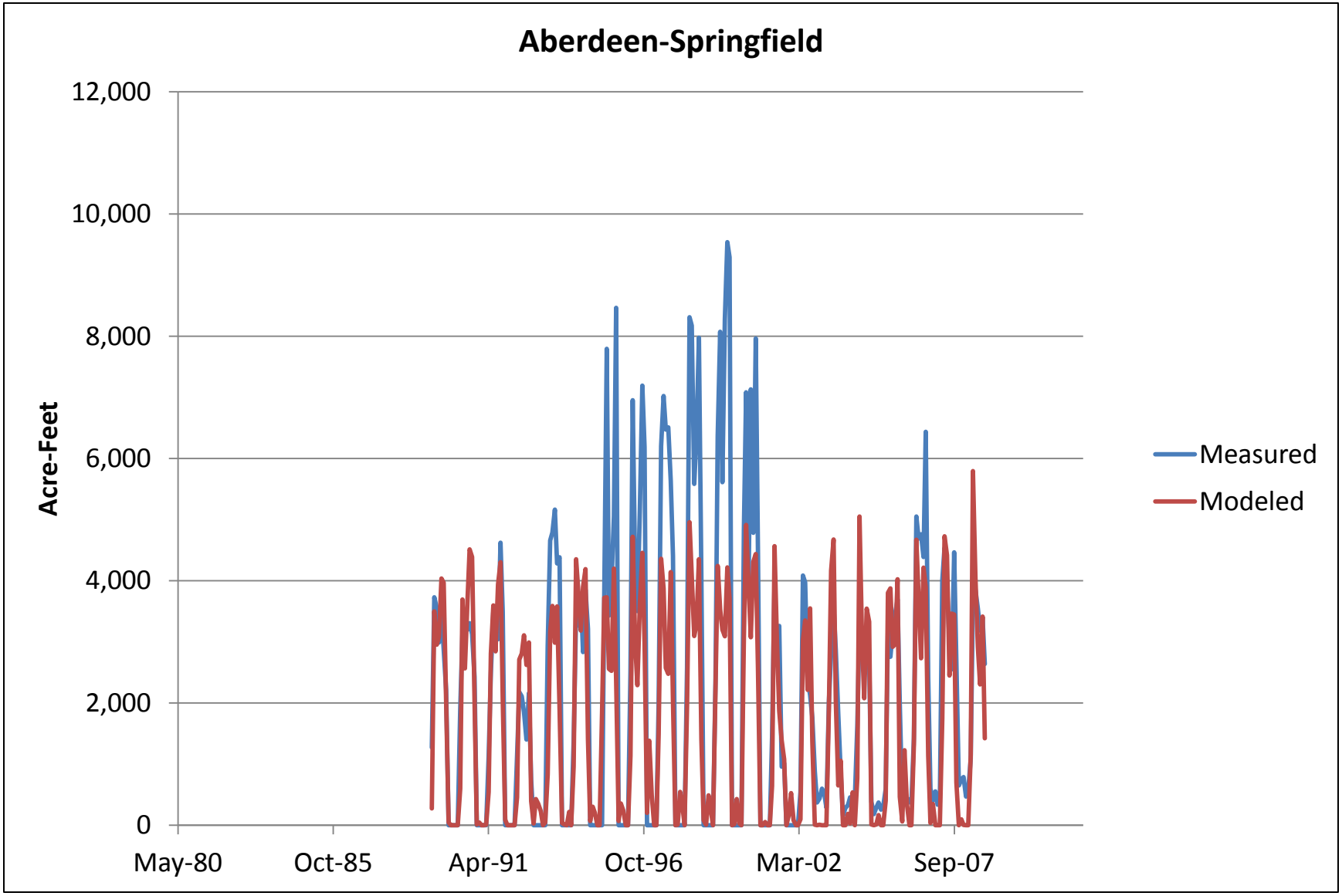

Figure 113. Measured and modeled return flows at Aberdeen-Springfield.

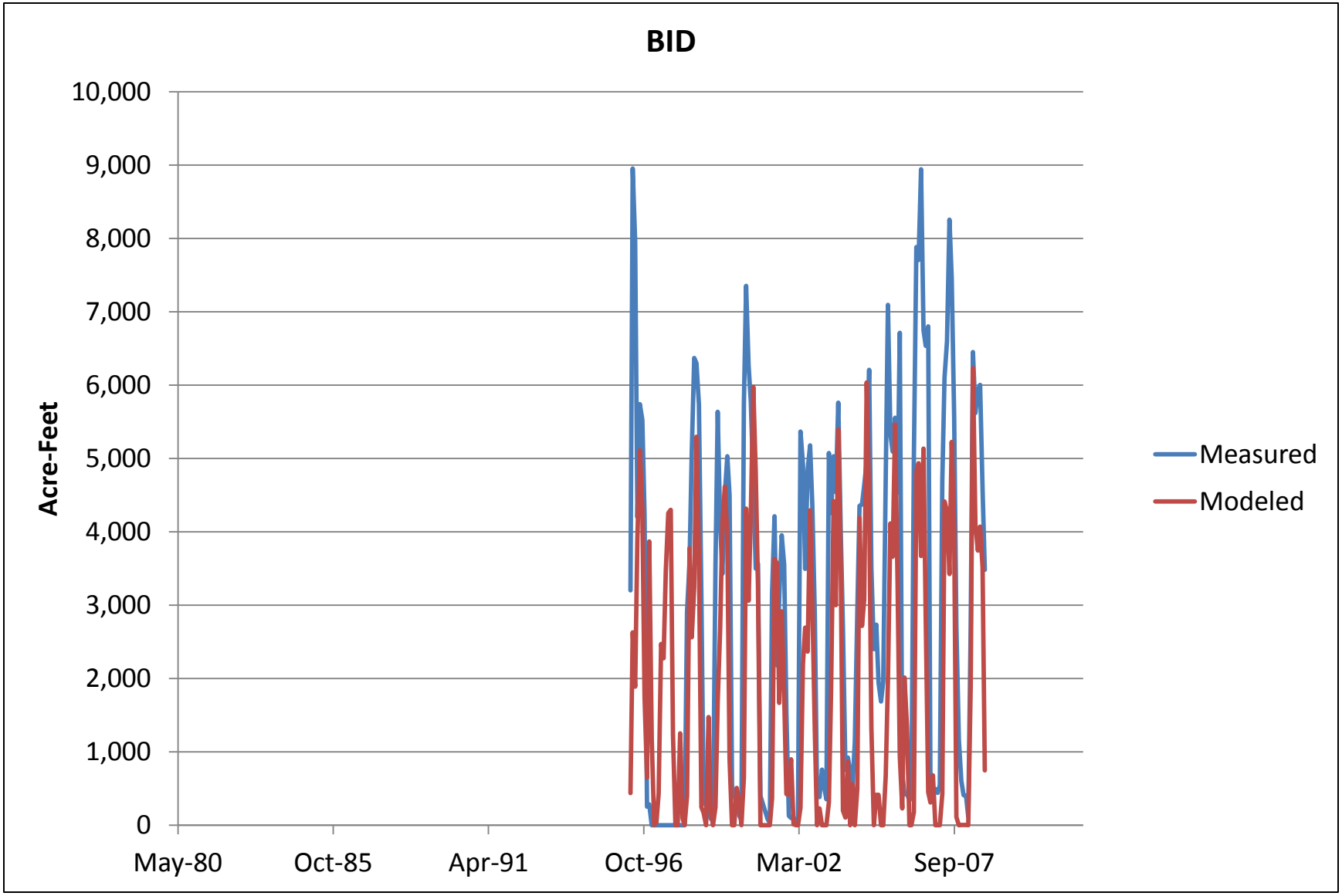

Figure 114. Measured and modeled return flows at Burley Irrigation District.

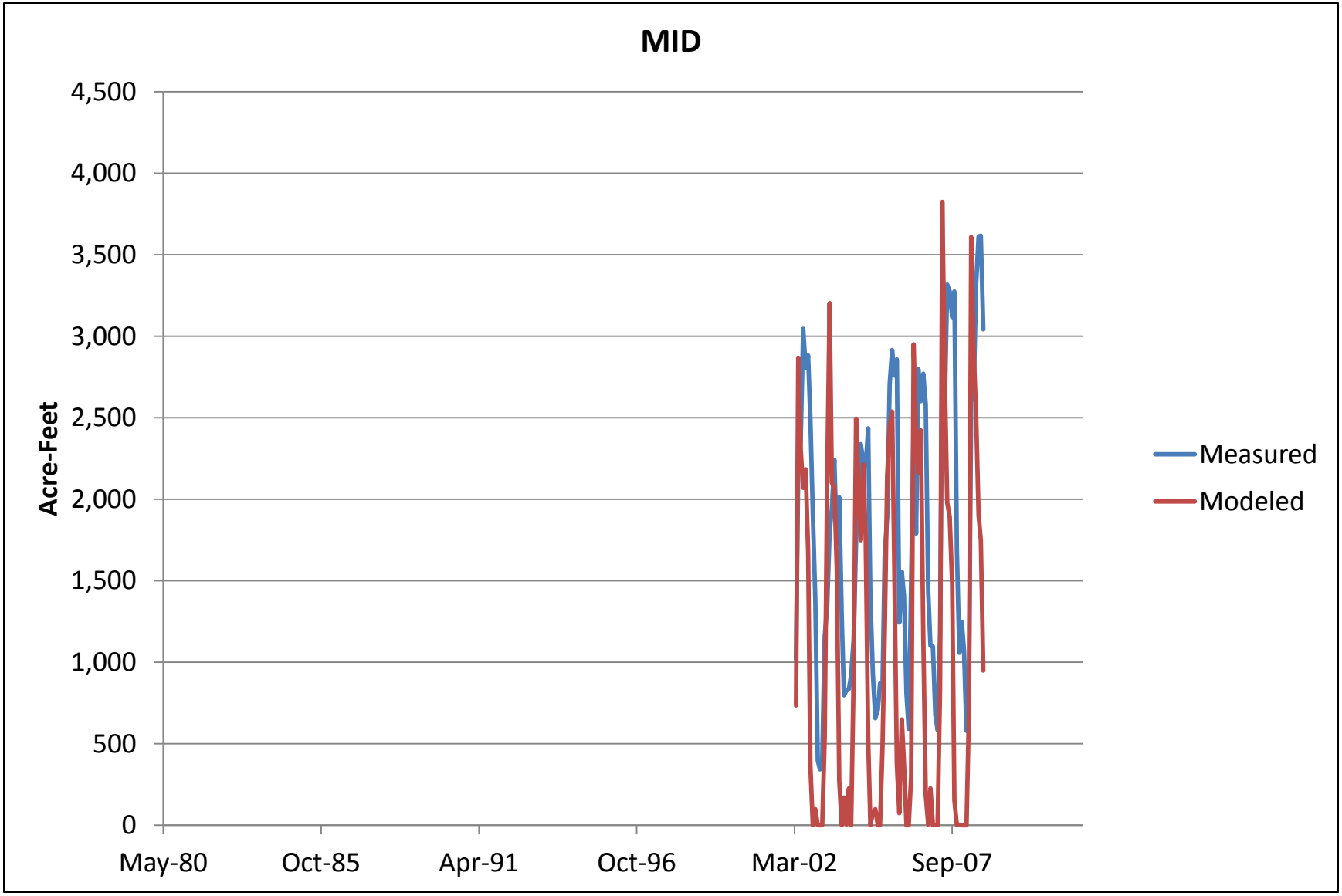

Figure 115. Measured and modeled return flows at Minidoka Irrigation District.

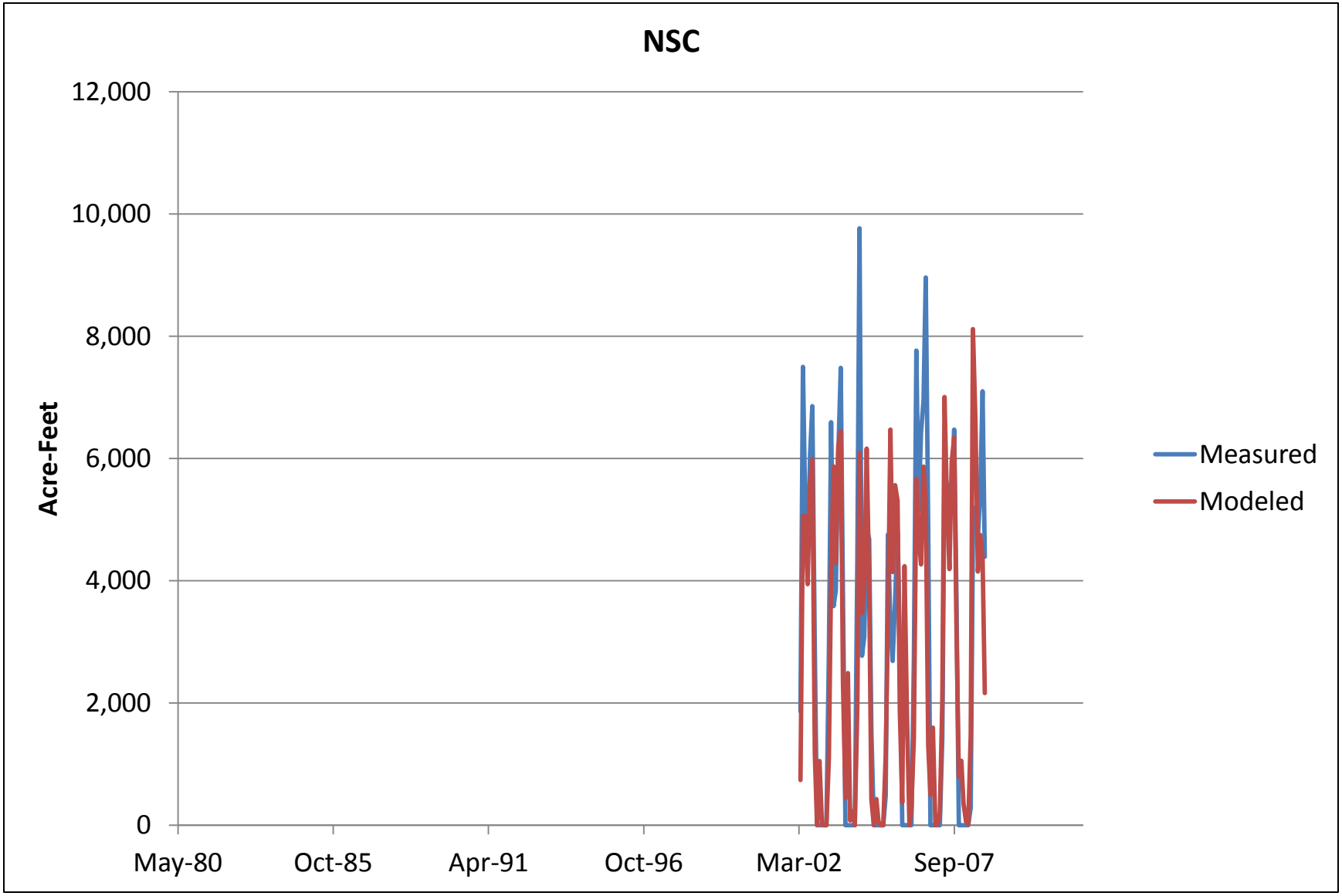

Figure 116. Measured and modeled return flows in the Northside Canal Company service area.

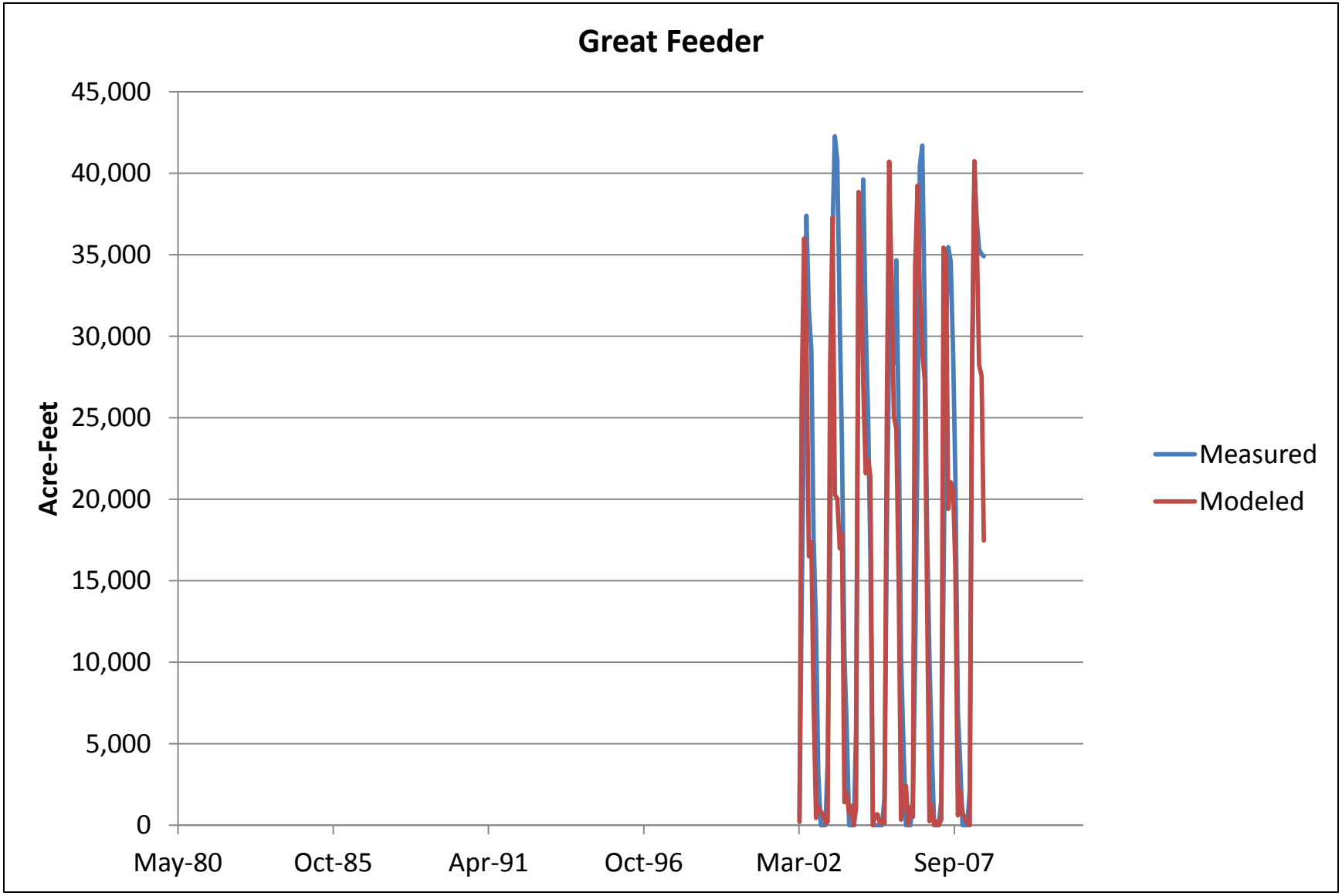

Figure 117. Measured and modeled return flows in the Great Feeder area.